POLYMORPHIC PHASE AND PIEZOELECTRIC PROPERTIES IN LEAD-FREE PIEZOELECTRIC BARIUM TITANATE-BASED CERAMICS

JITKASEM MAYAMAE

A THESIS SUBMITTED IN PARTIAL FULFILLMENT
OF THE REQUIREMENT FOR THE DEGREE OF
MASTER OF SCIENCE IN NANOSCIENCE AND NANOTECHNOLOGY
COLLEGE OF NANOTECHNOLOGY
KINGMONGKUT'S INSTITUTE OF TECHNOLOGY LADKRABANG
2017
KMITL-2017-NT-M-001-003

รอยต่อเฟสและสมบัติเพียโซอิเล็กทริกในวัสดุเพียโซอิเล็กทริกไร้สารตะกั่ว ของเซรามิกที่มีแบเรียมไททาเนตเป็นองค์ประกอบหลัก

POLYMORPHIC PHASE AND PIEZOELECTRIC PROPERTIES IN LEAD–FREE PIEZOELECTRIC BARIUM TITANATE–BASED CERAMICS

จิตเกษม มะยาแม

JITKASEM MAYAMAE

วิทยานิพนธ์นี้เป็นส่วนหนึ่งของการศึกษาตามหลักสูตรปริญญาวิทยาศาสตรมหาบัณฑิต

สาขาวิชานาโนวิทยาและนาโนเทคโนโลยี

วิทยาลัยนาโนเทคโนโลยีพระจอมเกล้าลาดกระบัง

สถาบันเทคโนโลยีพระจอมเกล้าเจ้าคุณทหารลาดกระบัง

พ.ศ.2560

KMITL-2017-NT-M-001-003

POLYMORPHIC PHASE AND PIEZOELECTRIC PROPERTIES IN LEAD–FREE PIEZOELECTRIC BARIUM TITANATE–BASED CERAMICS

JITKASEM MAYAMAE

A THESIS SUBMITTED IN PARTIAL FULFILLMENT

OF THE REQUIREMENT FOR THE DEGREE OF

MASTER OF SCIENCE IN NANOSCIENCE AND NANOTECHNOLOGY

COLLEGE OF NANOTECHNOLOGY

KINGMONGKUT'S INSTITUTE OF TECHNOLOGY LADKRABANG

2017

KMITL-2017-NT-M-001-003

หัวข้อวิทยานิพนธ์	รอยต่อเฟสและสมบัติเพียโซอิเล็กทริกในวัสดุเพียโซอิเล็กทริกไร้สารตะกั่วของเซรามิกที่มีแบเรียมไททาเนตเป็นองค์ประกอบหลัก
นักศึกษา	นางสาวจิตเกษม มะยาแม
รหัสประจำตัว	56607008
ปริญญา	วิทยาศาสตรมหาบัณฑิต
สาขาวิชา	นาโนวิทยาและนาโนเทคโนโลยี
พ.ศ.	2560
อาจารย์ที่ปรึกษาวิทยานิพนธ์	ผศ.ดร. วรรณวิลัย วิทยากร
อาจารย์ที่ปรึกษาวิทยานิพนธ์ร่วม	รศ.ดร. นราธิป วิทยากร

บทคัดย่อ

วิทยานิพนธ์นี้ศึกษาความสัมพันธ์ระหว่างโครงสร้างและสมบัติของเซรามิกที่มีแบเรียมไททาเนตเป็นองค์ประกอบหลัก งานวิจัยทำการออกแบบแบเรียมไททาเนตให้เกิดเฟสร่วมสองเฟสหรือมากกว่าสองเฟสอยู่ร่วมกันใกล้อุณหภูมิห้องเพื่อศึกษาสมบัติเพียโซอิเล็กทริก จากทฤษฎีการเกิดเฟสร่วมในวัสดุเฟอร์โรอิเล็กทริกได้ให้ความสนใจในเซรามิกระบบไตรภาคของ $BaTiO_3$–$SrTiO_3$–$BaSnO_3$ และ $BaTiO_3$–$Bi_{0.5}Na_{0.5}TiO_3$–$Bi(Mg_{0.5}Ti_{0.5})O_3$ ซึ่งเซรามิกทั้งหมดสองระบบทำการเตรียมขึ้นด้วยกระบวนการปฏิกิริยาสถานะของแข็ง โดยในระบบแรกทำการศึกษา $(0.975\text{-}y)BaTiO_3$–$0.025SrTiO_3$–$y BaSnO_3$ (เรียกย่อว่า BT–ST–yBS) ที่สัดส่วนองค์ประกอบ y = 0.00, 0.02, 0.04, 0.06, 0.08 และ 0.10 งานวิจัยในระบบนี้ได้ศึกษาผลของการเจือ Sn ใน BT–ST–yBS ซึ่งส่งผลต่อโครงสร้างผลึก การเปลี่ยนแปลงเฟส สมบัติทางไดอิเล็กทริก เฟอร์โรอิเล็กทริก และเพียโซอิเล็กทริก จากการทดลองพบว่าที่สัดส่วนองค์ประกอบ y = 0.04 มีการอยู่ร่วมกันของเฟสที่หลากหลายส่งผลให้สัดส่วนนี้แสดงสมบัติทางไฟฟ้าที่โดดเด่น ซึ่งแสดงค่าคงที่ไดอิเล็กทริกสูงสุด 11500 ในขณะเดียวกันก็มีค่าความเครียด 0.12 % ภายใต้สนามไฟฟ้า 10 kV/cm และค่าสัมประสิทธิ์ความเครียดได้สูงถึง 1280 pm/V

ในระบบที่สองทำการศึกษา $0.9BaTiO_3$–$(0.1\text{-}x)Bi_{0.5}Na_{0.5}TiO_3$–$xBi(Mg_{0.5}Ti_{0.5})O_3$ (เรียกย่อว่า BT–BNT–xBMT) ที่สัดส่วนองค์ประกอบ x = 0.00, 0.02, 0.04, 0.06, 0.08 และ 0.10 โดยศึกษาผลของการเจือ BMT ลงใน BT–BNT ส่งผลต่อโครงสร้างผลึก การเปลี่ยนแปลงเฟส ลักษณะทางสัณฐานวิทยา สมบัติไดอิเล็กทริก เฟอร์โรอิเล็กทริก และเพียโซอิเล็กทริก จากผลการทดลองพบว่าเมื่อปริมาณของ BMT เพิ่มขึ้นโครงสร้างผลึกของระบบ BT–BNT–xBMT เปลี่ยนจากโครงสร้างเททระโกนอลไปเป็นคิวบิกเสมือน และมีการเปลี่ยนเฟสเฟอร์โรอิเล็กทริกไปเป็นเฟสเสมือนรีแล็กเซอร์เมื่อปริมาณของ

BMT เพิ่มขึ้น นอกจากนี้พบว่าค่าโพลาไรเซชันคงเหลือ ค่าสนามไฟฟ้าบังคับ และค่าสัมประสิทธิ์ความเครียดมีแนวโนมที่ลดลงเมื่อปริมาณ BMT เพิ่มขึ้น

คำสำคัญ : วัสดุเพียโซอิเล็กทริกไร้สารตะกั่ว แบเรียมไททาเนต วิธีปฏิกิริยาสถานะของแข็ง

Thesis Title	Polymorphic Phase and Piezoelectric Properties in Lead–Free Piezoelectric Barium Titanate–Based Ceramics
Student	Miss Jitkasem Mayamae
Student ID	56607008
Degree	Master of Science
Program	Nanoscience and Nanotechnology
Year	2017
Thesis Advisor	Asst. Prof. Dr. Wanwilai Vittayakorn
Thesis Co-advisor	Assoc. Prof. Dr. Naratip Vittayakorn

ABSTRACT

The structure-properties relationship of barium titanate–based system were studied in this work. To study piezoelectric properties, the design of two phases or multiphase near room temperature in $BaTiO_3$–based was focused in this work. Ternary system of $BaTiO_3$–$SrTiO_3$–$BaSnO_3$ and $BaTiO_3$–$Bi_{0.5}Na_{0.5}TiO_3$–$Bi(Mg_{0.5}Ti_{0.5})O_3$ were selected for investigation. The ceramics of $(0.975\text{-}y)BaTiO_3$–$0.025SrTiO_3$–$yBaSnO_3$ (abbreviated as BT–ST–*y*BS) with y = 0.00, 0.02, 0.04, 0.06, 0.08 and 0.10 were synthesized via conventional solid state reaction. This system was carried out to study the effect of Sn on the crystal structure, phase transition, dielectric, ferroelectric, and piezoelectric properties of BT–ST–*y*BS ceramics. A room temperature, the composition *y* = 0.04 exhibited multi-coexistence phase which shows high relative permittivity (ε_r) of 11500 and high reversible strain of 0.12% with the normalized piezoelectric coefficient (*S*max/*E*max) of 1,280 pm/V at a low electric field (10 kV/mm).

In the second system, the $0.9BaTiO_3$–$(0.1\text{-}x)Bi_{0.5}Na_{0.5}TiO_3$–$xBi(Mg_{0.5}Ti_{0.5})O_3$ (abbreviated as BT–BNT–*x*BMT) ceramic, *x* = 0.00, 0.02, 0.04, 0.06, 0.08 and 0.10, were prepared. The effect of BMT on crystal structure, phase transition, morphology, dielectric, ferroelectric, and piezoelectric properties of BT–BNT ceramics were studied as a function of composition. The crystal structure of BT–BNT–*x*BMT successively transforms from tetragonal to pseudocubic symmetry, with increased BMT content. Temperature dependence of dielectric constant (ε_r) and dielectric loss ($tan\delta$) for BT–

BNT–*x*BMT at various frequencies showed that phase transition of ceramics changed from ferroelectric to relaxor-like behavior as BMT content increased. Furthermore, remanent polarization (P_r), coercive field (E_c) and the normalized strain (d_{33}^*) of BT–BNT–*x*BMT ceramics tend to decrease with increasing BMT concentration.

Keywords : Lead-free piezoelectric materials, Barium titanate, Solid state reaction

ACKNOWLEDGMENT

This thesis has been accomplished in the Electroceramic Research Laboratory, College of Nanotechnology, King Mongkut's Institute of Technology Ladkrabang, Bangkok, Thailand.

Throughout the period of 4 years ago in master's degree, I must acknowledge many people who have great assistance me. First, I would like to thank my co-advisor, Assoc. Prof. Dr. Naratip Vittayakorn who has guided me though these years for all invaluable advices, inspiration and supports throughout my education. I would like also to thank my advisor, Asst. Prof. Dr. Wanwilai Vittayakorn who has all the supports, kind advices and encourage in this study

I would like to thank to thank my committee members, Assoc. Prof. Dr. Wisanu Pecharapa, Asst. Prof. Dr. Thutiyaporn Thiwawong and Dr. Usa Sukkha, for their comment, valuable advices and questions.

I am grateful to Assist. Prof. Dr. Soodkhet Pojprapai and Asst. Prof. Dr. Theerachai Bongkarn, is credited for piezoelectric measurement, Dr. Rangson Muanghlua, Department of Electronics, Faculty of Engineering, King Mongkut's Institute of Technology Ladkrabang, is credited for dielectric measurement.

Addition, I wish to thank ECRL members for all helps, assistance and encourage me.

Finally, I would like to express my deepest thanks to my family, my father, Adun Mayamae, my mother, Kannika Mayamae, , my old sister, Aksara Mayamae, and my old brother, Kittikhun Mayamae, who have always encourage, helps, assistance and support me in everything until through all the difficulties during my studied.

Jitkasem Mayamae

TABLE OF CONTENTS

TABLE OF CONTENTS (II)

TABLE OF CONTENTS (III)

LIST OF TABLES

LIST OF ILLUSTRATIONS

Figure **Page**

LIST OF ILLUSTRATIONS (II)

Figure **Page**

LIST OF ILLUSTRATIONS (III)

LIST OF ILLUSTRATIONS (IV)

Figure **Page**

ABBREVIATIONS AND SYMBOLS

d_{ij}	Piezoelectric coefficient
E	Electric field
E_C	Coercive field
T_C	Curie temperature
ε_r	Relative permittivity
$tan\delta$	Dielectric loss
K	Electromechanical coupling factor
k_p	Planar electromechanical coupling factor
P	Polarization
P_S	Saturated polarization
P_r	Remanent polarization
PPT	Polymorphic phase transition
MPB	Morphotropic phase boundary
S	Strain
t	Tolerance factor

CHAPTER 1
INTRODUCTION

1.1 Overview

Piezoelectric materials have been studied widely and used extensively in many electronic devices such as electromechanical transducers, sensors and actuators, due to their excellent ferroelectric and piezoelectric properties [1]. It is known that Lead – based piezoelectric materials, for example, lead zirconate titanate (PZT) and PZT – family have been used widely in many piezoelectric applications [2]. However, lead – based piezoelectric materials contain over 60 wt% of lead, which is a serious threat to the environment. The fabrication process of these materials also uses lead oxide, which enhances toxicity further due to volatilization at a high temperature, predominantly during calcination and the sintering process, thus causing environmental pollution [3]. Consequently, legislations from the European Union (EU), including Restriction of Hazardous Substances (RoHS), Waste from Electrical and Electronic Equipment (WEEE), and End of Life Vehicles (ELV), have been put into effect in order to restrict the use of hazardous substances such as lead and other heavy metals in electronic devices [4–6]. There have been many previous scientific works that have substituted lead-free piezoelectric materials, but the properties used were not nearly as effective as those in the PZT system. Candidate lead – free perovskite systems are fundamentally Barium Titanate ($BaTiO_3$; BT), Bismuth Sodium Titanate $(Bi_{0.5}Na_{0.5})TiO_3$ and Potassium Sodium Niobate $(K_{0.5}Na_{0.5})NbO_3$ ceramics [7].

BT–based ceramics are a lead-free piezoelectric material candidate, due to their outstanding piezoelectric properties [8]. It is known that the coexistence of different ferroelectric phases plays a crucial role in enhancing piezoelectric properties in lead and lead-free piezoelectric properties. The piezoelectric properties of BT ceramic have been modified by doping with either A– and/or B – site substitutions into the ABO_3 structure. The binary system of tin-doped into barium titanate ($BaTiO_3$–$x$$BaSnO_3$) recently showed high dielectric permittivity (ε_r) ~ 75,000 and piezoelectric coefficient (d_{33}) ~ 697 pC/N at the quasi-quadruple point, at which Cubic, Tetragonal, Orthorhombic and Rhombohedral phases coexist [9]. Xusheng Wang et al. reported a

high electrostriction strain value of ~ 0.22% in the binary systems of $BaTiO_3$–$CaTiO_3$, where diphasic or tetragonal and orthorhombic phases occur at room temperature [10]. Wei Li et al. investigated the polymorphic phase transition (PPT) from orthorhombic to tetragonal phase in the BT–BZ–CT system, and a high piezoelectric constant (d_{33}) of ~ 365 pC/N and planar electromechanical coupling (k_p) at ~ 48.5% were recorded at the PPT composition [11-12]. Extremely high piezoelectric properties; d_{33} = 568 pC/N, k_p = 47.7%, ε_r = 23000 and normalized strain (dS/dE) = 1013 pm/V, were found recently at the orthorhombic-tetragonal coexistence phase composition [13]. The multiphase coexistence of rhombohedral–pseudocubic–orthorhombic phase (R–PC–O) composition exhibited an ultrahigh d_{33} = 670 pC/N at room temperature [14]. Complex perovskite was used also recently to modify the piezoelectric properties of BT ceramics. Wada et al. studied the combination between $BaTiO_3$ and $Bi(Mg_{0.5}Ti_{0.5})O_3$ (BMT) and found that BMT can enhance Curie temperature (T_C) of BT with the highest T_C (about 360°C) for $0.5BaTiO_3$ - 0.5BMT ceramics [15]. Qi Wang et al. studied lead-free $Bi_{0.5}Na_{0.5}TiO_3$ -$Bi(Mg_{0.5}Ti_{0.5})O_3$ systems and reported that BMT could improve piezoelectric properties and enhance T_C of BNT ceramic. The 0.95BNT–0.05BMT ceramic showed the highest d_{33} at about 110 pC/N, with high T_C at 352°C [16].

In this work, the substituting system in BT is classified into two classes; substituting with a simple perovskite (ABO_3) system (such as CT, BS, ST and BSn) and a complex perovskite ($A'A''\ B'B''O_3$) system (such as BMT, BNT, KNN). Based on information from the literature review, the ferroelectric phase diagram of BT–ST–BS and BT–BNT–BMT has been created to explore the effect of substituting with a simple perovskite (ABO_3) system and a complex perovskite ($A'A''\ B'B''O_3$), respectively. Based on the phase diagram, the composition range in the $(0.975\text{-}y)BaTiO_3$–$0.025SrTiO_3$–$yBaSnO_3$ (abbreviated as BT–ST–*y*BS) system and $0.9BaTiO_3$–$(0.1\text{-}x)Bi_{0.5}Na_{0.5}TiO_3$–$xBi(Mg_{0.5}Ti_{0.5})O_3$ (abbreviated as BT–BNT–*x*BMT) system is expected to display the multiphase near room temperature. The goal of this study is to synthesize the lead-free piezoelectric ceramics of the barium titanium-based ternary system in two systems:

1. The ternary system of (0.975-*y*)$BaTiO_3$–0.025$SrTiO_3$–*y*$BaSnO_3$, where *y* = 0.00, 0.02, 0.04, 0.06, 0.08 and 0.10.
2. The ternary system of 0.9$BaTiO_3$–(0.1-*x*)$Bi_{0.5}Na_{0.5}TiO_3$–*x*$Bi(Mg_{0.5}Ti_{0.5})O_3$, where *x* = 0.00, 0.02, 0.04, 0.06, 0.08, 0.10

Based on the PPT concept, high piezoelectric properties are expected to be obtained near the PPT composition. The structure – properties relationship will be studied systematically and explored.

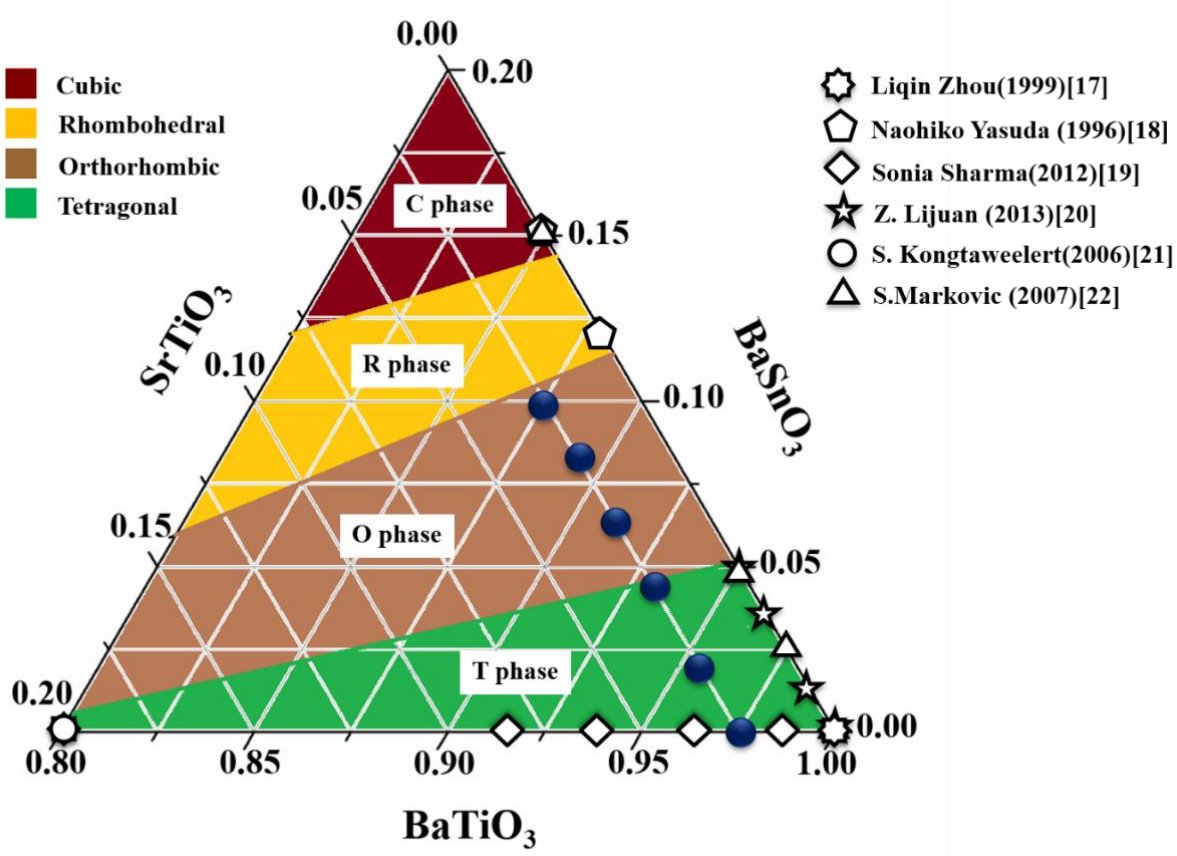

Figure 1.1 Phase diagram and composition studied in ternary BT–ST–*y*BS system

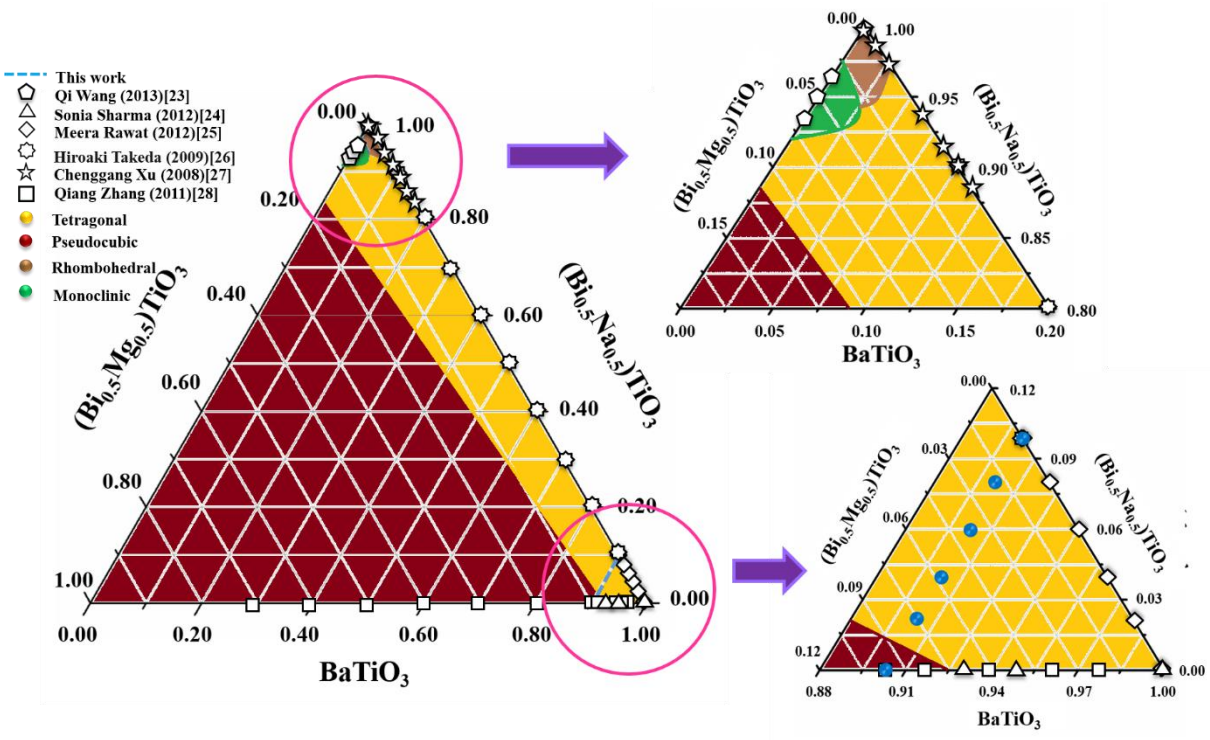

Figure 1.2 Phase diagram and composition studied in ternary BT–BNT–*x*BMT system

1.2 Scope of this work

The goal of this study is to synthesize lead-free piezoelectric ceramics of the barium titanium-based ternary system in two systems. The first system is (0.975-*y*)$BaTiO_3$–0.025$SrTiO_3$–*y*$BaSnO_3$, where *y* = 0.00, 0.02, 0.04, 0.06, 0.08 and 0.10 and the second 0.9$BaTiO_3$–(0.1-*x*)$Bi_{0.5}Na_{0.5}TiO_3$–*x*$Bi(Mg_{0.5}Ti_{0.5})O_3$, where *x* = 0.00, 0.02, 0.04, 0.06, 0.08 and 0.10. These two systems are fabricated via solid state reaction with metal oxide used for starting materials. The effect of cations substitution on crystal structure and phase transition was examined by the X–ray diffraction technique (XRD), dielectric measurement and Raman spectroscopy. The morphology of ceramics was determined using scanning electron microscopy (SEM). Electrical measurements such as dielectric, ferroelectric and piezoelectric properties of ceramics also were investigated.

1.3 Objectives of this work

1.3.1 To prepare $(0.975\text{-}y)BaTiO_3–0.025SrTiO_3–yBaSnO_3$ and $0.9BaTiO_3–(0.1\text{-}x)Bi_{0.5}Na_{0.5}TiO_3–xBi(Mg_{0.5}Ti_{0.5})O_3$ ceramics by the conventional solid state mixed oxide method.

1.3.2 To study effect of the composition on the crystal structure and phase transition as well as electrical properties $(0.975\text{-}y)BaTiO_3–0.025SrTiO_3–yBaSnO_3$ and $0.9BaTiO_3–(0.1\text{-}x)Bi_{0.5}Na_{0.5}TiO_3–xBi(Mg_{0.5}Ti_{0.5})O_3$ ceramics.

1.3.3 To study the crystal structure and phase transition of $(0.975\text{-}y)BaTiO_3 – 0.025SrTiO_3–yBaSnO_3$ and $0.9BaTiO_3–(0.1\text{-}x)Bi_{0.5}Na_{0.5}TiO_3–xBi(Mg_{0.5}Ti_{0.5})O_3$ ceramics by Raman spectra, XRD and dielectric measurement.

1.3.4 To study the morphology and grain size of $0.9BaTiO_3–(0.1\text{-}x)Bi_{0.5}Na_{0.5}TiO_3–xBi(Mg_{0.5}Ti_{0.5})O_3$ ceramics by Scanning electron microscope.

1.3.5 To investigate the dielectric ferroelectric and piezoelectric properties of $(0.975\text{-}y)BaTiO_3–0.025SrTiO_3–yBaSnO_3$ and $0.9BaTiO_3–(0.1\text{-}x)Bi_{0.5}Na_{0.5}TiO_3–xBi(Mg_{0.5}Ti_{0.5})O_3$ ceramics.

1.4 References

[1] Setter, N. E. 2002. “Piezoelectric material in devices”.

[2] Uchino, K. 2000. “Ferroelectric Devices” Marcel Dekker, Inc., New York.

[3] Olaf, A. 1919. “The Volatilization of Lead Oxide from Lead Silicate Melts” **J. Am. Ceram. Soc**. 2(10): 784 – 789.

[4] EU-Directive 2002/96/EC: Waste Electrical and Electronic Equipment (WEEE). Off. J. Eur. Union 2003, 46 (L37), 24.

[5] EU-Directive 2002/95/EC: Restriction of the Use of Certain Hazardous Substances in Electrical and Electronic Equipment (RoHS). Off. J. Eur. Union 2003, 46 (L37), 19.

[6] Regulations Relating to Restrictions on the Manufacture, Import, Export, Sale and Use of Chemicals and Other Products Hazardous to Health and the Environment, Produktforskriften (Product Regulations Norway), 2004.

[7] Jaffe, B., Cook, W.R., and Jaffe, H. 2000. “Piezoelectric Ceramics” Academic, New York.

[8] Rawat, M., and Yadav, KL. 2013. “Structural, dielectric and ferroelectric properties of $Ba_{(1-x)}(Bi_{0.5}Na_{0.5})xTiO_3$ ceramics” **Ceram Int**. 39: 3627-3633.

[9] Yonggang, Y., Chao, Z., Duchao, L., Dong, W., Haijun, W., Yaodong, Y., and Xiaobing, R. 2012. “Large piezoelectricity and dielectric permittivity in BaTiO – xBaSnO$_3$ systems: The role of phase coexisting” **Europhys. Lett**. 98: 27008.

[10] Xusheng, W., Hiroshi, Y., and Chao, N. X. 2005. “Large electrostriction near the solubility limit in $BaTiO_3$ – $CaTiO_3$ ceramics” **Appl Phys Lett**. 86: 022905.

[11] Wei, L., Zhijun, X., Ruiqing, C., Peng, F., and Guozhong Z. 2010. “Piezoelectric and Dielectric Properties of $(Ba_{1-x}Ca_x)(Ti_{0.95}Zr_{0.05})O_3$ Lead-Free Ceramics” **J. Am Ceram. Soc**. 93[10]: 2942 – 2944.

[12] Su-wei, Z., Hailong, Z., Bo-Ping, Z., and Sui, Y. 2010. “Phase-transition behavior and piezoelectric properties of lead-free $(Ba_{0.95}Ca_{0.05})(Ti_{1-x}Zr_x)O_3$ ceramics” **J. Alloys Compd**. 506: 131–135.

[13] Li-Feng, Z., Bo-Ping, Z., Xiao-Kun, Z., Lei, Z., Peng-Fei, Z. and Jing-Feng, L. 2013 “Enhance Piezoelectric Properties of $(Ba_{1-x}Ca_x)(Ti_{0.92}Sn_{0.08})O_3$ Lead-Free Ceramics” **J. Am. Ceram. Soc**. 96 [1]: 241–245.

1.4 References (II)

[14] Li-Feng, Z., Bo-Ping, Z., Xiao-Kun, Z., Lei, Z., and Fang-Zhou, Y. 2013. "Phase transition and high piezoelectricity in (Ba,Ca)($Ti_{1-x}Sn_x$)O_3 lead-free ceramics" **Appl. Phys. Lett**. 103: 072905.

[15] Wadda, S., Yamato, K., Pulpan, P., Kumada, N., Lee, BY., Iijima, T., Moriyoshi, C., and Kuroiwa, Y. 2010. "Preparation of barium titanate–bismuth magnesium titanate ceramics with high Curie temperature and their piezoelectric properties" **J. Ceram Soc Jpn**. 118(8): 683-687.

[16] Wang, Q., Chen, J., Fan, L., Liu, L., Fang, L., and Xing, X. 2013. "Preparation and Electric Properties of $Bi_{0.5}Na_{0.5}TiO_3$–$Bi(Mg_{0.5}Ti_{0.5})O_3$ Lead-Free Piezoceramics" **J. Am. Ceram. Soc**. 96(4): 1171-1175.

[17] Ligin, Z., Vilarinho, P. M., and Baptista, J. L. 1999. "Dependence of the Structural and Dielectric Properties of $Ba_{1-x}Sr_xTiO_3$ Ceramic Solid Solutions on Raw Material Processing" **J. Eur. Ceram. Soc.** 19.

[18] Naohiko, Y., Hidehiro, O., and Shigeto, A. 1996. "Dielectric Properties and Phase Transition of $Ba(Ti_{1-x}Sr_x)O_3$ Solid Solution" **J. Appl. Phys.** 35: 5099-5103.

[19] Sonia, S., Kumar, P., and Palei, P. 2012. "Dielectric and piezoelectric properties of low temperature synthesized iso-valent modified BT ceramics" **Ceram. Int.** 38: 5597-5603.

[20] Zhang, L., Wang, L., Liu, J., Cheng, B., Zhao, M., and Ye, B. 2013. "Dielectric properties and structural defects in ceramics" **J. Phys.: Conf. Ser.** 443 012014.

[21] Kongtaweelert, S., Sinclair, D. C., and Panichphant, S. 2006. "Phase and morphology investigation of $BaSr_{1-x}Ti_xO_3$ (x = 0.6, 0.7 and 0,8) powders" **Curr. Appl. Phys.** 6: 474-477.

[22] Markovic, S., Mitric, M., Cvjeticanin, N., and Uskokovic, D. 2007. "Preparation and properties of $BaTi_{1-x}Sr_xO_3$ multilayered ceramics" **J. Eur. Ceram. Soc.** 27: 505-509.

[23] Qi, W., Jun, C., Longlong, F., Laijun, L., Liang, F., and Xianran, X. 2013. "Preparation and Electric Properties of $Bi_{0.5}Na_{0.5}TiO_3$-$Bi(Mg_{0.5}Ti_{0.5})O_3$ Lead- Free Piezoceramics" **J. Am. Ceram. Soc.** 96(4): 1171-1175.

[24] Meera, R., and Yadav, K.L. 2013. "Structural, dielectric and ferroelectric Properties of $Ba_{1-x}(Bi_{0.5}Na_{0.5})TiO_3$ ceramics" **Ceram. Int.** 39: 3627-3633.

1.4 References (III)

[25] Hiroaki, T., Takeshi, S., Yoshiaki, K., and Tadashi, S. 2009. "Fabrication and operation limit of lead-free PTCR ceramics using $BaTiO_3$-$(Bi_{1/2}Na_{1/2})TiO_3$ system" **J. Electroceram.** 22: 263-269.

[26] Chenggang, X., Dunmin L., and Kwok K.W. 2008. "Structure, electrical properties and depolarization temperature of $(Bi_{0.5}Na_{0.5})TiO_3$-$BaTiO_3$ lead-free piezoelectric ceramic" **Solid State Sci.** 10(7): 934-940.

[27] Qiang, Z., Zhenrong, L., Fei, L., and Zhuo, X. 2011. "Structural and Dielectric Properties of $Bi(Mg_{1/2}Ti_{1/2})O_3$-$BaTiO_3$ Lead-Free Ceramics" **J. Am. Ceram. Soc.** 94(12): 4335-4339.

CHAPTER 2

LITERATURE REVIEW

2.1 Piezoelectricity

The first phenomenon of piezoelectric effect was discovered in 1880 by French physicists Pierre and Jacques Curie in quartz [1]. *Piezo* word is press or squeeze in Greek and electric word is relate to electric charge or electrical energy. Two different of piezoelectricity are direct and indirect effect, which this materials must have switching of both effect. The direct effect or direct piezoelectric effect is the generation of electricity when compression or stress is applied into piezoelectric material as shown in Figure 2.1 (a). The direct effect is used in sensor applications such as gas igniters, accelerometer and microphones, as shown in figure 2.2. Conversely, for indirect effect or converse piezoelectric effect is distortion in the crystal when an electric field is applied (see in Figure 2.1 (b)). These indirect effect is a have been applied in actuator device include liquid inkjet printers, common rail diesel injection, dual – stage actuator in HDDs, and camera shutter, as shown in figure 2.2.

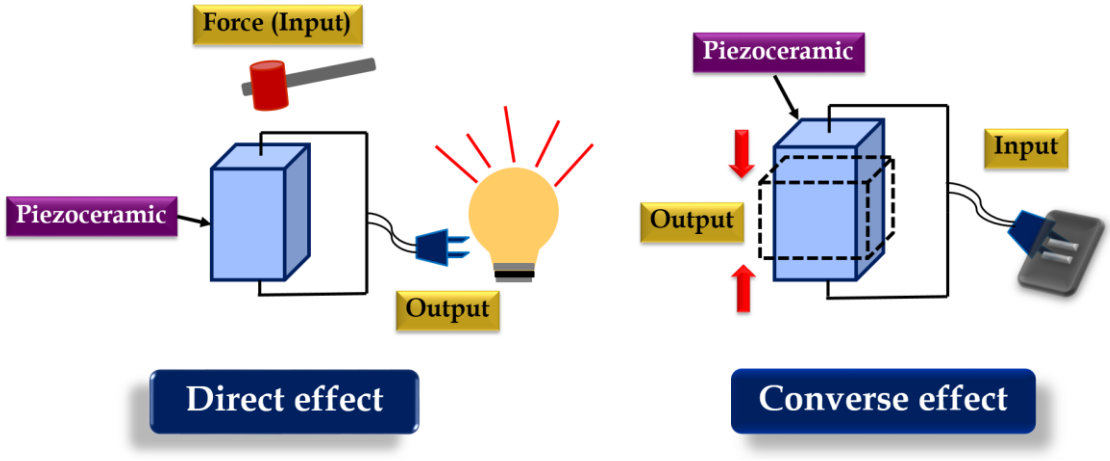

Figure 2.1 Direct (a) and indirect (b) effect of piezoelectricity (Modified from [4])

Common rail diesel injection

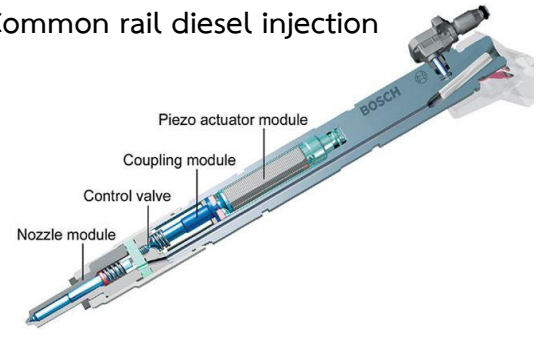

Dual – stage actuator in HDDs

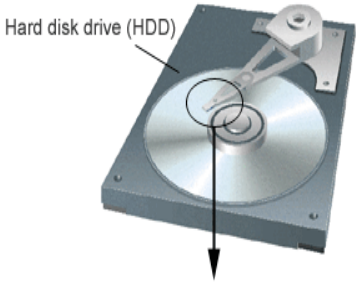

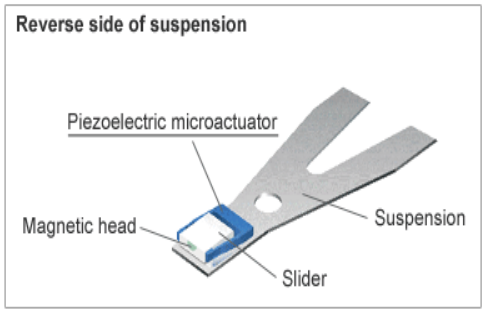

Accelerometer

Gas igniters

Camera shutter

Liquid inkjet printers

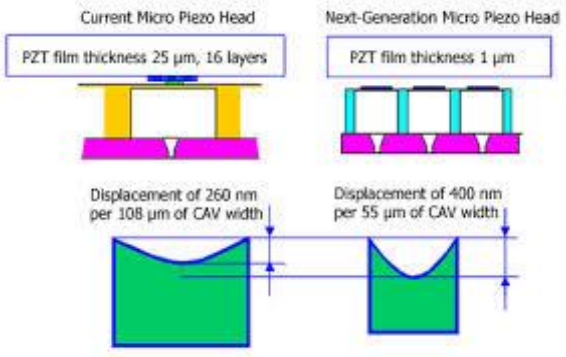

Figure 2.2 Piezoelectric applications [2, 3]

Piezoelectricity is the coupling between electrical and mechanical displacements in a material. The direct and converse piezoelectric effect can be described by basic equations 2.1 and 2.2 respectively [4]

Direct effect:

$$D = d_1 T + \varepsilon^T E \tag{2.1}$$

where *D* is dielectric displacement, *T* is the mechanical stress, ε^T is the permittivity at constant stress, *E* is the electric field and d_1 is piezoelectric charge coefficients direct piezoelectric effect.

Converse effect:

$$S = s^E T + d_2 E \tag{2.2}$$

where *S* is mechanical strain, s^E is mechanical compliance, *T* is mechanical stress, *E* is the electric field and d_2 is piezoelectric charge coefficients for converse piezoelectric effect.

Furthermore, the piezoelectric ceramics demonstrate an anisotropic effect. The direction of the induced polarization depends on the direction of the applied electric field or the mechanical force with piezoelectric materials. However, the direction of polarization is conventionally taken as the 3 axis by the Z – axis of a rectangular system. Direction X, Y, or Z is represented by the subscript 1, 2, or 3, respectively, and shear stains about one of these axes is represented by the subscript 4, 5 or 6, respectively [5], as shown in Figure 2.3. Therefore, *d* is a tensor and many other physical properties of piezoelectric materials have two subscripts that indicate the directions of two related quantities. For example, piezoelectric constant d_{33} is measure when the induced polarization is generated in direction 3 due to a stress applied in direction 3 and d_{31} represents the induced polarization in direction 3 per unit stress applied along direction 1 [4]. High piezoelectric constants are desirable in order to increase the charge or strain developed per force or electric field applied.

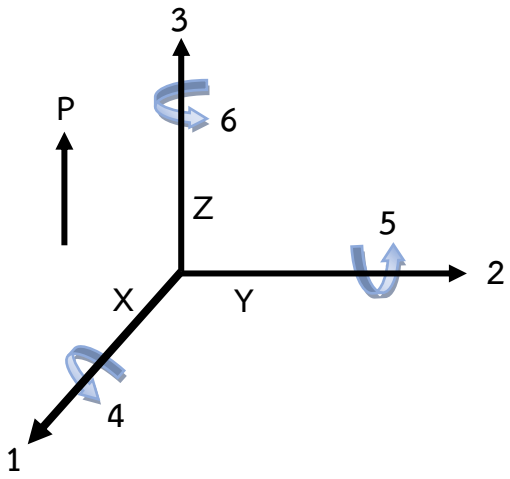

Figure 2.3 Directional axes (Modified from [5])

Another important parameter used to describe piezoelectric efficacy is the electromechanical coupling factor (*k*). The k factor represents the ability of a piezoceramic material from electrical to mechanical form or vice versa and it depends on degree of poling for ceramics [5].

$$k = \sqrt{\frac{\text{input mechanical energy converted into electrical energy}}{\text{input mechanical energy}}} \tag{2.3}$$

$$k = \sqrt{\frac{\text{input electrical energy converted into mechanical energy}}{\text{input electrical energy}}} \tag{2.4}$$

The subscripts denote the relative directions of electrical and mechanical quantities and the kind of motion involved such as k_{33}, k_{31}. For a thin piezoelectric ceramic disc is the planar coupling factor (k_p).

The crystals can be divided into these 32 symmetry point groups. Out of these 32 point groups, 21 are noncentrosymmetric with one or more crystallographically unique directional axes and 11 are centrosymmetric (Non-piezoelectric), meaning the centre of positive and negative charge coincides with each other. Out of these 21 point groups, 20 belongs to the class of piezoelectric. Out of these 20 point groups, 10 are pyroelectrics. The ferroelectrics are a subgroup of pyroelectrics [6], as shown in figure 2.4.

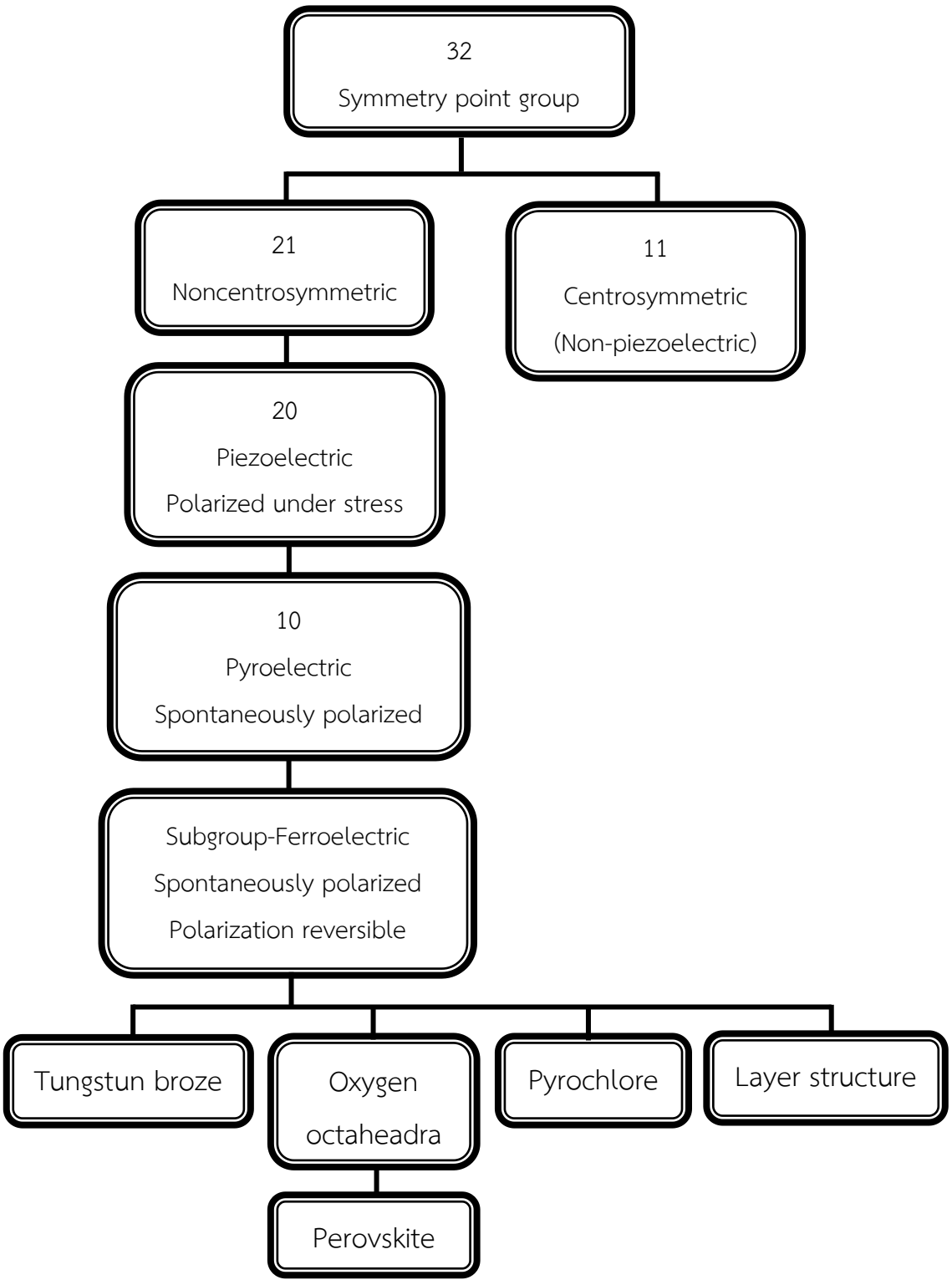

Figure 2.4 Relationship of piezoelectricity and its subdivisions with symmetry groups [6]

2.2 Ferroelectricity

2.2.1 Ferroelectrics

A subgroup ferroelectric are pyroelectric and the sub set of pyroelectric are piezoelecric. Thus relationship between ferroelectrics and piezoelectrics is exhibited in the Venn diagram in figure 2.5. In the year 1921, ferroelectricity was first discovered in Rochelle salt (sodium potassium tartarate tetrahydrate; $NaKC_4H_4O_6.4H_2O$) by Joseph Valasek [7]. Ferroelectrics are materials which possess a spontaneous electric polarization (P_s) in the absence of an electric field and this polarization can be reversed by applying a suitable electric field (E) [8]. An important feature of ferroelectric materials are hysteresis loop (abbreviated as P – E loop), which displays relationship between the polarization (P) and applied electric field (E).

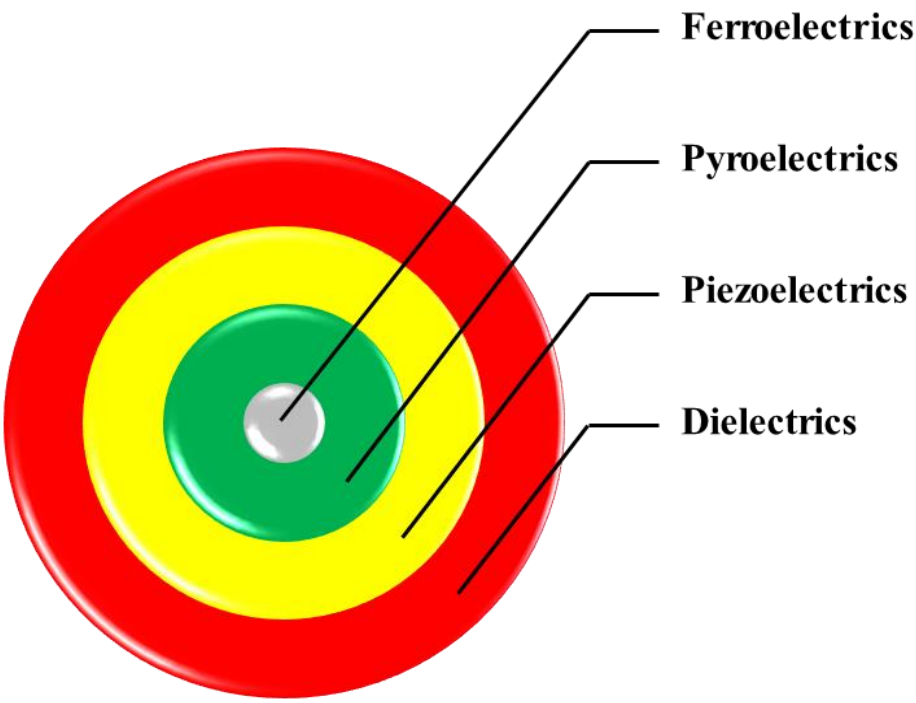

Figure 2.5 Venn diagram showing of dielectric materials [7]

The P – E hysteresis loop occur from the energy needed to switch the domain and polarization in the direction of the external field. As shown in figure 2.6, when an electric field is applied to a crystal with randomly oriented dipoles (or domains), they begin to line up with the field from points O to B, until the saturation polarization (P_s) is reached at points C, and all of the dipoles are aligned. When the field is

removed, there is some remanent polarization (P_r) at point D due to coupling between all of the dipoles, and the material is permanently polarized. When the electric field is applied in the opposite direction, the dipoles are reversed. A coercive field (E_c) must be applied in order to remove the remanent polarization (point F), and create a random dipole orientation. As the reversed field is further increased, saturation occurs with the opposite polarization at point G. As the field continues to alteate, a hysteresis loop is formed. The area inside the loop is a function of the energy required to switch the direction of the polarization 180° [9].

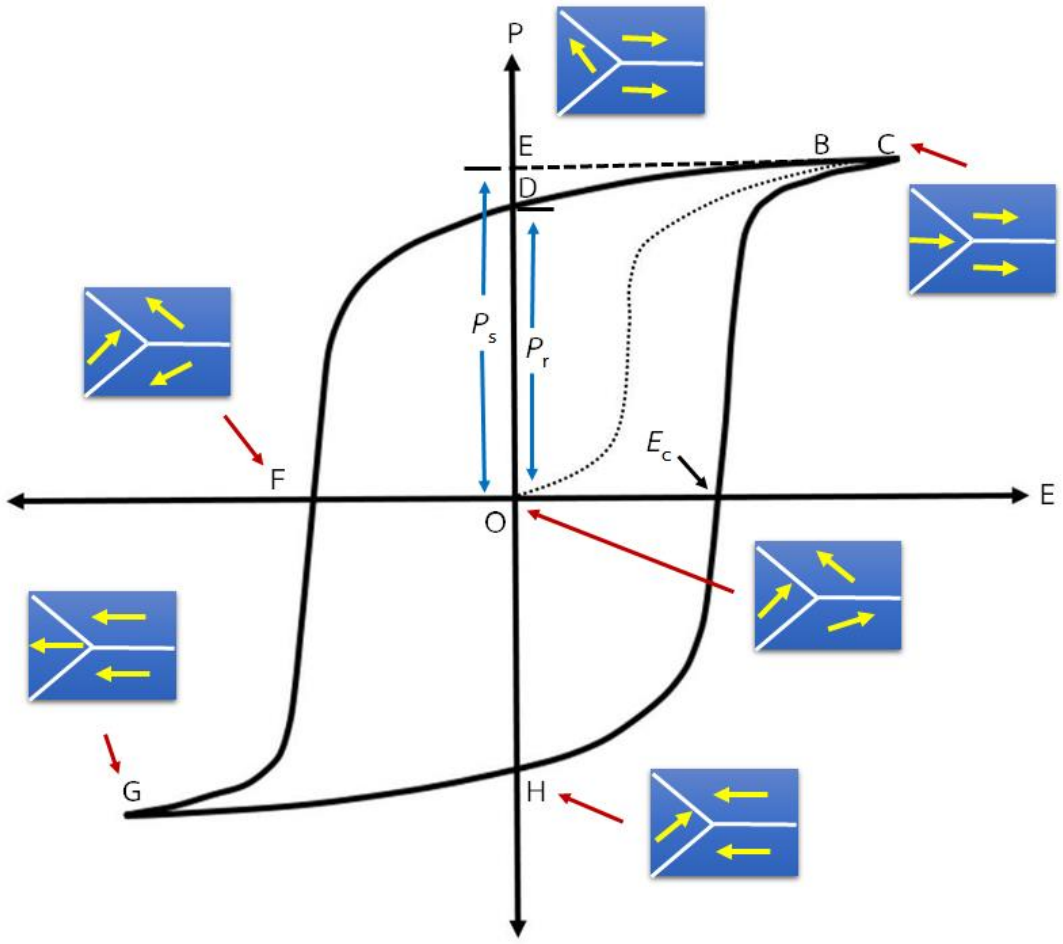

Figure 2.6 A typical ferroelectric hysteresis loop ((P – E) hysteresis loop) [10]

For ferroelectric materials, another important characteristic is the temperature of structural phase transition from the paraelectric phase to the ferroelectric phase which is called Curie temperature (T_c). The temperature is above T_c the crystal does

not exhibit ferroelectricity. On the other hand, when the temperature falls below T_c, the crystal exhibits ferroelectricity. According to the Curie – Weiss law equation [10];

$$\frac{1}{\varepsilon} = \frac{(T - T_0)}{C} \tag{2.5}$$

Where, C is the Curie – Weiss constant, T is the temperature, T_0 is the Curie – Weiss temperature which is formula constant obtained by extrapolation and is less than T_c. While T_c is actual temperature when crystal structure changes.

2.2.2 Relaxor ferroelectrics

Relaxor ferroelectrics or relaxors are a class of ferroelectric materials that were first discovered in the 1950's by Smolenskii *et al*. [11]. The Relaxor ferroelectrics can be categorized into two structural families: the first is complex perovskites and the last is tungsten bronze system. For some examples of common relaxor ferroelectrics are $Pb(Mg_{1/3}Nb_{2/3})O_3$, $(Pb_{1-3x/2}La_x)(Zr_yTi_{1-y})O_3$, $Pb_{1-x}Ba_xNb_2O_6$, and $Pb(Zn_{1/3}Nb_{2/3})O_3$. These materials have high piezoelectric, dielectric, pyroelectric and electro-optic properties. Therefore, application of relaxor ferroelectric have been widely used in industry such as high permittivity capacitors, phase conjugate mirrors, piezoelectric sensors and actuators [12]. The hysteresis loop of relaxor this zero field polarization is significantly smaller owing to the fact that the the nanodomains being randomly distributed. Three qualitative features of the dielectric response of relaxors can be summarized as follows [13, 14]: the first, the peak at phase transition are characterized rounded and broad peaks in the temperature dependence of the dielectric permittivity. Secondly, the relaxors exhibit frequency dependent maximum dielectric permittivity, when the temperature of maximum relative permittivity (T_m) increasing and maximum relative permittivity (ε_{max}) decreasing with increasing frequency and the last, the temperature of maximum relative permittivity is called T_m.

In order to further characterize the relaxor behavior, a modified Curie – Weiss law (is called quadratic Curie – Weiss) was used for description a broad relative permittivity and diffuseness of phase transition [15].

$$\frac{\varepsilon_{\max}}{\varepsilon} = 1 + \frac{(T - T_m)^{\gamma}}{\delta_{\gamma}^2} \tag{2.6}$$

Where, $\varepsilon_{\max}$ is the maximum value of relative permittivity and T_m is the temperature of dielectric maximum. The γ value expresses the degree of dielectric relaxation in relaxor ferroelectric material which this value is in the range of $1 \leq \gamma \leq 2$. When γ value is equal 1, becomes the classic Curie Weiss law valid in the case of normal ferroelectric. The value of δ_{γ} represents the degree of diffuseness for transition peaks. Both δ_{γ} and γ were determined from the slope and intercept of $\ln(\frac{1}{\varepsilon} - \frac{1}{\varepsilon_m})$ versus $\ln(T - T_m)$.

2.3 Perovskite structure

Perovskites is an important class of piezoelectric materials. Perovskite is orginally the name of the mineral calcium titanate ($CaTiO_3$) [16]. An idea perovskite structure can be described as a simple cubic unit cell with a closed-packed face center cubic (FCC) structure. The perovskite structure is written as ABO_3, where A illustrate a cation with a larger ionic radius on the comers, and B show a cation with a smaller ionic radius in the body center or octahedral interstitial site and O is oxygen in the center of the faces [17], as shown in Figure 2.7. The A site is in 12–fold coordination, the B site is in 6–fold coordination, and the O site is 6–fold coordinated anions. There are many complex perovskites which can be describe with the formula $(A', A'')^{XII}(B', B'')^{VI}O_3$ where XII and VI represent coordination number. In KNN, K^+ or Na^+ ions are situated at the corner of the unit cell (A – site), Nb^{5+} at body center positions (B – site).

Ideal perovskite structure is simple cubic lattice. The simple geometrical relationship between cations and anions which can be used to describe the stability of the perovskite structure proposed by Goldschmidt in early 1920 [19]. The stability of the perovskite structure is the tolerance factor which can be expressed as following equation [1]:

$$t = \frac{(R_A + R_O)}{\sqrt{2}(R_B + R_O)} \tag{2.7}$$

where t is tolerance factor. R_A R_B and R_o are the ionic radius of the large cation occupying the A – site, small cation occupying the B – site, and anion (oxygen) respectively. For ideal cubic symmetry, the tolerance factor is equal to 1. The stable perovskite structure, tolerance factor should be in the between range $0.88 < t < 1.09$. In general, the perovskite with $t > 1$ has tetragonal symmetry and the perovskite with $t < 1$ has rhombohedral or monoclinic symmetry [20].

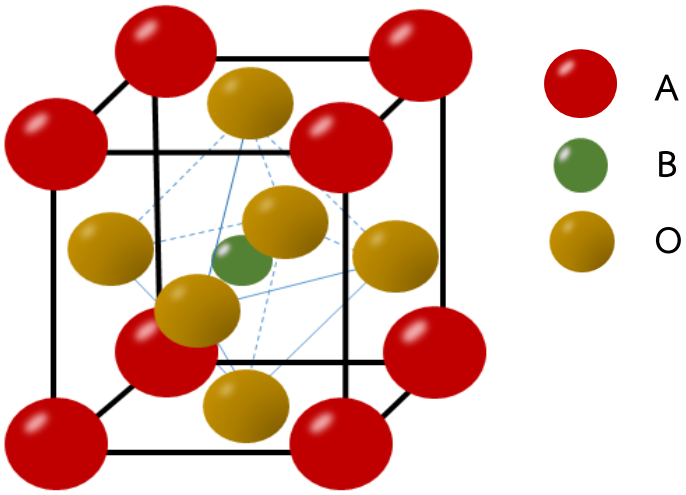

Figure 2.7 ABO_3 perovskite type unit cell (Modified from [18])

2.4 Lead–based piezoelectric materials

The commercially most important piezoelectric material lead zirconate titanate ($PbZr_{1-x}Ti_xO_3$; PZT) was developed since in 1950's [21].Lead zirconate titanate is solid solution of lead zirconate ($PbZrO_3$) and lead titanate ($PbTiO_3$) which it is a perfect sample of polycrystalline ceramics. Currently, the lead zirconate titanate is the most widely used piezoelectric material for numerous electronic devices utilizing actuators, sensors and transducers [22]. Above the Curie temperature (T_c), lead zirconate titanate obtains the cubic perovskite structure where the A – site is Pb^{2+}(Large cation) on the comers, B – site are Zr^{4+} and Ti^{4+} in the body center and O is oxygen in the face centers [23], as shown in figure 2.8.

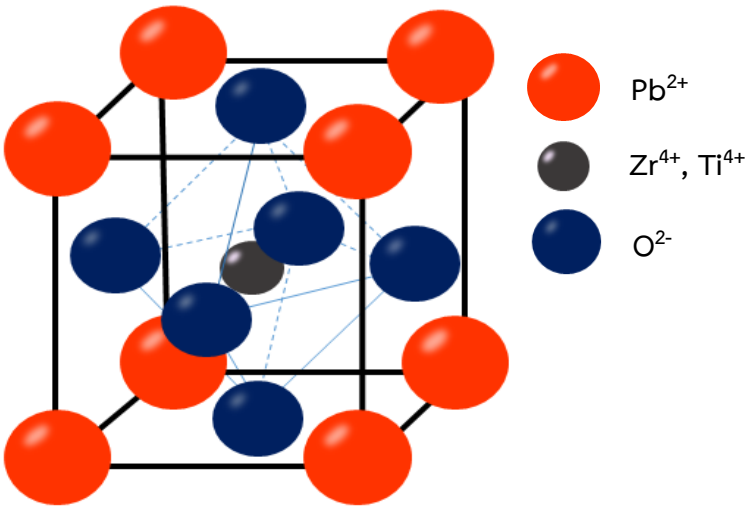

Figure 2.8 Perovskite structure of lead zirconate titanate (Modified from [24])

The form of the crystalline structure exhibited by lead zirconate titanate is dependent on the percentage concentration of metal oxides. The phase diagram of the lead zirconate titanate system as a function of temperature and chemical composition is shown in figure 2.9. The morphotropic phase boundary (MPB) defines the composition at which there is an abrupt structure change, the composition being almost independent of temperature. Moreover, the nearly vertical line separates the ferroelectric phase region of tetragonal phase on the Ti rich side (F_T) and rhombohedral phase on the Zr rich side (F_R). The T_c line is the boundary between the cubic paraelectric phase (P_c) and the ferroelectric phase (F). For below T_c line, the substitution of Zr^{4+} for Ti^{4+} in $PbTiO_3$ changes the rhombohedral distortion in favour of the tetragonal symmetry in the PZT perovskite structure. The nearly vertical morphotropic phase boundary (MPB) at 52:48 for Zr/Ti cation ratio, had coexistence phase of a tetragonal and rhombohedral phase. This compositions in the morphotropic phase boundary region are commercially interesting because they have shown high dielectric permittivity and piezoelectric electromechanical coupling factors, as shown in figure 2.10 [26]. The enhanced dielectric and piezoelectric properties of the commercial composition is generally associated with a large ionic displacement upon field application due to the rotation of the polar axis. Furthermore, other system of lead base systems exhibit excellent piezoelectric and

dielectric properties such as $Pb(Mg_{1/3}Nb_{2/3})O_3$-$PbTiO_3$ [27], $Pb(Zn_{1/3}Nb_{2/3})O_3$-$PbTiO_3$ [28, 29] and $Pb(Zr_{1/2}Ti_{1/2})O_3$ – $Pb(Zn_{1/3}Nb_{1/3})O_3$ [30].

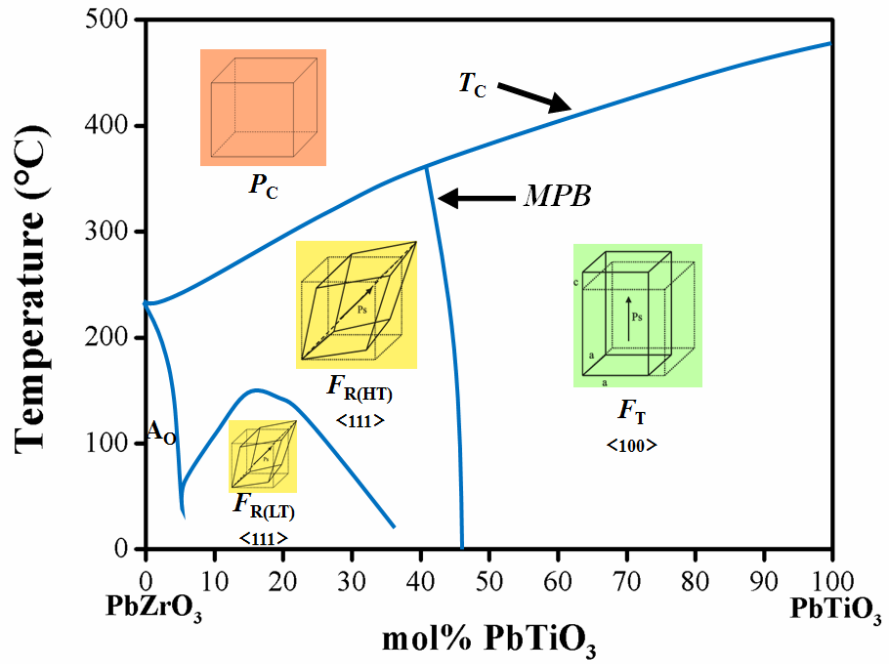

Figure 2.9 Lead zirconate titanate phase diagram (Modified from [25])

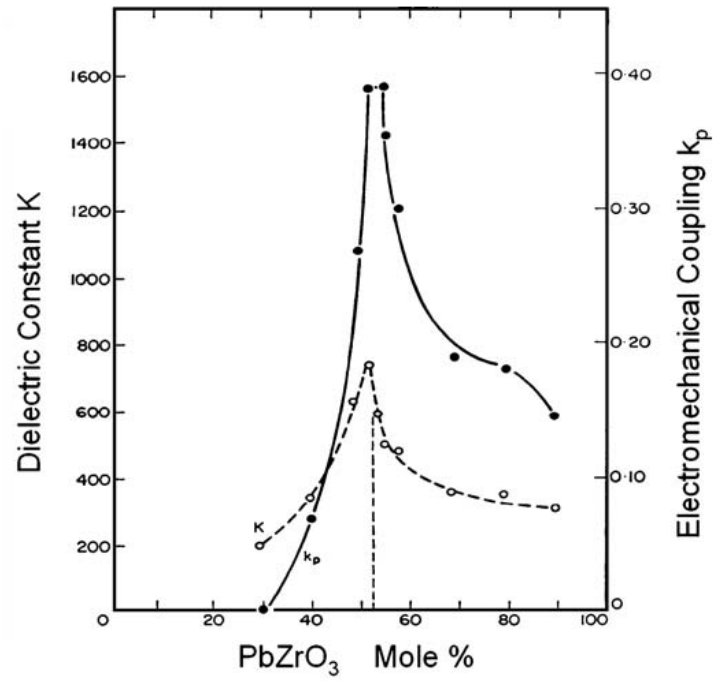

Figure 2.10 Enhanced dielectric and piezoelectric properties in lead zirconate titanate [26]

However, the lead base materials contain lead which it is not environmental friendly and dangerous to human because toxicity of lead oxide in volatile during processing. Therefore, legislation of European Union such as Waste from Electrical and Electronic Equipment (WEEE) and Restriction of Hazardous Substances (RoHS) directives and End-of Life Vehicles (ELV) restrict the use of six hazardous substances including lead in electronic equipment. To prevent generation of new waste, and re-use or recycle electrical waste and electronic equipment [31, 32, 33]. Therefore, lead free friendly piezoelectric ceramics have been received considerable attentions to replace lead-based piezoelectric materials.

2.5 Lead–free piezoelectric materials

Current research is mostly focus on lead free piezoelectric materials Among the lead free materials, Potassium sodium niobate with the chemical formula (K, Na)NbO_3 (abbreviated as KNN), is a solid solution of ferroelectric $KNbO_3$ and the antiferroelectric $NaNbO_3$. The phase diagram of $KNbO_3$–$NaNbO_3$ is exhibited in Figure 2.11. The MPB at near the 50-50 ratio of $KNbO_3$–NaNbO3 separates two tetragonal phases at high temperatures and two orthorhombic phases at room temperature, with different tilting of the oxygen octahedral [5, 34]. Moreover, $(K_{0.5}Na_{0.5})NbO_3$, is a good candidate because it has a fairly high Curie temperature (T_c) about 420°C, which is high temperature application. Nevertheless, it's difficult to obtain fully dense $(K_{0.5}Na_{0.5})NbO_3$ ceramics by ordinary sintering.

In addition to, the bismuth–based perovskite lead-free materials is bismuth potassium titanate, $(Bi_{0.5}K_{0.5})TiO_3$ (abbreviated as BKT) and bismuth sodium titanate $(Bi_{0.5}Na_{0.5})TiO_3$ (abbreviated as BNT). The $(Bi_{0.5}K_{0.5})TiO_3$ is a typical ferroelectric material with tetragonal structure at room temperature and has a higher Curie temperature about 380°C [35]. In 1961, Smolenskii et al. discovered $(Bi_{0.5}Na_{0.5})TiO_3$ [36]. At room temperature, it shows large remnant polarization (P_r) 38 μC/cm2 and coercive field (E_c) 73 kV/cm. $(Bi_{0.5}Na_{0.5})TiO_3$ has rhombohedral structure at room temperature with a high Curie temperature about 320°C [37]. However the piezoelectric properties are not good enough due to its large coercive field and relatively high conductivity, thus pure BNT is hard to pole. Some electrical properties of pure $(Bi_{0.5}K_{0.5})TiO_3$ [38] and $(Bi_{0.5}Na_{0.5})TiO_3$ [5] is shown in table 2.1

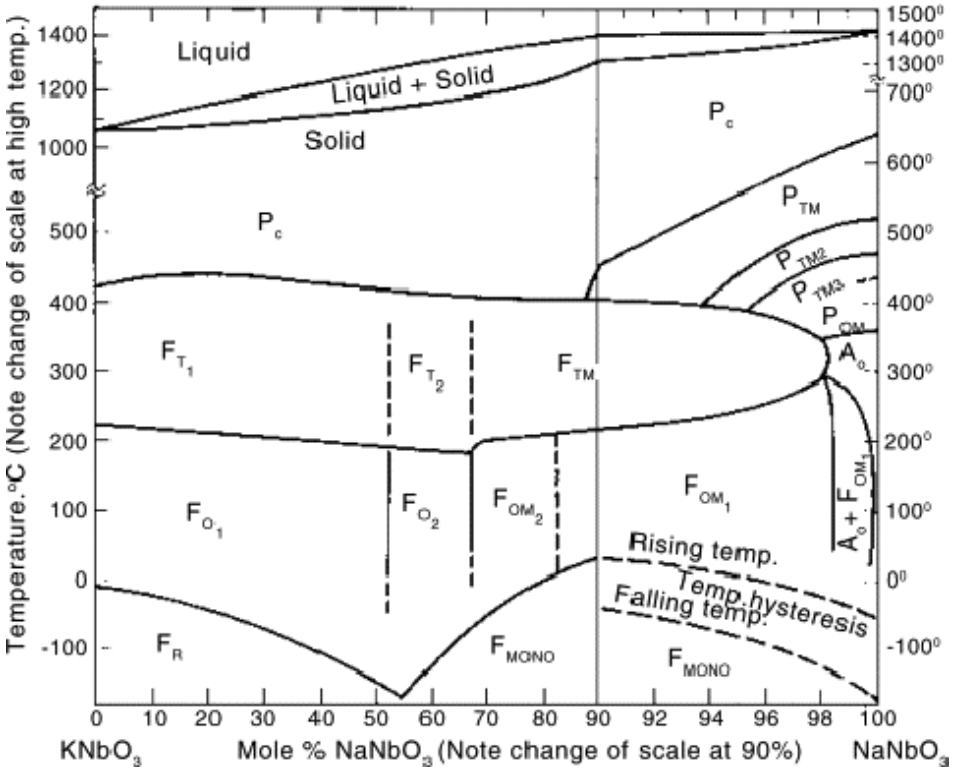

Figure 2.11 Phase diagram of $KNbO_3$–$NaNbO_3$ [5]

Table 2.1 Some electrical properties of pure $(Bi_{0.5}K_{0.5})TiO_3$ and $(Bi_{0.5}Na_{0.5})TiO_3$

	ε_r	$\tan\delta$	k_{33}	d_{33} (pC/N)	P_r (μC/cm2)	E_c (MV/m)
$(Bi_{0.5}K_{0.5})TiO_3$	300	1.1	0.4	70.0	38.0	7.30
$(Bi_{0.5}Na_{0.5})TiO_3$	517	7.1	0.28	69.8	22.2	5.25

Therefore, this thesis work focuses on developing ferroelectric and piezoelectric material that are lead free materials of barium titanate base

2.5.1 Barium titanate ($BaTiO_3$, BT)

In 1945, Wol and Goldman discovered $BaTiO_3$ with the chemical formula $BaTiO_3$ (abbreviated as BT) [39]. $BaTiO_3$ was the first ferroelectric material and later on the first piezoelectric ceramic. It is widely used a dielectric material for ceramic capacitors, and as a piezoelectric material for microphones and other transducers [4].

Furthermore, It possesses the perovskite crystallographic structure where the A – site is Ba^{2+} on the comers, B – site is Ti^{4+} in the body center and O is O^{2-} in the face centers. These four crystal structures of $BaTiO_3$ are rhombohedral, orthorhombic, tetragonal and cubic. $BaTiO_3$ has various phase transition as a function of the temperature. At the Curie temperature about 130°C change from tetragonal (ferroelectric) to cubic (paraelectric) phase. Above 130°C, it has a cubic structure which it is centro – symmetric and possesses no spontaneous dipole. As the low Curie temperature, the structure is slightly distorted to the tetragonal phase with a dipole moment with the [001] direction. The phase transition at temperature -80°C change from rhombohedral to orthorhombic phase, whereas a transition from orthorhombic to tetragonal phase occur temperature near 0°C. The phase transition of $BaTiO_3$ is illustrated in figure 2.12 [1]. Moreover, the phase transition of $BaTiO_3$ are corresponded to change in values of the lattice parameter, Relative permittivity and spontaneous polarization, as shown in figure 2.13 [1], 2.14 [40] and 2.15 [1] respectively.

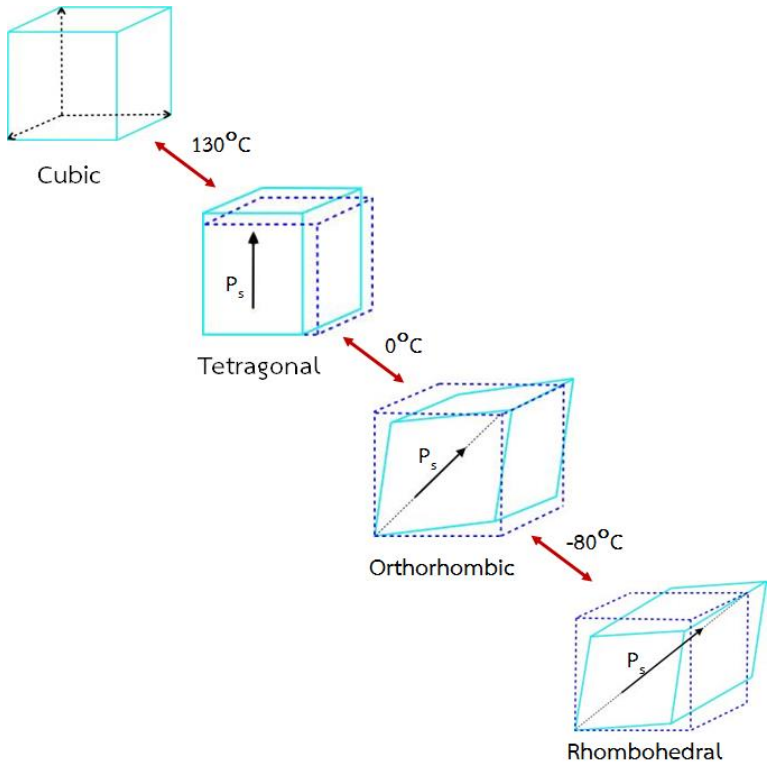

Figure 2.12 Unit cell distortions of $BaTiO_3$ structure [1]

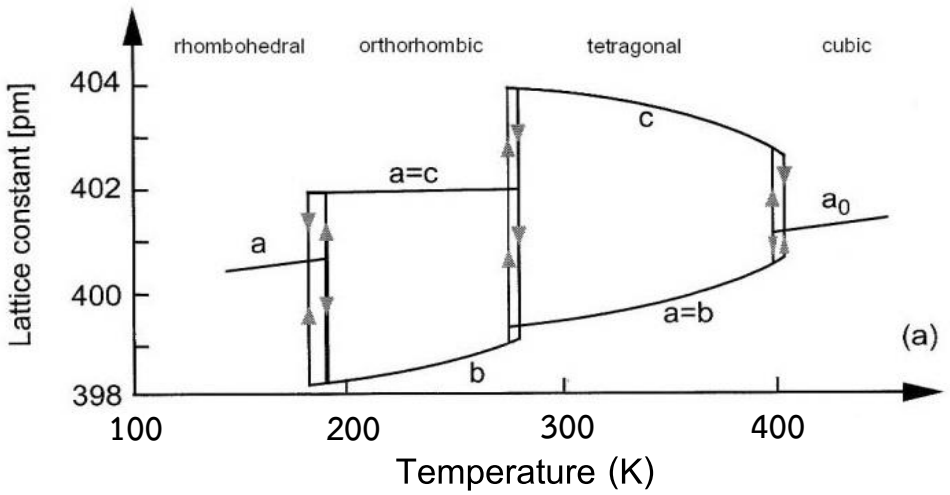

Figure 2.13 Lattice parameters versus temperature [1]

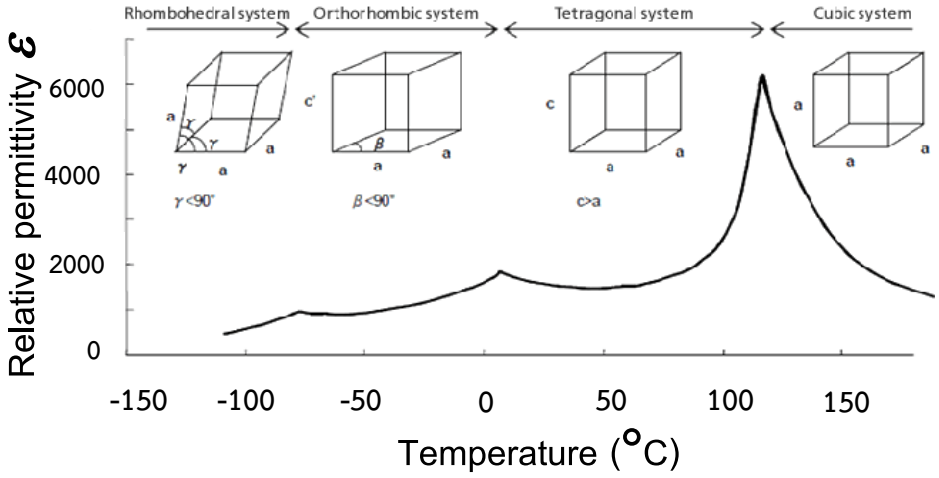

Figure 2.14 Relative permittivity versus temperature [40]

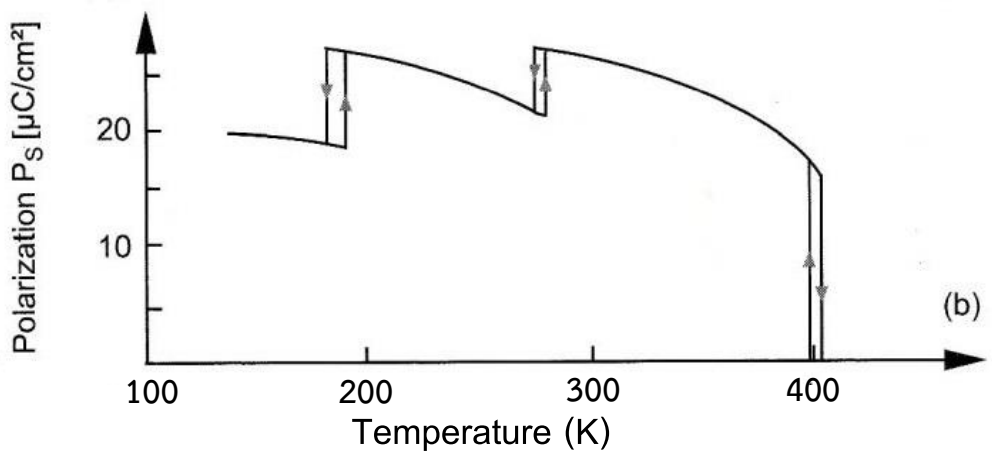

Figure 2.15 Spontaneous polarization versus temperature [1]

The electrical properties of $BaTiO_3$ ceramics such as dielectric ferroelectric and piezoelectric properties is shown in Table 2.2 [41]. It is seen that $BaTiO_3$ has good ferroelectric and piezoelectric properties. Nevertheless, the comparison electrical properties of pure $BaTiO_3$ and PZT material is also quite evident that electrical properties of PZT material is higher than pure $BaTiO_3$ material, as show in figure 2.16 and 2.17 [41].

Table 2.2 Some parameter of electrical properties for Barium titanate ceramics [41]

Electrical parameter	Value
Curie Temperature, T_C (°C)	130
Relative permittivity, ε_r (at 1 kHz)	1700
Dielectric loss, $\tan\delta$ (at 1 kHz)	0.01
Remnant polarization, P_r ($\mu C/cm^2$)	13.3
Piezoelectric d_{33} coefficient (pC/N)	190
Piezoelectric d_{31} coefficient (pC/N)	-78
Electromechanical coupling coefficient, k_{33}	0.49

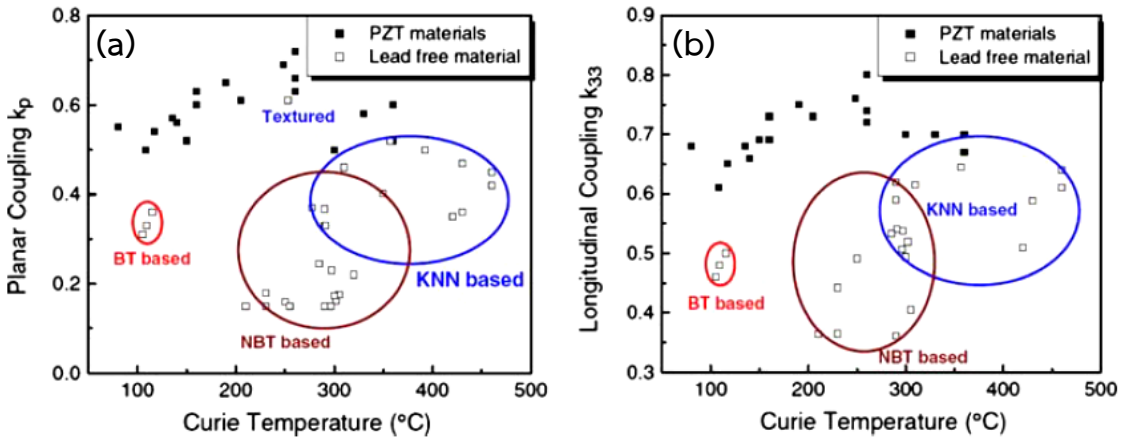

Figure 2.16 (a) Planar Coupling; k_p and (b) Longitudinal Coupling; k_{33} versus Curie temperature [41]

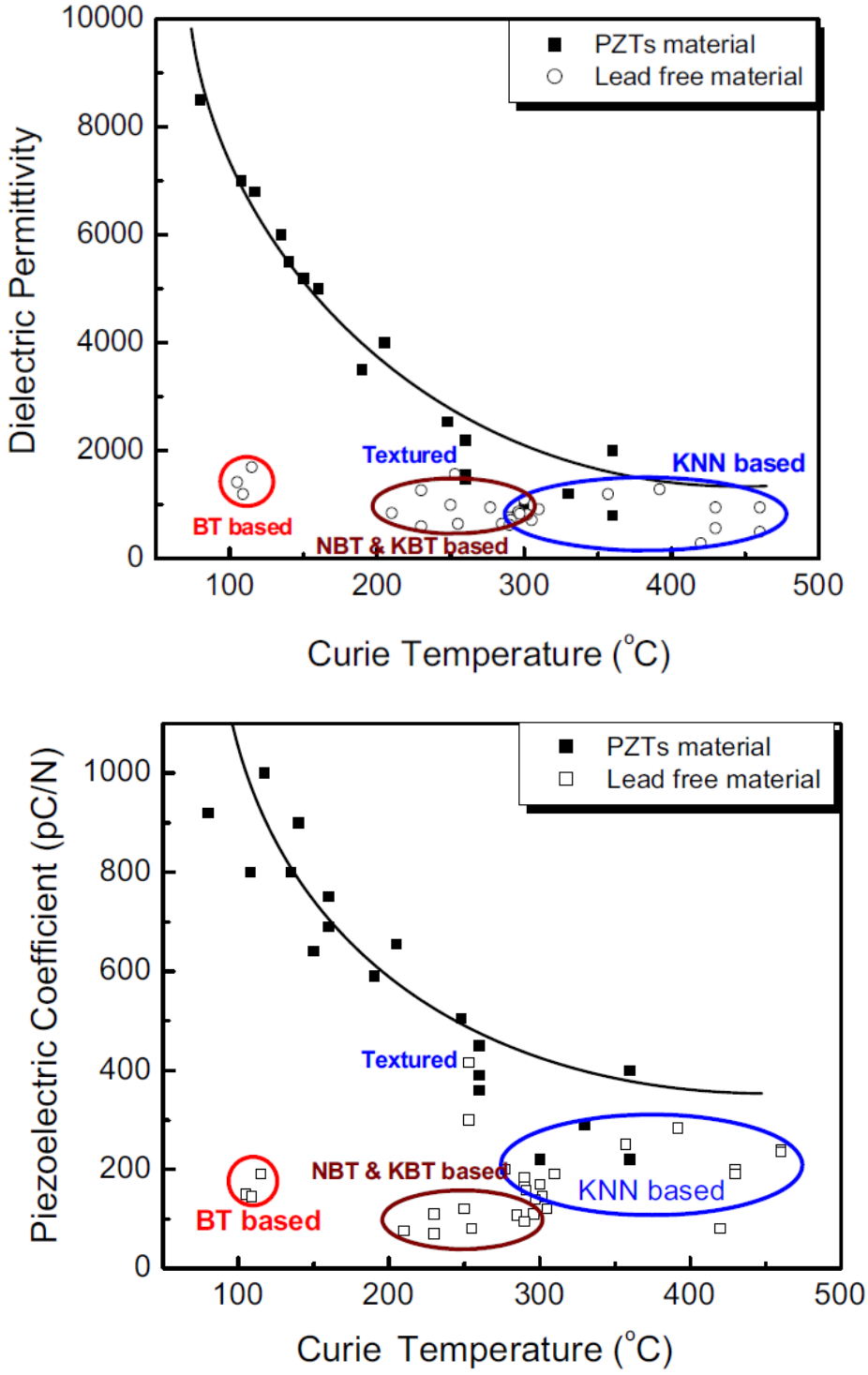

Figure 2.17 Dielectric permittivity and Piezoelectric Coefficient versus Curie temperature [41]

Therefore, the attention is improve electrical properties of $BaTiO_3$ material with comparable to electrical properties of PZT material. Many paper of BT-base have been modified by doping with either A or/and B site substitutions. In addition to, research is focus on morphotropic phase boundary (MPB) or polymorphic phase transition (PPT) due to it excellent electrical properties.

2.5.1.1 Binary system of $BaTiO_3$ material

In a few decades, Guo *et al.* studied $BaTiO_3$–$K_{1/2}Na_{1/2}NbO_3$ ceramics. They found that the phase transition at x = 0.02 and 0.06 of $BaTiO_3$ changed tetragonal to cubic symmetry and orthorhombic to tetragonal symmetry, respectively. For composition x = 0.02 exhibited enhanced piezoelectric and ferroelectric properties including $P_r \sim$ 7.5 μC/cm^2, $E_C \sim$ 12 kV/cm, $d_{33} \sim$ 104 pC/N, $k_p \sim$ 0.29 and $T_C \sim$ 358°C [42].

Meanwhile many researchers studied the binary system of $BaTiO_3$– $Bi_{0.5}Na_{0.5}TiO_3$ [43, 44]. Takenaka *et al.* studied $BaTiO_3$–$Bi_{0.5}Na_{0.5}TiO_3$ system. Researchers found a morphotrobic phase boundary between rhombohedral and tetragonal phases at 6 mol% of BT as illustrated in figure 2.18. These MPB had excellent electrical properties such as $T_C \sim$ 288°C, $\varepsilon_{33}^T/\varepsilon_0 \sim$ 580, $tan\delta \sim$ 1.3%, $d_{33} \sim$ 125 pC/N, and $k_{33} \sim$ 55.0% [43]. In 2013 Rawat *et al*. studied $BaTiO_3$–$Bi_{0.5}Na_{0.5}TiO_3$ system. They reported that the P_r and E_c increasing with increasing BNT content and the $T_C \sim$ 155°C at 10 mol% of BNT addition [45]. Furthermore, Wada *et al*. studied lead free $BaTiO_3$ and $Bi(Mg_{0.5}Ti_{0.5})O_3$ (BT–BMT) ceramic. They found that the highest $T_C \sim$ 360°C at 0.05 mol% of BMT [46].

In 2005 Xusheng *et al*. prepared (1-x)$BaTiO_3$–$xCaTiO_3$ system via conventional solid-state reaction. They reported that the composition x = 0.23 exhibited high electrostriction strain ~ 0.22% due to it had two of tetragonal $Ba_{0.8}Ca_{0.2}TiO_3$ and orthorhombic $Ba_{0.07}Ca_{0.93}TiO_3$ solid solution [47]. After that, Dong *et al.* studied (1-x) $BaTiO_3$–$xBaZrO_3$ ceramic. They found that the diffused phase transition behavior was enhanced with increasing BZ content. At composition x = 0.06 had high piezoelectric and dielectric properties (d_{33} = 420 pC/N, d_{31} = -138 pC/N, k_p = 0.49 and ε_r = 2500) [48]. At the same time, Yonggang *et al.* studied the effect of $BaSnO_3$ observed large piezoelectricity and dielectric permittivity in $BaTiO_3$–$xBaSnO_3$ systems. They found that four phase coexistence of Cubic–Tetragonal–Orthorhombic–Rhombohedral

phase at x = 0.11, exhibited large piezoelectricity and dielectric permittivity (ε_r ~ 75,000 and d_{33} ~ 697 pC/N), as shown in figure 2.19 [49].

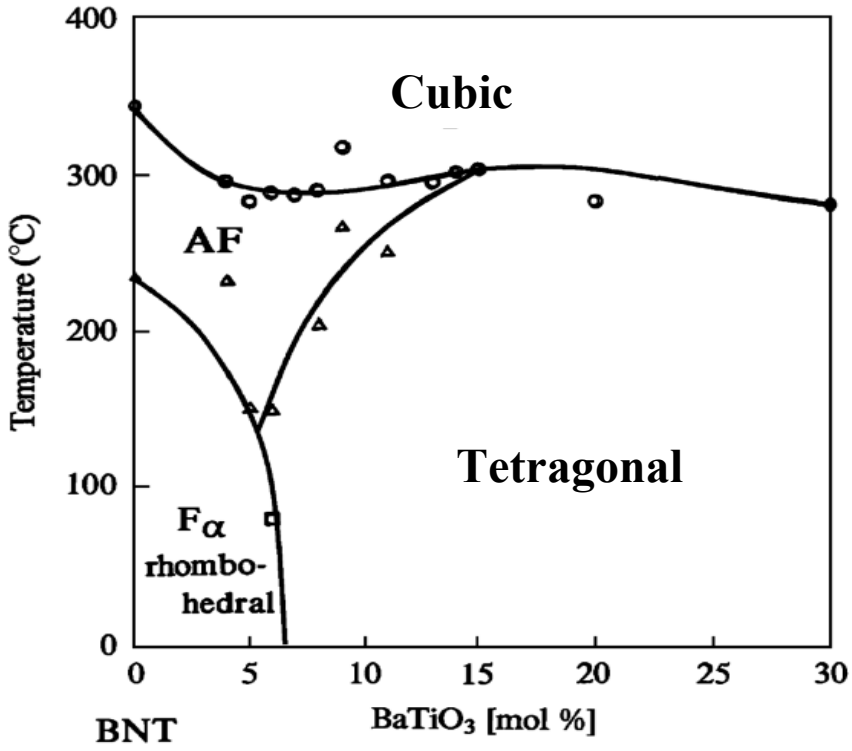

Figure 2.18 Temperature–composition phase diagram of BT–BNT [13]

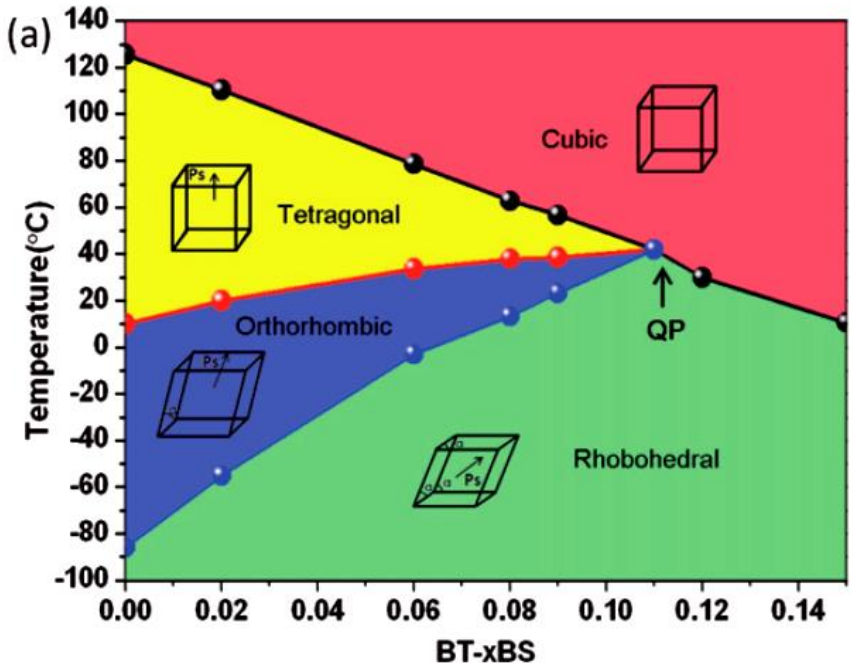

Figure 2.19 Temperature–composition phase diagram of $BaTiO_3$–$x BaSnO_3$ [49]

2.5.1.2 Ternary system of $BaTiO_3$ material

Meanwhile, many research focus on ternary system of $BaTiO_3$ material. In 2008, Zhang *et al.* studied lead free *x*BT–(1-*x*-*y*)BNT–*y*KNN system. They found that lead free 6BT–92BNT–2KNN ceramics exhibited the giant strain about 0.45% under both a unipolar and bipolar electric field at 80 kV/mm, as shown in figure 2.20 [50]. Afterward, Rahman et al. prepared lead free $6.5BaTiO_3$–$(93.5-x)Bi_{0.5}Na_{0.5}TiO_3$–$xBaZrO_3$ (BNBT–*x*BZ) by conventional solid-state reaction method. They reported that BNBT–0.03BZ ceramic had high d^*_{33} ~ 542 pm/V and strain ~ 0.38% at an applied field of 7 kV/mm [51].

Moreover, Trelcat *et al.* studied lead free $xBaTiO_3$–$yBi_{0.5}Na_{0.5}TiO_3$–$zBi_{0.5}K_{0.5}TiO_3$ system (*x*BT–*y*BNT–*z*BKT). Researcher reported that the 3.5BT–86.5BNT–10BKT ceramic exhibited high piezoelectric constant and electromechanical coupling factors (d_{33} ~ 133 pC/N, k_p ~ 0.26 and k_t ~ 0.26) [52].

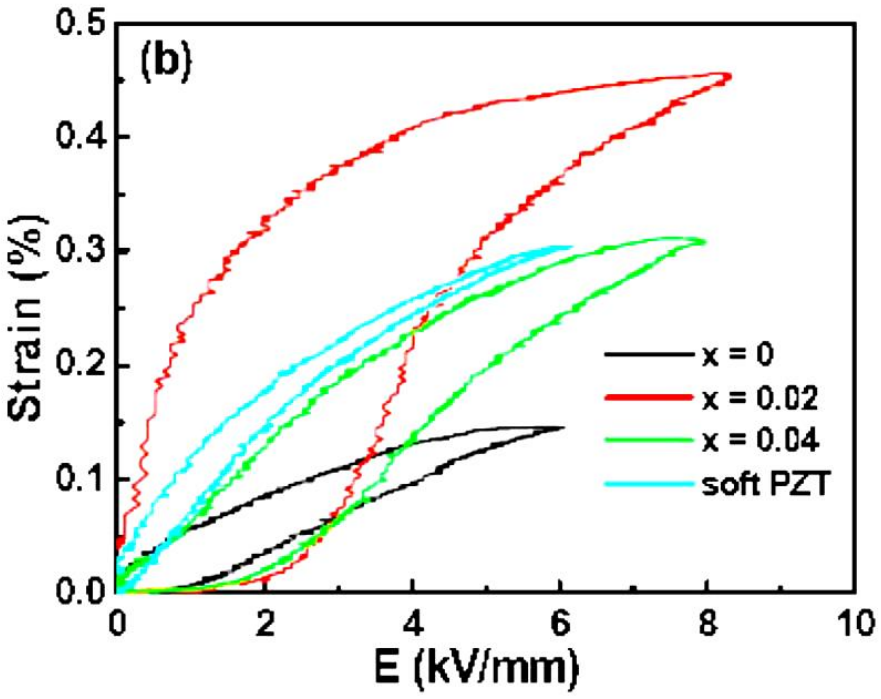

Figure 2.20 The relative plot of unipolar strain (%) of *x*BT–(1-*x*-*y*)BNT–*y*KNN ceramic as a function of electric field (kV/cm) [50]

In recent years, Li *et al.* synthesized $(Ba_{1-x}Ca_x)(Ti_{0.95}Zr_{0.05})O_3$ system using a solid-state reaction technique. They reported that the PPT from orthorhombic to

tetragonal phase at x = 0.08 showed high piezoelectric properties (d_{33} ~ 365 pC/N and k_p ~ 48.5%) [53]. . In 2010, Sutapun *et al.* studied $0.87BaTiO_3$–$(0.13\text{-}x)BaZrO_3$–$xCaTiO_3$ ceramic. They found that the multiphase coexistence of the rhombohedral and tetragonal phase at x = 0.06 (figure 2.21) exhibited high d_{33}^* ~ 1280 pm/V at electric field 10 kV/cm and strain ~ 0.23% at electric field 40 kV/cm [54].

Recently, Zhu *et al.* synthesized $(Ba_{1-x}Ca_x)(Ti_{0.92}Sn_{0.08})O_3$ [55] and $(Ba,Ca)(Ti_{1-x}Sn_x)O_3$ [56] ceramics. For $(Ba_{1-x}Ca_x)(Ti_{0.92}Sn_{0.08})O_3$ ceramics, they found that the PPT from orthorhombic phase to tetragonal phase at x =0.05 presented high dielectric and piezoelectric properties (ε_r ~ 23000, k_p ~ 47.7%, d_{33} ~ 568 pC/N and d_{33}^* ~ 1013 pm/v) [55]. Another $(Ba,Ca)(Ti_{1-x}Sn_x)O_3$ system, they reported that the multiphase coexistence of R–PC–O at x = 0.11 (figure 2.22) exhibited ultrahigh d_{33} ~ 670 pC/N and electrostrain 0.061% [56].

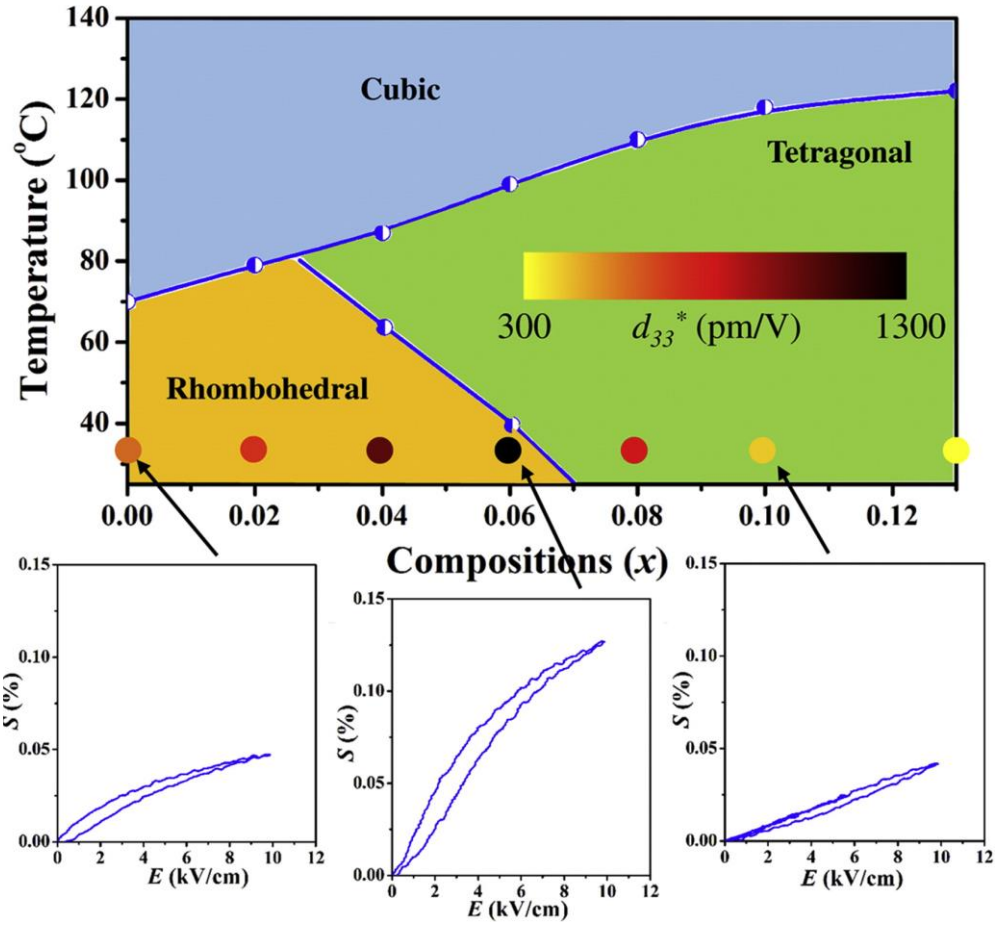

Figure 2.21 Composition–temperature ferroelectric phase diagram of BT–BZ–xCT ceramics [54]

Hao-Ran Li *et al.* studied lead free $(Ba_{1-x}Sr_x)(Zr_{0.05}Ti_{0.95})O_3$ or BSTZ ceramic. They found that BSTZ with x = 0.11 showed enhance piezoelectric properties (d_{33} ~ pC/N and k_p ~ 0.38) [57]. In 2009, Yanxia Li *et al.* prepared $Ba_{1-x}Sr_xTi_{0.94}Sn_{0.06}O_3$ (BSTS) ceramics by solid-state reaction method. Researchers reported that the BSTS at x = 0.02 exhibited maximum tunability of 63.5% at applied electric field of 6 kV/cm [58].

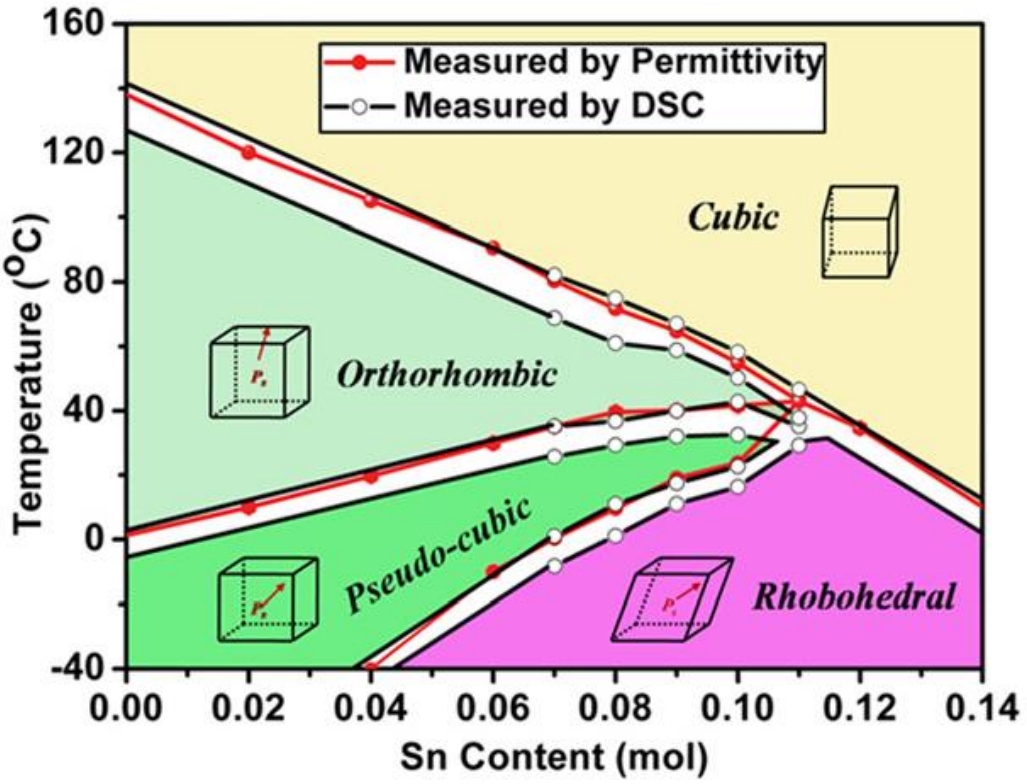

Figure 2.22 Temperature-composition phase diagram of $(Ba,Ca)(Ti_{1-x}Sn_x)O_3$ [56]

Jiagang Wu *et al*. prepared BT-base ceramic by combining $(1-x)Ba_{0.98}Ca_{0.02}Ti_{0.94}Sn_{0.06}O_3$–$xBa_{0.85}Ca_{0.15}Ti_{0.90}Zr_{0.10}O_3$ ((1-*x*)BCTS–*x*BCTZ) system. The phase boundary coexistence of orthorhombic and tetragonal phase was observed at around 4 mol% BCTZ which show good dielectric and piezoelectric properties (ε_r ~ 5500, $tan\delta$ ~ 0.3% and d_{33} ~ 407 pC/N) [59]. In 2009, Liu and Ren studied lead free $Ba(Ti_{0.8}Zr_{0.2})O_3$–$(Ba_{0.7}Ca_{0.3})TiO_3$ (BZT–BCT) system which it showed high d_{33} ~ 620 pC/N and d_{33}^* ~ 1140 pm/V at 50BZT–50BCT composition. The MPB of BZT–BCT ceramic exhibited tricritical triple point of a cubic paraelectric phase, ferroelectric rhombohedral, and tetragonal phases, which leads to a nearly vanishing polarization

between [001] tetragonal and [111] rhombohedral states, as illustrated in figure 2.23 [60].

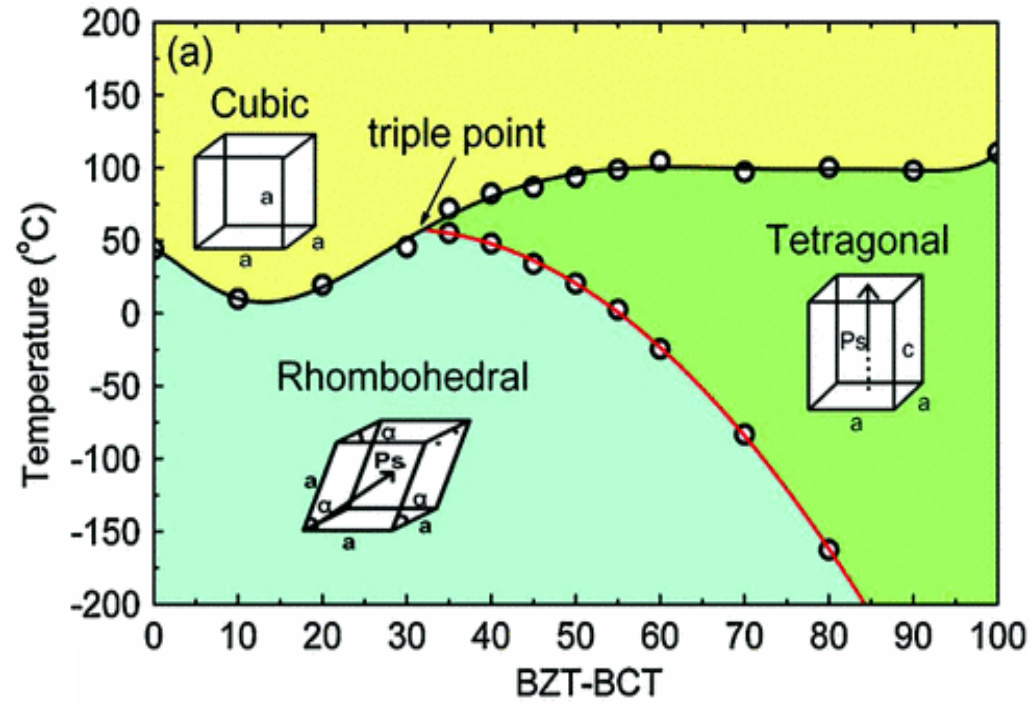

Figure 2.23 Phase diagram of $Ba(Ti_{0.8}Zr_{0.2})O_3$–$(Ba_{0.7}Ca_{0.3})TiO_3$ ceramic [60]

2.6 References

[1] Moulson, A. J., and Herbert J. M. 2003. “Electroceramic: Materials, properties, Application.” 2nd Ed. West Sussex : Jonh Wiley & Son Ltd.

[2] Uchino, K. 1997. “Piezoelectric Actuators and Ultrasonic Motors” springer.

[3] Uchino K. 2000. “Ferroelectric Devices” Taylor & Francis.

[4] Haertling, G. H. 1999. “Ferroelectric ceramics: History and technology” **J. Am. Ceram. Soc.** 82 : 797-818.

[5] Jaffe, B., Cook, W. R., and Jaffe, H. 1971. “Piezoelectric Ceramics” Academic, New York.

[6] Kittel, C. 2007. “Introduction to Solid State Physics” John Wiley&Sons, Singapore, New York, seventh edition, Ch.13, 393-394.

[7] Valasek, J. 1921. **Phys. Rev**. 17 : 475.

[8] Werner K. 1957. “ferroelectrics and antiferroelectrics” in Fredrick seitz, T.P.Das, David Turnbull, E.L. Hahn. Solid state physics 4.

[9] Askeland, D.R. 1996. “The Science and Engineering of Materials” 3rd S.I. Edition. London, UK, Chapman & Hall.

[10] Xu Y. 1991. “Ferroelectric Material and Their Application” Amsterdam: Elsavier.

[11] Smolenskii, G.A., and Agranovskaya, A.L. 1958. “Dielectric polarization and losses of some complex compound” **Sov. Phys.-Tech. Phys**. 1380-1382.

[12] Granzow, T. 2004. **Phys. Rev. Lett.** 92 065701-1.

[13] Cross, L.E. 1994. “Relaxor Ferroelctrics: An Overview” **Ferroelectrics**. 151 : 305-320.

[14] Mishima, T., Fujioka, H., Nagakari, S., Kamigaki, K., and Nambu, S. 1997. “Lattice Image Observations of Nanoscale Ordered Regions in $Pb(Mg_{1/3}Nb_{2/3})O_3$” **Jpn. J. Appl. Phys.** 36 : 6141-6144.

[15] Unico, K. and Nomura, S. 1982. “Critical Exponents of the Dielectric Constant in Diffused – Phase – Transition Crystals” **Ferroelectrics Lett**. 44 : 55 -61.

[16] Bhalla, A. S., Guo, R. and Roy, R. 2000. “The Perovskite Structure – a Review of Its Role in Ceramic Science and Technology” **Mat. Res. Innovat.** 4 : 3 – 26.

2.6 References (II)

[17] Izyumskaya, N., Alivov, Y. I., Cho, S. J., Morkoc, H., Lee, H., and Kang, Y. S. 2007 "Processing, structure, properties and applications of PZT thin films," **Crit. Rev. Solid State and Mater Sci.** 32.

[18] http://www.mrl.ucsb.edu/~dshoe/218/

[19] Goldschmidt, V.M., Skrifer Norske Videnskaos – Akad. Oslo, I. Mat. –Nat., 1926. 8.

[20] Feng, G., Rongzi, H., Jiaji, L., Zhen, L., Lihong, C. and Changsheng, T. 2009. "Phase Formation and Characterization of High Curie Temperature xBiYbO$_3$ – (1-x)PbTiO$_3$" **J. Eur. Ceram. Soc.** 29 : 1687 – 1693.

[21] Berlincourt, D., SC-4203(TR), Sandia Corp. Tech. Rept. U.S. Dept. Commerce, Washington, 1958.

[22] Lu, J., 2003. "Microstructure and electrical properties of Pb(Zr, Ti)O$_3$ thick film prepared by electrostatic spray deposition", **Sensor. Actuat. A-Phys.** 108 : 2-6.

[23] Guo, R., Cross, L.E., Park, S.E., Noheda, B., Cox, D.E., and Shirane, G. 2000. "Origin of the high piezoelectric response in PbZr$_{1-x}$Ti$_x$O$_3$" **Phys. Rev. Lett.** 84(23).

[24] http://cst-www.nrl.nary.mil/lacttice/struk.picts/e2_1.s.png.

[25] Jaffe B. 2012. "Piezoelectric ceramic" Elsevier Science.

[26] Jaffe,B., Roth, R.S., and Marzullo S. 1954. "Piezoelectric Properties of Lead Zirconate-Lead Titanate Solid-Solution Ceramics" **J. Appl Phys.** 25 : 809 – 810.

[27] Seung-Eek, P., and Shrout, T. R. 1997. "Ultrasonics Ferroelectrics and Frequency Control" **IEEE Transactions**. 44 : 1140-1147.

[28] Takenaka T., Muramata, K., and Fujiu, T. 1992. "PmC4. Piezoelectric properties of Pb(Zn$_{1/3}$Nb$_{2/3}$)O$_3$-PbTiO$_3$ prepared by HIP" **Ferroelectrics** 134(1) : 133-138

[29] Kuwata, J., Uchino, K., and Nomura, S., 1982. "Dielectric and Piezoelectric Properties of 0.91Pb(Zn$_{1/3}$Nb$_{2/3}$)O$_3$ - 0.09PbTiO$_3$ Single Crystals" **Jpn. J. Appl. Phys.** 21 : 1298-1302.

[30] Vittayakorn, N., Puchmark, C., Rujijanagul, G., Tan, X., and Cann, D.P. "Piezoelectric properties of (1-x)Pb(Zr$_{1/2}$Ti$_{1/2}$)O$_3$ – xPb(Zn$_{1/3}$Nb$_{1/3}$)O$_3$ ceramics prepared by the columbite (wolframite) precursor method" **Curr. Appl. Phys.** 6 : 303.

2.6 References (III)

[31] EU-Directive 2002/96/EC: Waste Electrical and Electronic Equipment (WEEE). Off. **J. Eur. Union** 2003, 46 (L37), 24.

[32] EU-Directive 2002/95/EC: Restriction of the Use of Certain Hazardous Substances in Electrical and Electronic Equipment (RoHS). Off. **J. Eur. Union** 2003, 46 (L37), 19.

[33] Maeder, M.D., Damjanovic, D., and Setter, N. 2004. "Lead free piezoelectric materials" **J. Electroceram**. 13 : 385 – 392.

[34] Shirane, G., Newnham, R., and Pepinsky, R. 1954. "Dielectric properties and phase transition of $NaNbO_3$ and $(Na,K)NbO_3$" **Phys. Rev.** 96(3) : 581-588.

[35] Buhler, C. F. 1962. "Some properties of bismuth perovskites" **J. Chem. Phys.** 36(3).

[36] Smolenskii, G. A., Isupov, V. A., Agranovskaya, A. I., and Kainik,N. N. 1961. "New ferroelectrics of complex composition," **Soviet Phys. : Solid State.** 2(11) : 2651–2654.

[37] Suchanicz, J., Roleder, K., Kania, A., and Handerek, J. 1988, "Electrostrictive strain and pyroeffect in the regon of phase coexistence in $Na_{0.5}Bi_{0.5}TiO_3$" **Ferroelectrics**. 77 : 107.

[38] Hiruma, Y., Aoyagi, R., Nagata, H., and Takenaka, T. 2005. "Ferroelectric and Piezoelectric Properties of $(Bi_{1/2}K_{1/2})TiO_3$ Ceramics" **Jpn. J. Appl Phys.** 44(7).

[39] Goldman, I. 1946. M. C. R. Acad. Sci. Russ. 46 : 139.

[40] http://www.murata.com/support/faqs/products/capacitor/mlcc/char/0013.

[41] Zhang, S., Xia R., and Thomas, R.S. 2007. "Lead-free piezoelectric ceramics vs. PZT?" **J. Electroceram.** 19 : 251–257.

[42] Guo, Y. P., Kakimoto, K., and Ohsato, H. 2004. "Structure and electrical properties of lead-free $(Na_{0.5}K_{0.5})$ NbO_3-$BaTiO_3$ ceramics" **Jpn. J. Appl. Phys.** Pt. 1. 43 : 6662–6666.

[43] Takenaka, T., Maruyama, K., and Sakata, K. 1991. "$(Bi_{1/2}Na_{1/2})TiO_3$-$BaTiO_3$ System for Lead Free Piezoelectric Ceramics" **Jpn. J. Appl. Phys.** 30 : 2236-2239.

2.6 References (IV)

[44] Chen, M., Xu, Q, Kim, B. H., Ahn, B. K., Ko, J. H., Kang, W. J. and Nam, O. J. 2008. "Structure and electrical properties of $(Na_{0.5}Bi_{0.5})_{(1-x)}Ba_xTiO_3$ piezoelectric ceramics" **J. Eur. Ceram. Soc.** 28 : 843–849.

[45] Gao, L., Huang, L., Hu, Y., and Du, H. 2007. "Dielectric and ferroelectric properties of (1-x)$BaTiO_3$–x$Bi_{0.5}Na_{0.5}TiO_3$ ceramics" **Ceram. Int.** 33 : 1041-1046.

[46] Wadda, S., Yamato, K., Pulpan, P., Kumada, N., Lee, BY., Iijima, T., Moriyoshi, C., and Kuroiwa, Y. 2010. "Preparation of barium titanate–bismuth magnesium titanate ceramics with high Curie temperature and their piezoelectric properties" **J. Ceram. Soc. Jpn.** 118(8) : 683-687.

[47] Wang, X., Yamada, H., and Xu, C. N. 2005. "Large electrostriction near the solubility limit in $BaTiO_3$ – $CaTiO_3$ ceramics" **Appl. Phys. Lett.** 86.

[48] Dong, L., Stone, D. S., and Lake, R. S. 2012. "Enhanced dielectric and piezoelectric properties of *x*$BaZrO_3$-(1-*x*)$BaTiO_3$ ceramics" **J. Appl. Phys.** 111 : 084107.

[49] Yao, Y., Zhou, C., Duchao L.v, Dong Wang, Haijun Wu, Yaodong Yang and Xiaobing Ren, 2012. "Large piezoelectricity and dielectric permittivity in BaTiO – x$BaSnO_3$ systems: The role of phase coexisting" **EPL.** 98(2) : 27008.

[50] Zhang, S., Kounga, AB., Aulbach, E., Granzow, T., Jo, W., Kleebe, H., and Rödel, J. 2008. "Lead-free piezoceramics with giant strain in the system $Bi_{0.5}Na_{0.5}TiO_3$-$BaTiO_3$ - $K_{0.5}Na_{0.5}NbO_3$. I. Structure and room temperature properties" **J. Appl. Phys.** 103 : 034107.

[51] Rahman, JU., Hussain, A., Maqbool, A., Ryu, GH., Song, TK., Kim, W., and Kim, M. H. 2014. "Field induced strain response of lead-free $BaZrO_3$-modified $Bi_{0.5}Na_{0.5}TiO_3$-$BaTiO_3$ ceramics" **J. Alloy Compd**. 593 : 97-102.

[52] Trelca, JF., Courtois, C., Rguiti, M., Leriche, A., Duvigneaud, PH., Segato, T. 2012. "Morphotropic phase boundary in the BNT–BT–BKT system" **Ceram Int.** 38 : 2823–2827.

[53] Li, W., Xu, Z., Chu, R., Fu, P., and Zang, G. 2010. "Piezoelectric and Dielectric Properties of $(Ba_{1-x}Ca_x)(Ti_{0.95}Zr_{0.05})O_3$ Lead-Free Ceramics" **J. Am. Ceram. Soc.** 93(10) : 2942–2944.

2.6 References (V)

[54] Sutapun, M., Vittayakorn, W., Muanghlua, R., and Vittayakorn, N. 2015. "High piezoelectric response in the new coexistent phase boundary of $0.87BaTiO_3$–$(0.13-x)\ BaZrO_3$–$xCaTiO_3$" **Mater. Design.** 86 : 564-574.

[55] Zhu, L.-F., Zhang, B.-P., Zhao, X.-K., Zhao, L., Zhou, P.-F. and Li, J.- F. 2013. "Enhanced Piezoelectric Properties of $(Ba_{1-x}Ca_x)(Ti_{0.92}Sn_{0.08})O_3$ Lead-Free Cermics **J. Am. Ceram. Soc.** 96(1) : 241-245.

[56] Zhu, L.-F., Zhang, B.-P., Zhao, X.-K., Zhao, L., Fang-Zhou Yao et al., 2013. "Phase transition and high piezoelectricity in $(Ba,Ca)(Ti_{1-x}Sn_x)O_3$ lead-free cermics" **Appl. Phys. Lett.** 103 : 072905.

[57] Li, H.-R., Chen C.-X. and Zheng R.-K. 2014. "Effects of Sr substitution on the structural, dielectric, ferroelectric, and piezoelectric properties of $Ba(Zr,Ti)O_3$ lead-free ceramics" **J. Mater. Sci : Mater Electron.** 26(5) : 3057 - 3063.

[58] Li Y., Yao X., Wang X. and Fu L., 2009. "Tunability and Dielectric Properties of $Ba_{1-x}\ Sr_xTi_{0.94}Sn_{0.06}O_3$ Ceramics" **Ferroelectric.** 384(1) : 79-83

[59] Liu, W., and Ren, X. 2009. "Large piezoelectric effect in Pb-Free ceramics" **Phys. Rev. Lett.** 103 : 257602.

[60] Wu, J., Habibul, A., Cheng, X., Wang, X., Zhang, B. "Orthorhombic–tetragonal phase coexistence and piezoelectric behavior in $(1-x)(Ba,Ca)(Ti,Sn)O_3$–$x(Ba,Ca)(Ti,Zr)O_3$ lead-free ceramics" Mater Res. Bull. 48(10) : 4411-4414.

CHAPTER 3
EXPERIMENTAL PROCEDURES

In this section explains experimental procedures used for the preparation powders ceramic processing and characterization of ternary barium titanate base ceramics. The characterizations of BT–based ceramics were describes physical and electrical properties.

3.1 Powder preparation

In this studies, BT–based powders of (0.975-*y*)$BaTiO_3$–0.025$SrTiO_3$–*y*$BaSnO_3$ and 0.9$BaTiO_3$–(0.1-*x*)$Bi_{0.5}Na_{0.5}TiO_3$–*x*$Bi(Mg_{0.5}Ti_{0.5})O_3$ systems were prepared using a solid-state by mixed carbonate and oxide method. The chemical purity and supplier of raw materials were used for preparations BT–based systems are listed in Table 3.1. For the raw material of (0.975-*y*)$BaTiO_3$–0.025$SrTiO_3$–*y*$BaSnO_3$ system were mixed by vibratory milled and 0.9$BaTiO_3$–(0.1-*x*)$Bi_{0.5}Na_{0.5}TiO_3$–*x*$Bi(Mg_{0.5}Ti_{0.5})O_3$ system were mixed by rotational ball milled. The starting materials were treated and dried in oven at 100°C before use. The oxide and carbonate powder were weighted according to the molar ratios of unit formula mixed and milled with yttrium-stabilized zirconia media in ethyl alcohol (ethanol). After that the mixture was dried in oven at 100°C for 24 hours and calcined in closed alumina crucibles for an optimized temperature range for each system. Then the calcined powders were ground and sieved. The procedure of all powder preparations in this studied is shown in figure 3.1.

Table 3.1 Specifications of starting precursors used in this study

Chemical	Purity (%)	Suppliers
Barium carbonate ($BaCO_3$)	99.9%	Inframal Advance Materials
Bismuth oxide (Bi_2O_3)	99.9%	Sigma-Aldrich
Sodium carbonate (Na_2CO_3)	99.8%	Riedel-de Hean
Titanium dioxide TiO_2	99.9%	Sigma-Aldrich
Magnesium oxide (MgO)	99%	Fluka
Tin oxide (SnO_2)	99.9%	Sigma-Aldrich
Strontium carbonate ($SrCO_3$)		Inframal Advance Materials

3.1.1 Powder preparation of (0.975-*y*)$BaTiO_3$–0.025$SrTiO_3$–*y*$BaSnO_3$

The composition series of (0.975-*y*)$BaTiO_3$–0.025$SrTiO_3$–*y*$BaSnO_3$ (abbreviated as BT –ST–*y*BS), where *y* = 0.00, 0.02, 0.04, 0.06, 0.08 and 0.10 ceramics were fabricated via solid – state reaction technique. The metals oxide and carbonate powder of $BaCO_3$, $SrCO_3$, TiO_2 and SnO_2 were used as starting materials. In the mixing process, the stoichiometric amount of raw materials were weights by following the equation (3.1).

$$0.975BaCO_{3(S)} + 0.025SrCO_{3(S)} + (1\text{-}x)\,TiO_{2(S)} + xSnO_{2(S)} \longrightarrow (0.975\text{-}x)BaTiO_3\text{–}0.025SrTiO_3\text{–}xBaSnO_{3(S)} \quad (3.1)$$

These powders were mixed in ethanol with yttrium-stabilized zirconia and then vibro-milling for 6 hours. The mixture were dried and calcined in alumina crucible at 1200°C for 4 hours with heating / cooling rate 5°C/min. The calcined powder were ground and sieved. The procedure of BT–ST–*y*BS powder preparations in this studied is showed in Figure 3.1.

3.1.2 Powder preparation of 0.9$BaTiO_3$–(0.1-*x*)$Bi_{0.5}Na_{0.5}TiO_3$–*x*$Bi(Mg_{0.5}Ti_{0.5})O_3$

Lead free 0.9$BaTiO_3$–(0.1-*x*)$Bi_{0.5}Na_{0.5}TiO_3$–*x*$Bi(Mg_{0.5}Ti_{0.5})O_3$ (abbreviated as BT–BNT–*x*BMT) ceramics, where *x* = 0.00, 0.02, 0.04, 0.06, 0.08, 0.10, were synthesized by the solid state reaction, as shown figure 3.2. Bi_2O_3, $BaCO_3$, Na_2CO_3, TiO_2 and MgO powders were used raw materials. First, stoichiometric amounts of raw materials were weighted by following the equation (3.2)

$$0.9BaCO_{3(S)} + \frac{(0.1+x)}{4}\,Bi_2O_{3(S)} + \frac{(0.1-x)}{4}\,Na_2CO_{3(S)} + \frac{(2-x)}{2}\,TiO_{2(S)} + \frac{x}{2}\,MgO_{(S)} \longrightarrow 0.9BaTiO_3\text{–}(1\text{-}x)(Bi_{0.5}Na_{0.5})TiO_3\text{–}xBi(Mg_{0.5}Ti_{0.5})O_{3(S)} \quad (3.2)$$

The raw materials were mixed and ball-milled with yttrium-stabilized zirconia in ethanol media for 18 hours. After drying the mixture for 24 hours in an oven and the mixed powder was calcined at 900°C for 4 hours with heating/cooling rate 10°C/min. Finally procedure of powder preparation, the calcined powder were ground and sieved.

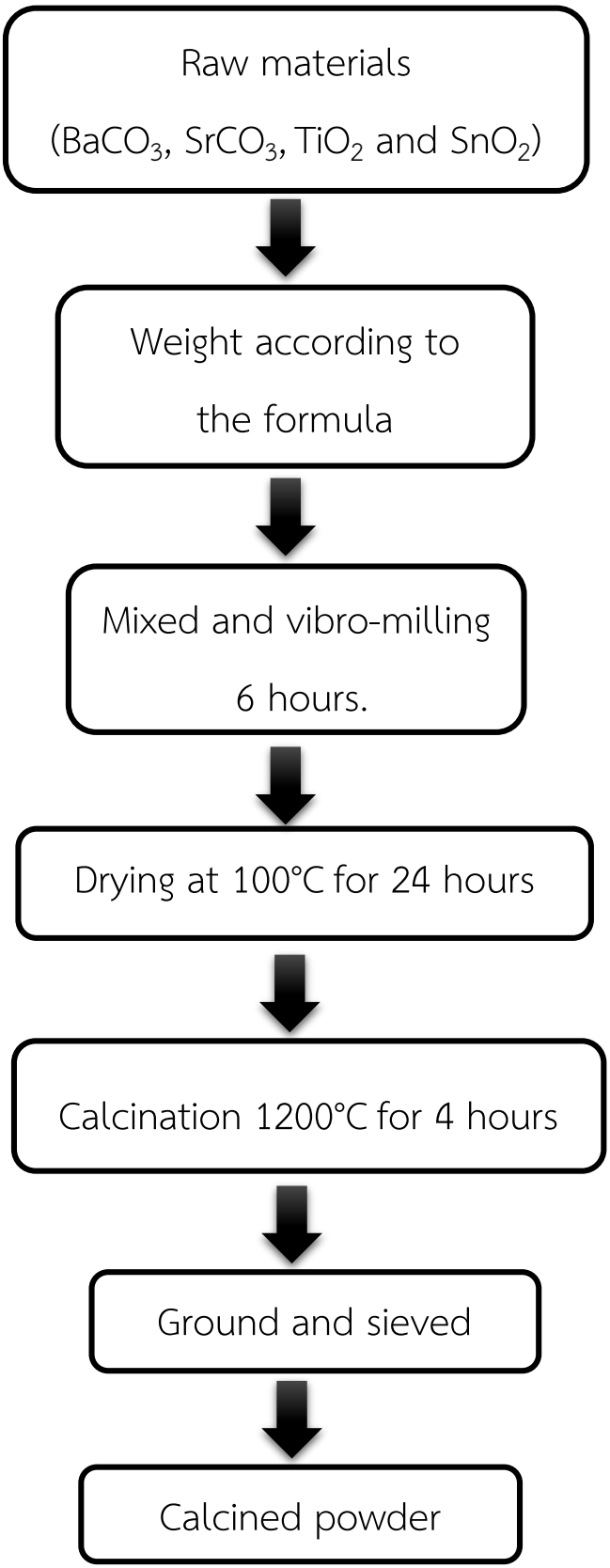

Figure 3.1 The powder preparation procedure of BT–ST–*y*BS

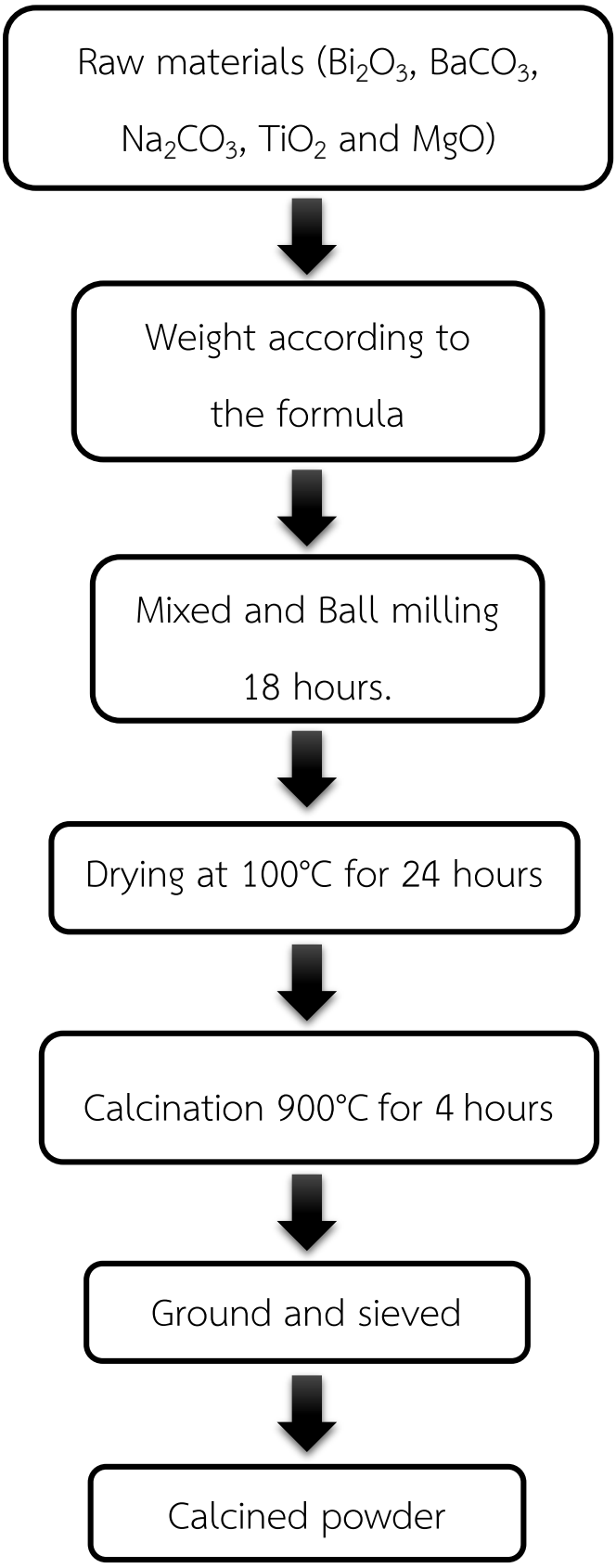

Figure 3.2 The powder preparation procedure of BT–BNT–*x*BMT

3.2 Ceramic processing

3.2.1 (0.975-*y*)$BaTiO_3$–0.025$SrTiO_3$–*y*$BaSnO_3$ ceramics

All BT–ST–*y*BS powder were weighted about 0.8 g. These powder were mixed with 5% polyvinyl alcohol (PVA) binder and pressed into green pellet of 11 mm diameter by uniaxial pressing. Then the binder inside the discs can be burnt out at 500°C and dwell time of 2 hours with heating rate 2°C/min. After that the samples were sintered 1375°C for 4 hours with heating/cooling rate 5°C/min which the disks were placed on an alumina plate. The samples deal is shown in figure 3.3.

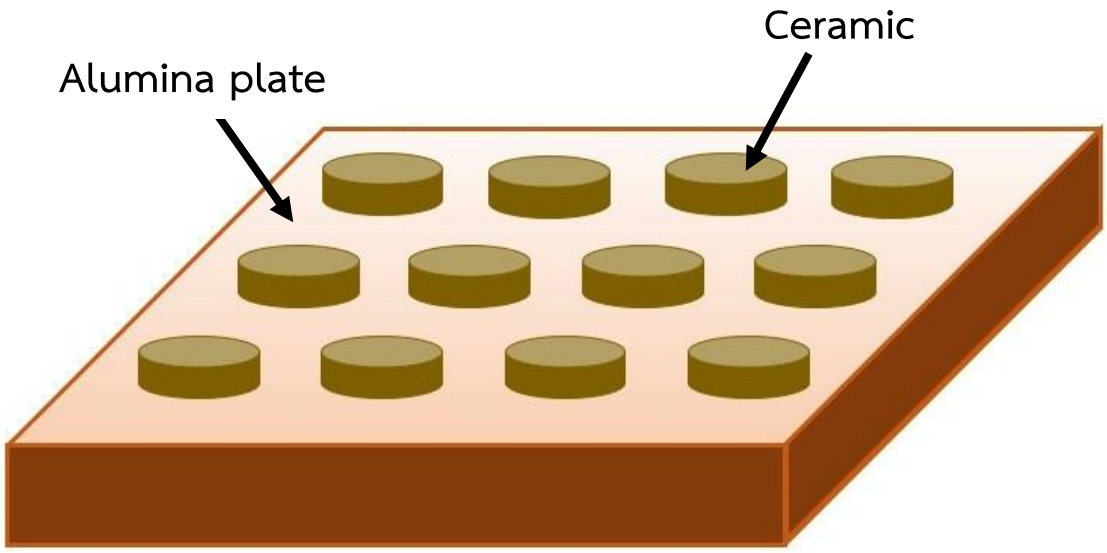

Figure 3.3 Arrangement of ceramics for the sintering process of BT–ST–*y*BS system

3.2.2 0.9$BaTiO_3$–(0.1-*x*)$Bi_{0.5}Na_{0.5}TiO_3$–*x*$Bi(Mg_{0.5}Ti_{0.5})O_3$ ceramics

The calcined powder of BT–BNT–*x*BMT systems were weighted about 1.2 g. and mixed continuously with 5% polyvinyl alcohol (PVA) as a binder to obtain homogeneous mixture. These powder were pressed into disks with 15 mm diameter by cold uniaxial pressing. Then the green pellet were placed on the alumina powder-bed inside alumina crucible which had a layer of alumina and $BaTiO_3$ powder, as shown in figure 3.4. After that the PVA binder inside the sample can be burnt out at around 500°C and holding for 2 hours with slowly heating rate 2°C/min. After the PVA burnout process, the disks were sintered 1150–1250°C for 4 hours with heating/cooling rate 5°C/min.

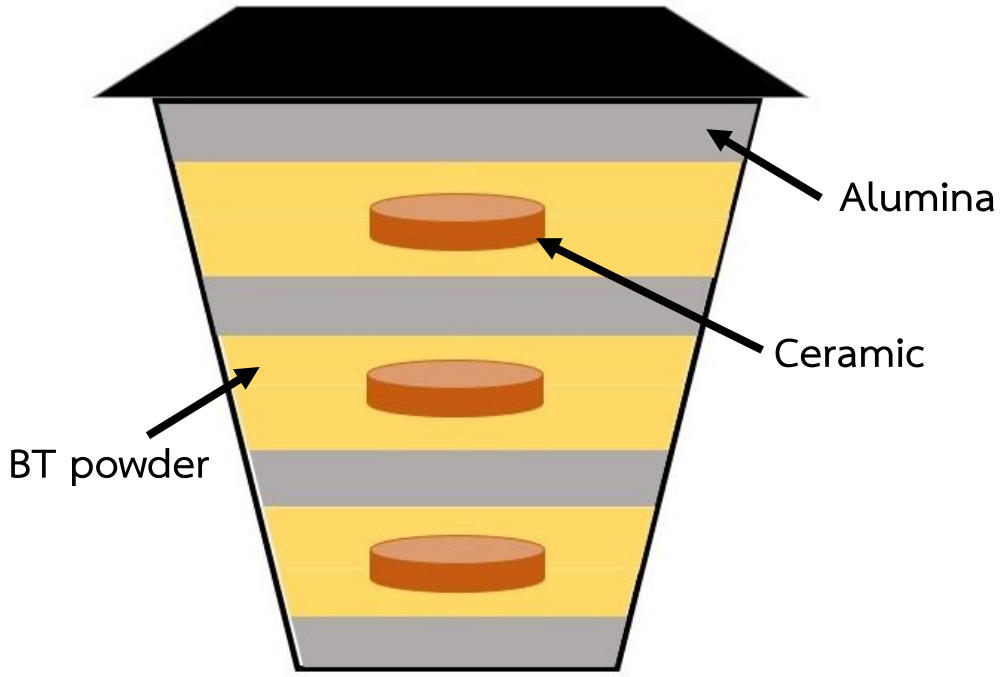

Figure 3.4 Arrangement of ceramics for the sintering process of BT–BNT–*x*BMT system

3.3 Characterization of ceramics

3.3.1 Physical properties and structure determination

3.3.1.1 Density measurement [1]

The density of sintered pellet is an index of its quality which is dependent on impurities and pores. It was determined using a water immersion technique at room temperature based on the Archimedes' principle. The density of each sample could be calculated (Equation 3.3)

$$\rho = \frac{W_d}{W_0 - W_i} \times \rho_{water} \tag{3.3}$$

Where, W_d = dry weight, W_i = ceramic weight in the water and W_0 = the weight of ceramic after issuing from water.

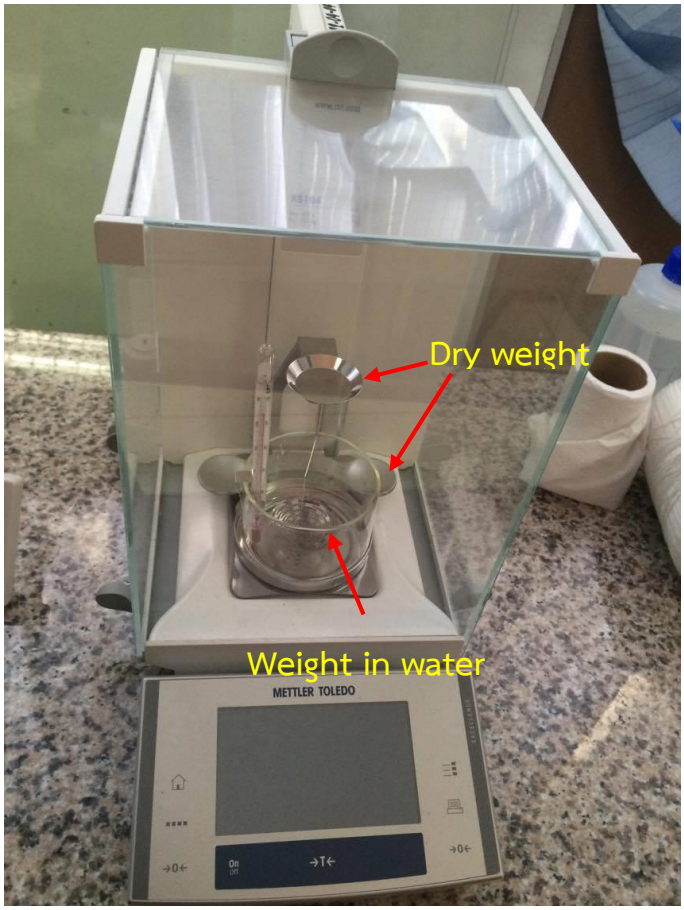

Figure 3.5 Laboratory weights scale (Mittler Toledo)

3.3.1.2 X – ray diffraction analysis [2]

After sintering of green pallet, the crystal structure and phase transition of all ceramics was carried out X–ray diffraction technique. The scattering of X–ray is related to the interaction between X–ray and crystal lattice of the materials by the X–ray scattered from different lattices interfere with each other and produces a diffraction pattern upon the change of incident angle of the X–ray beam. The incident rays interact with the samples and produces constructive interference when conditions satisfy Bragg's law

$$n\lambda = 2d\sin\theta \tag{3.4}$$

Where, *d* = perpendicular distance between lattice planes of miller indices, λ= wavelength of the incident, θ = glancing angle, n = an integer- 1, 2, 3... etc

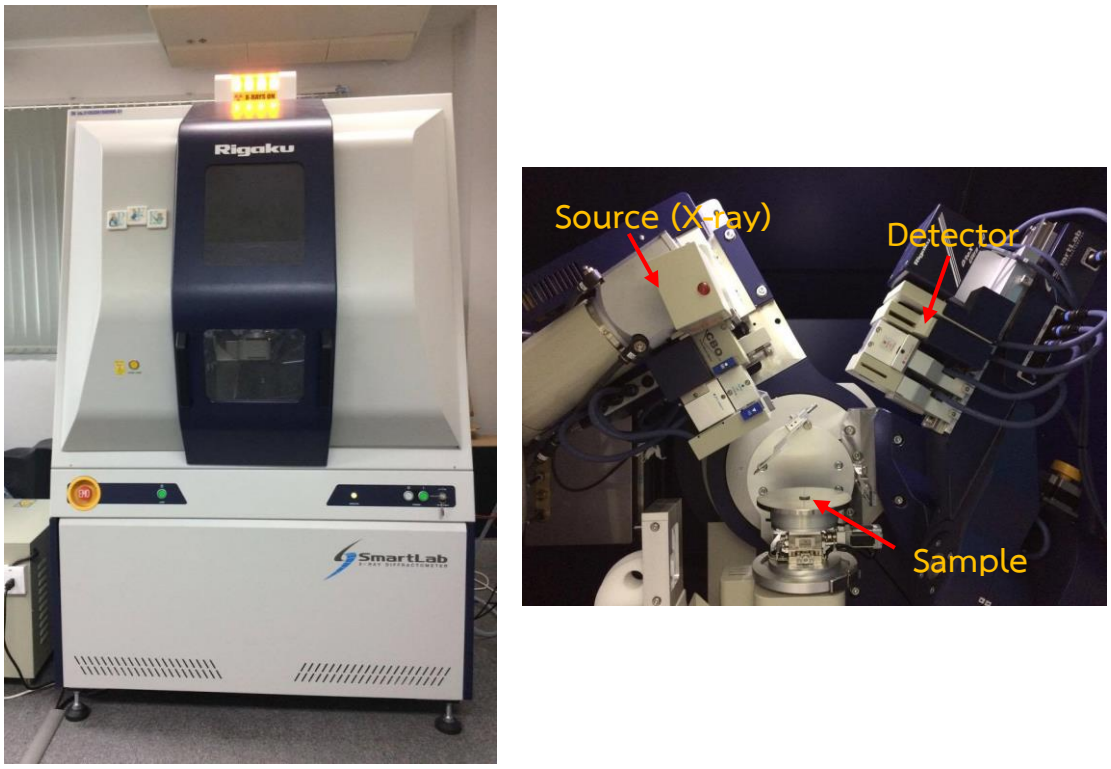

Figure 3.6 SmartLab X-ray diffractometer

In this studies, The X-ray diffraction results were obtained a SmartLab X-ray diffractometer (Figure 3.6). The source of X-ray used Cu-K_α radiation with λ = 1.5418 Å. The Data of X-ray diffraction were collected in the 2θ scan range of 20 - 80°, with a step size of 0.02° at a scanning rate of 1.2° per minute. The phases were determined by comparing the major peaks to the values listed on the Joint Committee on Powder Diffraction Standards (JCPDS) and the peaks of X–ray diffraction pattern were calculated lattice parameter.

3.3.1.3 Scanning Electron Microscopy (SEM) [3]

Microstructure of the ceramic can be exanimated using scanning electron microscopy. In this studies, the surface morphology of ceramics was observed using scanning electron microscope (EVO®MA10) (Figure 3.7) by attaching the ceramic on stainless steel stubs using carbon adhesive tape. After that, the top surface of the sample was coated by gold layer. The calculation of average grain size of the ceramics were using linear intercept method.

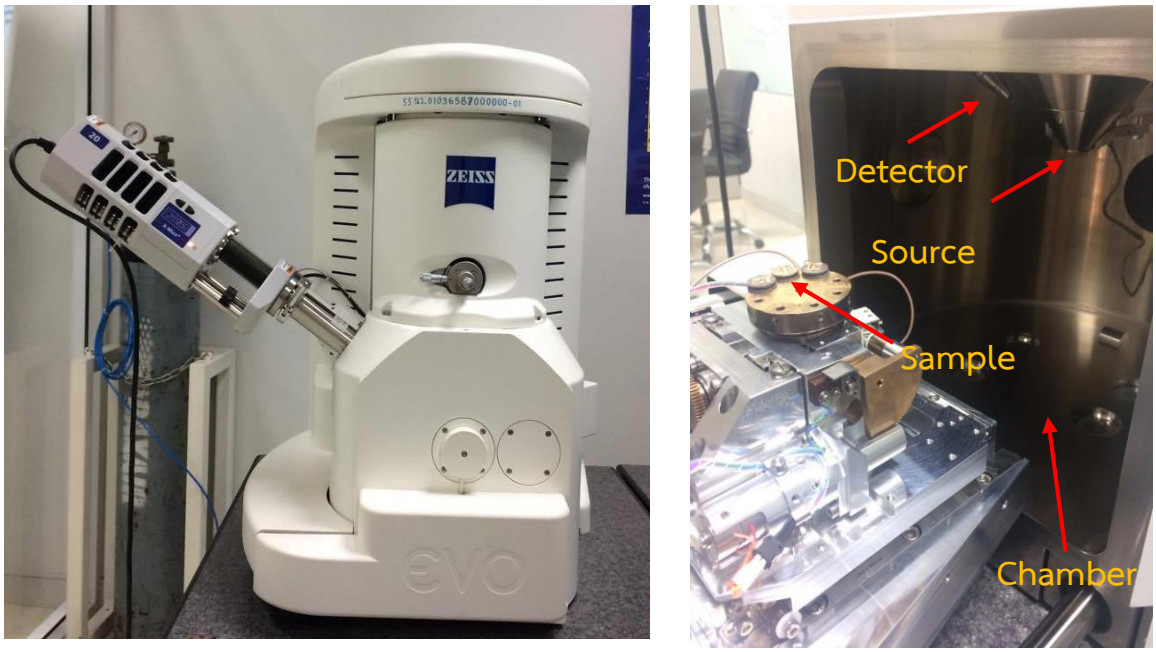

Figure 3.7 Scanning electron microscope (EVO®MA10)

3.3.1.4 Raman spectroscopy [4]

Raman spectroscopy is a spectroscopic technique based on inelastic scattering of monochromatic light, usually from a laser source. The ceramics, Raman spectroscopy is used to investigate the vibration modes and sensitivity of local structure in inorganic materials. In this work, Raman spectra were studied using Thermo Scientific DXR Raman microscope (Figure 3.8) with a He – Ne laser in 100 – 1000 cm^{-1} for wavenumber.

Figure 3.8 Thermo Scientific DXR Raman microscope [7]

3.3.2 Electrical Analysis

3.3.2.1 Sample preparation

Before the measurement of electric properties, all samples were polished for both sides and made parallel. They were cleaned with ethanol in an ultrasonic bath before electrode coating with silver paste (C1000, Heraeus) on both surfaces. Silver paste was heated on at 750°C for 20 min with heating/cooling rate 5°C/min and before measurement of the piezoelectric constant d_{33} poling of the sample was done.

3.3.2.2 Dielectric property measurement [5]

The dielectric property measurement are mention the determination of the phase transition temperature, relative permittivity (ε_r) or dielectric constant and loss tangent ($tan\delta$). The relative permittivity and loss tangent value were determined from capacitance measurements based on the following equation 3.5.

$$C = \frac{\varepsilon_0 \varepsilon_r A}{d} \tag{3.5}$$

Where *C* is the capacitance (Farad), *d* is the ceramic thickness, *A* is the surface area of sample, and ε_0 is the permittivity of free space, 8.854 x 10-12 F/m.

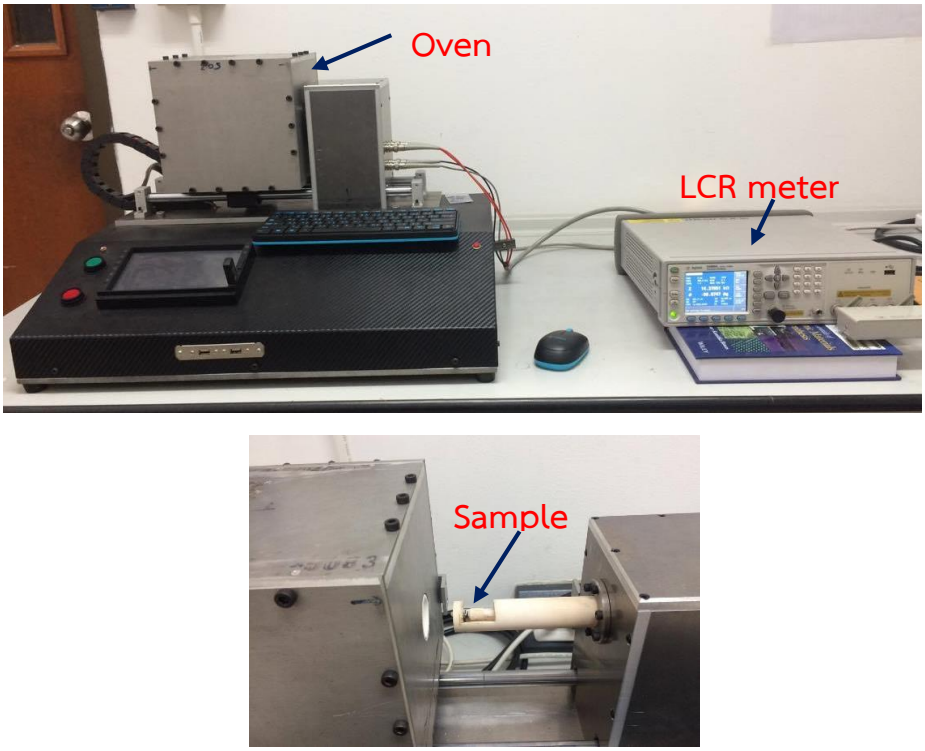

Figure 3.9 LCR analyzer (HP – 4284, Hewlette Packard Inc.)

In this work, the dielectric property measurements were done using programmable furnace with an LCR analyzer (HP – 4284, Hewlette Packard Inc.), as shown in figure 3.9 and temperature varied at room temperature to 250°C for BT–BNT–*x*BMT ceramics and at room temperature to 160°C for BT–ST–*y*BS ceramics.

3.3.2.3 Ferroelectric property measurement

Ferroelectric material are perform measurement of polarization as a function of electric field (P – E hysteresis loop). The P – E hysteresis loop describes the dynamic nonlinear polarization switch behavior as a function of field. The spontaneous polarization (P_s), remnant polarization (P_r) and coercive field (E_c) can be obtained from ferroelectric hysteresis loop. In this studies, polarization – electric field (P – E) hysteresis loop were determined at room temperature using Radiant Technologies, Inc (RT66A) at a frequency

4 Hz and an electric field of 10 – 60 kV/cm. During the measurement, the samples were immersed in silicone oil to prevent the breakdown of from the side area of the samples.

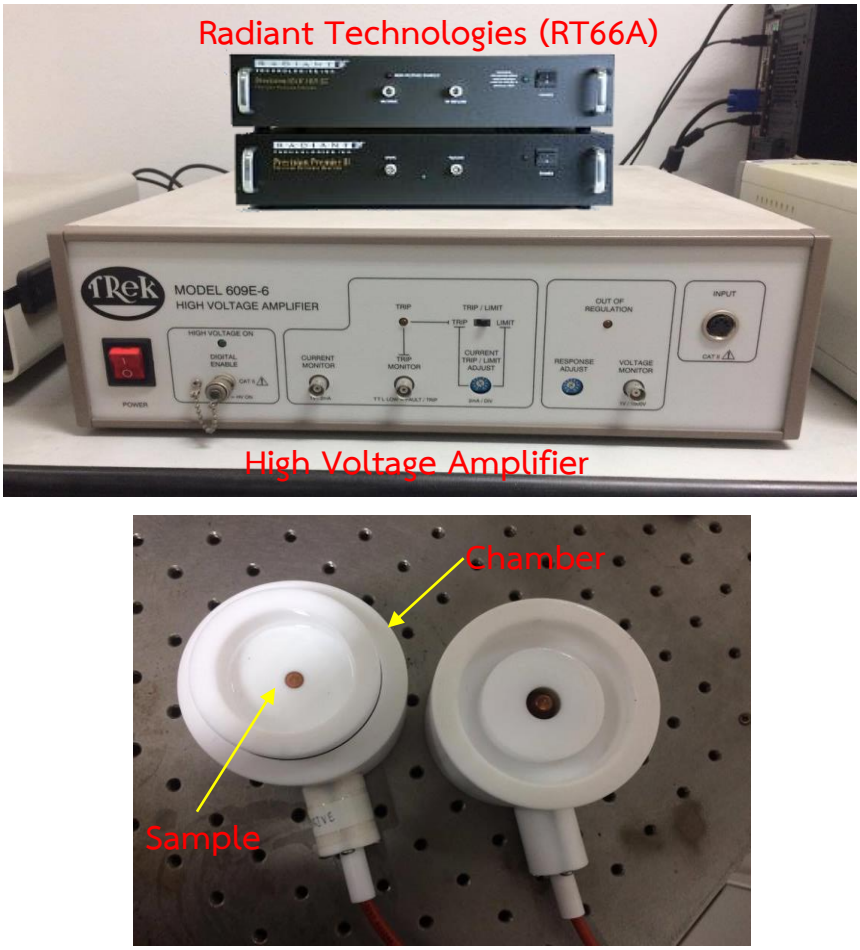

Figure 3.10 Ferroelectric Tester

3.3.2.4 Piezoelectric property measurement [6]

The piezoelectric properties mention the piezoelectric constant (d coefficient). These is the polarization generated per unit of mechanical stress applied to material (Direct effect) alternatively, is the mechanical strain produced by a piezoelectric material per unit of electric field applied (Converse effect). The d coefficient can be calculated from the following equation 3.6 and 3.7.

$$d_{ij} = \frac{short\ circuit\ charge\ density}{applied\ mechanical\ stress}\ (C/N) \quad (3.6)$$

$$= \frac{mechanical\ strain}{applied\ electric\ field}\ (m/V) \quad (3.7)$$

Where *i* indicates the direction of electric field or displacement and *j* indicates the direction of mechanical stress or strain.

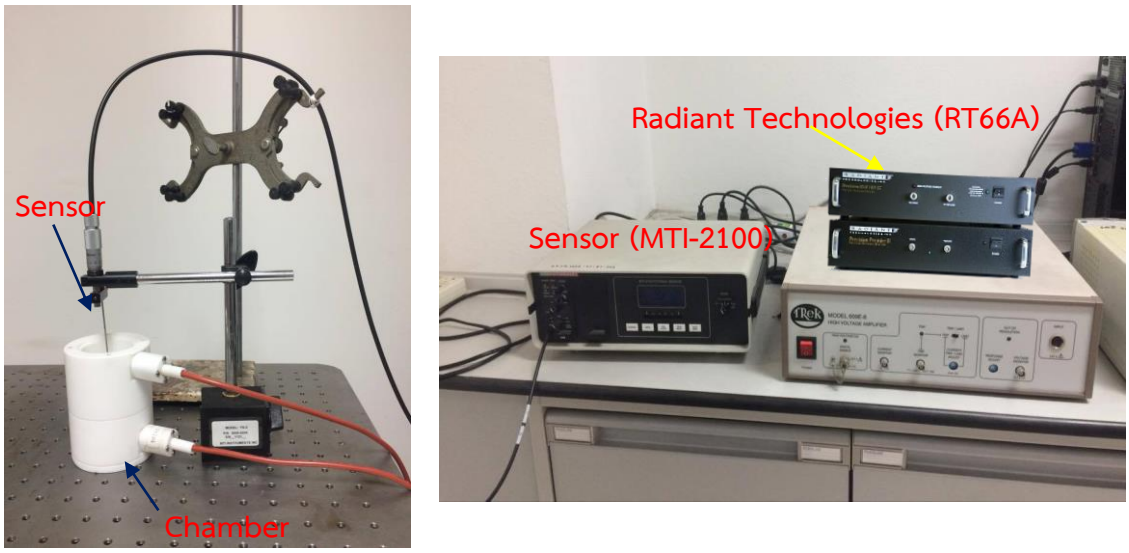

Figure 3.11 Instrument for strain measurement

In this work, the piezoelectric property, the strain measurement was done using an optical displacement sensor (MTI-2100) combined with the radiant ferroelectric test system at room temperature and an external electric field of 20 and 60 kV/cm. The normalized strain (d_{33}^{*}) value was calculated from the $\frac{S_{max}}{E_{max}}$ ratio for each composition. For the d_{33} measurements was determined at room temperature by using directly from a quasistatic d_{33} meter (YE2730A, APC International Ltd.). Before d_{33} measurements, the ceramics were poled at room temperature in silicone oil by applying a DC field at 35 – 40 kV/cm for 20 minutes.

3.4 References

[1] Reed J. S. 1995. “Principles of Ceramics Processing” Wiley Interscience, New York.

[2] Lesley E. S., and Elaine A. M. 2005. “Solid State Chemistry” Taylor & Francis, London.

[3] Lee W. E. and Rainforth W. M. 1994 “Ceramic Microstructures Property Control By Processing” Chapman & Hall, London.

[4] Bowley H. J., Gardiner D. J., Gerrard D. L., Graves P. R., Louden J. D., Turrell G. 1989 “Practical Raman spectroscopy”.

[5] Anthony R. W. 1999. “Basic Solid State Chemistry” John Wiley & Sons, New York.

[6] Jaffe B., Cook W. R., and Jaffe H. 1971. “Piezoelectric ceramics” Academic Press, New York.

CHAPTER 4

EFFECT OF Sn CONTENT ON THE DIELECTRIC AND PIEZOELECTRIC PROPERTIES OF THE TERNARY SYSTEM (0.975-*y*)$BaTiO_3$–0.025$SrTiO_3$–*y*$BaSnO_3$

Based on article published in Journal of Materials Science

Design of the polymorphic phase composition in the (0.975-*y*)$BaTiO_3$–0.025$SrTiO_3$–*y*$BaSnO_3$ ternary system was based on the ferroelectric phase diagram. The dense ceramic of (0.975-*y*)$BaTiO_3$–0.025$SrTiO_3$–*y*$BaSnO_3$ with y = 0.00, 0.02, 0.04, 0.06, 0.08 and 0.10 compositions was fabricated successfully via the solid state reaction method. The effect of Sn substitution on the ferroelectric phase transition and piezoelectric properties was explored in order to achieve high performance piezoelectric properties. All of the ceramics exhibited pure perovskite structures. Orthorhombic to tetragonal phase transition was evidenced clearly as a function of Sn content. The orthorhombic to tetragonal phase transition shifted close to ambient temperature by increasing the Sn content. The coexistent tetragonal and orthorhombic phases were exhibited at the composition, y = 0.04, and showed outstanding dielectric and piezoelectric properties, relative permittivity (ε_r) of 11500 and piezoelectric coefficient (d_{33}) of 450 pC/N. An outstanding reversible strain of about 0.12%, with a normalized piezoelectric coefficient (S_{max}/E_{max}) of 1,280 pm/V at a low electric field (10 kV/cm), was observed clearly at the composition of the coexistent phase. The (0.975-*y*)$BaTiO_3$–0.025$SrTiO_3$–*y*$BaSnO_3$ ceramics are the most promising candidate for lead–free piezoelectric materials.

4.1 Introduction

Lead-based piezoelectric ceramics such as lead zirconate titanate [$Pb(Zr_{1-x}Ti_x)O_3$; PZT] have been used most widely in actuator and sensor devices, due to their excellent piezoelectric properties [1]. Nevertheless, PZT ceramics are environmentally unfriendly and dangerous to human health, due to the toxicity of lead in fabrication

processing [2, 3]. Therefore, attention has been drawn to lead–free piezoelectric materials with a performance comparable to that in lead–based materials. Consequently, in recent years diverse systems have been explored, including bismuth – alkaline metal titanates and niobates, and especially $BaTiO_3$; BT solid solution [2–5].

Ferroelectric behavior was discovered in Barium titanate ($BaTiO_3$; BT) by Wul and Goldman in 1946 [6], which led to the widespread use of BT in capacitors and electromechanical devices [6, 7]. BT has a tetragonal perovskite structure at room temperature, and pure BT exhibits a piezoelectric constant ($\boldsymbol{d_{33}}$) of about 191 pC/N) [8] that is relatively low when compared to PZT-based ($\boldsymbol{d_{33}}$ = 300 – 600 pC/N) [8]. Therefore, BT has been modified by doping with A and/or B site substitutions [9–11]. The binary system of $BaTiO_3$–$BaSnO_3$; BT-BSn recently showed high dielectric permittivity ($\boldsymbol{\varepsilon_r}$) $\sim$ 75000 and excellent piezoelectric coefficient ($\boldsymbol{d_{33}}$) $\sim$ 697 pC/N at the quasi-quadruple point, which exhibited coexistent Cubic–Tetragonal–Orthorhombic–Rhombohedral phases in BT–BSn [12]. Wang et al. [13] reported a high electrostriction strain of $\sim$ 0.22% in the binary systems of $BaTiO_3$–$CaTiO_3$; BT–CT. Excellent piezoelectric properties also were obtained in the coexistent phase composition in the $BaTiO_3$–$BaZrO_3$–$CaTiO_3$; BT–BZ–CT and $BaTiO_3$–$BaZrO_3$–$CaTiO_3$; BT–BS–CT system [9, 14]. The $(Ba_{1-x}Ca_x)(Ti_{0.92}Sn_{0.08})O_3$ ceramics recently displayed high $\boldsymbol{d_{33}}$ = 568 pC/N, k_p = 47.7%, $\boldsymbol{\varepsilon_r}$ = 23,000 and normalized strain (dS/dE) = 1013 pm/V at the orthorhombic/tetragonal coexistent phase composition [15]. The coexistent phase composition in the Sn dope BT–CT system also exhibited ultra–high $\boldsymbol{d_{33}}$ (670 pC/N) and electrostrain (0.061%) [16]. Li et al. [17] recently reported a high piezoelectric coefficient ($\boldsymbol{d_{33}}$) of about 380 pC/N and k_p of about 38% in the Sr dope $Ba(Zr,Ti)O_3$; BZT system. The Sr substitute BZT, not only enhanced piezoelectric properties by shifting the ferroelectric phase transition close to room temperature, but also decreased the sintering temperature of the ceramic. In order to find new BT-based ceramics with excellent piezoelectric properties, Sn cation was selected to substitute the Sr–doped $BaTiO_3$ in this work. Sr doped BT was used as a base composition, due to Sr being able to enhance piezoelectric properties and slightly decrease the sintering temperature of the ceramic. Systematic study of how the Sn substitution affects crystal structure, and dielectric and piezoelectric behavior of $(0.975\text{-}y)BaTiO_3$–$0.025SrTiO_3$–$yBaSnO_3$; BT–ST–*y*BS ceramics, is still rare. The BT–ST–*y*BS ceramic, with *y* = 0.00, 0.02, 0.04, 0.06, 0.08 and 0.10 compositions, is designated in this study as a lead–free

composition that explores the compositional dependence of structure and piezoelectric behavior in Sn content. The development of piezoelectric properties by optimizing Sn content in BT–ST–*y*BS ceramics has been established.

4.2 Experimental procedure

The (0.975-*y*)$BaTiO_3$–0.025$SrTiO_3$–y$BaSnO_3$ ceramic with y = 0.00, 0.02, 0.04, 0.06, 0.08 and 0.10 compositions was fabricated via the solid–state reaction technique. The metal carbonate and oxide powder of $BaCO_3$ (99.9%, Inframal Advance Materials), $SrCO_3$ (99.5%, Inframal Advance Materials), TiO_2 (99.9%, Sigma-Aldrich) and SnO_2 (99.9%, Inframal Advance Materials) were used as raw materials. The stoichiometric amount of starting materials was mixed in ethanol with yttrium-stabilized zirconia in the first step, and then vibro-milled for 6 hours. The mixtures were dried and calcined at temperatures between 1,200 and 1,300°C for 4 hours, with a heating/cooling rate of 5°C/min. The calcined powders were ground and sieved. Finally, the resultant powders were pressed into pellets of 10 mm diameter, using 5 wt% polyvinyl alcohol (PVA) as a binder. The pellets were sintered at between 1,375 and 1,450°C for 4 hours with a heating/cooling rate of 5°C/min. Ceramics with more than 94% theoretical density were selected for investigating electrical properties. The crystal structure of ceramics was carried out with X-ray diffraction (Bruker-AXS D 8 Advance) using CuK_{α} radiation in the 2θ scan range of 20°-80°. In order to support crystal structure identification of the ceramics, Raman spectra were measured in the 100 – 1,000 cm^{-1} wave number range with a Thermo Scientific DXR Raman microscope, using the 532 nm exciting line of a He-Ne laser. Both sides of the samples were polished and paralleled for electrical measurements. Then, the pellets were coated on both surfaces with silver electrodes (C1000, Heraeus) and heated at 750°C for 20 min, with a heating/cooling rate of 5°C/min. The frequency (1, 10, 100 kHz) and temperature (room temperature to 160°C) dependence of relative permittivity (ε_r) and dielectric loss ($tan\delta$) were obtained by using an LCR analyzer (HP4284A, Hewlett-Packard, Palo Alto, CA). Ferroelectric hysteresis loops were determined at room temperature by using a ferroelectric tester (RT66A, Radiant Technologies, Inc.), and the strain – electric field (S – E) loop was measured by unipolar driving at 4 Hz using an MTI-2100 Fotonic sensor combined with a ferroelectric tester. The pellets of 10 mm diameter and 0.6 mm thickness were poled

under a DC field at 35 – 40 kV/cm for 30 min at room temperature and aged for 24 hours before piezoelectric measurements. The piezoelectric coefficient, d_{33}, was characterized using a quasi-static d_{33} meter (YE2730A, APC International Ltd.).

4.3 Results and discussion

The characteristics of crystal structured ceramics were examined by X-ray diffraction (XRD). XRD patterns of the BT–ST–*y*BS system, with compositions of y = 0.00, 0.02, 0.04, 0.06, 0.08 and 0.10, are shown in Fig. 4.1a–d. All of the samples demonstrated a single phase with the perovskite structure, and the secondary or impure phase was not observed in the XRD patterns, which indicates that both Sr and Sn ions are fully diffused into the $BaTiO_3$ lattice to form solid solution. The crystal structure of BT–ST–*y*BS at the compositions, $0.00 \leq y \leq 0.02$, has a tetragonal symmetry, identified by a single peak at 2θ of 38.7° (Fig. 4.1b) and splitting of (002) and (200) peaks at 2θ of 44.8 – 45.6° (Fig. 4.1c). At higher compositions of $0.06 \leq y \leq 0.10$, the XRD pattern exhibits splitting of two peaks [(102)/(120)] at around 38 – 39.5° and splitting of three peaks [(113)/(131)/(202)] at around 55.8 – 56.3°, which indicates an orthorhombic symmetry (Fig. 4.1d). Therefore, the results indicated that the crystal structure changed from tetragonal to orthorhombic phase with increasing Sn content. Meanwhile, it is anticipated that the tetragonal and orthorhombic phases for y = 0.04 coexist, which is confirmed by dielectric and piezoelectric measurements. It is seen clearly that the diffraction pattern of all compositions shifts gradually to low angles with increasing Sn content, which should induce expansion of the host lattice. Lattice parameter (Å) and unit cell volume ($Å^3$) were calculated and plotted as a function of Sn content, as shown in Fig. 4.2a, b. Regarding the compositions, $0.00 \leq y \leq 0.02$, with tetragonal symmetry, the unit cell a and c increase slightly with increasing Sn content, which corresponds with increased unit cell volume. The ostensibly discontinuous changes are noticed at $0.02 \leq y \leq 0.06$ when the tetragonal and orthorhombic phases coexist. The orthorhombic lattice parameters (a, b and c) and unit cell volume slightly increase for the compositions, $0.06 \leq y \leq 0.10$. This is consistent with the result reported by Zhu et al. [16]. The increase in the lattice parameter is caused mainly by the majority of Sn ions substitute Ti^{4+} ions the B site of the perovskite structure with Sn^{4+} state. However, it should be noted that the valency of the Sn ion is very sensitive

and allowed to adapt to a divalent, trivalent and tetravalent state in oxide ceramics [18]. Suzuki et al. [19] reported that under sintering conditions of reducing atmosphere, the Sn ions can substitute Ba^{2+} ions at the A-site of the perovskite structure with Sn^{2+} state. The oxidation states of the Sn ion in BT–ST–*y*BS ceramics must be considered for future investigation.

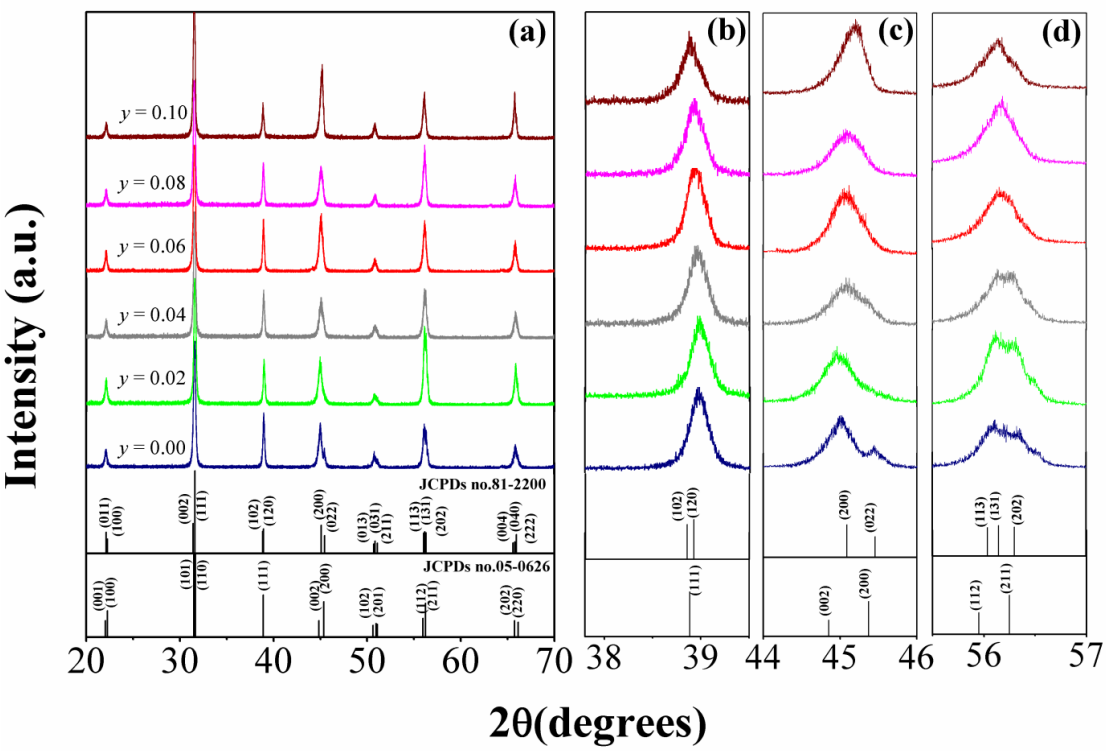

Figure 4.1 (a) X-ray diffraction patterns of (0.975-*y*)$BaTiO_3$–0.025$SrTiO_3$–*y*$BaSnO_3$ ceramic between the 2θ range of 20 – 80°, (b) expanded range of 38 – 39.5°, (c) expanded range of 44.8 – 45.6°, and (d) expanded range of 55.8 – 56.3°

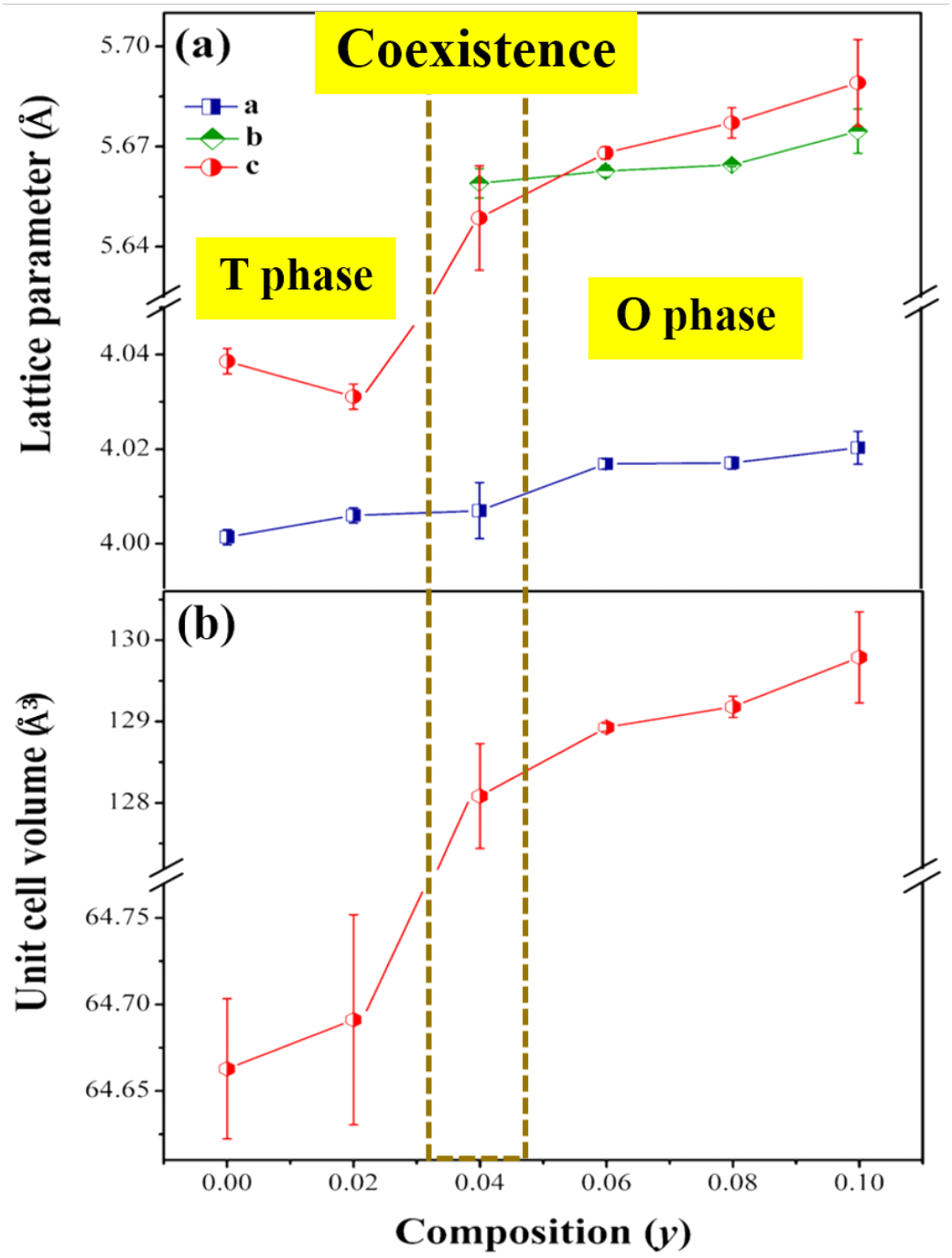

Figure 4.2 The relative plot between the (a) lattice parameter (Å), and (b) cell volume (Å^3) and composition *y* in (0.975-*y*)$BaTiO_3$–0.025$SrTiO_3$–*y*$BaSnO_3$ ceramic.

Dependence on the composition of Raman spectra for (0.975-*y*)$BaTiO_3$–0.025$SrTiO_3$–*y*$BaSnO_3$ systems was investigated at room temperature in the frequency range of 100–1,000 cm^{-1}, as shown in Figure 4.3(a–d). The ferroelectric phase with tetragonal symmetry corresponds with group theory analysis in normal optical mode, with each F_{1u} mode transforming into A_1 and E modes, whereas the F_{2u} mode gives rise to B_1 (silent) and E modes. All spectra generally display Raman–active modes of ferroelectric material. The interference dips at around 180 cm^{-1}, due to antiresonance between sharp $A_1(TO_1)$ and broad $A_1(TO_2)$ modes; such as a broad peak of $A_1(TO_2)$ mode near 257 cm^{-1}; sharp peak of $E(TO_2)$ mode at 295 cm^{-1}; broad peak of $A_1(TO_3)$ and E(TO) mode at around 515 cm^{-1}, which is a bending and stretching vibration of symmetric Ti-O in $[TiO_6]^{2-}$ and a broad peak of $A_1(LO_3)$ /$E(LO_3)$ mode at around 712 cm^{-1}[20]. Therefore, Raman spectra of all compositions are observed at a broad peak of $A_1(TO_2)$, $E(TO_2)$, $A_1(TO_3)$/E(TO), $A_1(LO_3)$/$E(LO_3)$ and interference dip mode (Figure 4.3a), which indicates that all compositions exhibit ferroelectric phase. The signature Raman mode of tetragonal phase for BT is generally; a broad $A_1(TO_2)$ mode, sharp $E(TO_2)$ mode, broad $A_1(TO_3)$/E(TO) mode, swelling $A_1(LO_2)$/E(LO) mode and broad $A_1(LO_3)$/$E(LO_3)$ mode [21]. Also, the mode of orthorhombic phase is a broad $A_1(TO_1)$, $A_1(TO_2)$, $A_1(TO_3)$/E(TO) and $A_1(LO_3)$/$E(LO_3)$ peak and sharp $E(TO_2)$ peak [21]. In the compositions, $0.00 \leq y \leq 0.02$, all of the Raman patterns show $A_1(TO_2)$, $E(TO_2)$, $A_1(LO_2)$/E(LO), $A_1(TO_3)$/E(TO) and $A_1(LO_3)$/$E(LO_3)$ at around 260, 303, 472, 517 and 720 cm^{-1}, respectively, which indicates a ferroelectric tetragonal phase. At the higher compositions, $0.04 \leq y \leq 0.10$, the $A_1(TO_1)$ mode appeared gradually at 190 cm^{-1} and $A_1(LO_2)$ /E(LO) mode at 472 cm^{-1}, but both were absent in the Raman spectrum. Therefore, the compositions, $0.06 \leq y \leq 0.10$, were considered as a signature of the ferroelectric orthorhombic phase by the presence of $A_1(TO_1)$, $A_1(TO_2)$, $E(TO_2)$, $A_1(TO_3)$/E(TO) and $A_1(LO_3)$/$E(LO_3)$ mode near 190, 222, 301, 514 and 716 cm^{-1}, respectively. A weak $A_1(TO_1)$, $A_1(TO_2)$, $E(TO_2)$, $A_1(TO_3)$/E(TO) and $A_1(LO_3)$/$E(LO_3)$ peak at the composition, y = 0.04, showed coexistence of the ferroelectric tetragonal and orthorhombic phase. These results identified that the phase transition changed from tetragonal to orthorhombic phase, which corresponds well with the XRD pattern.

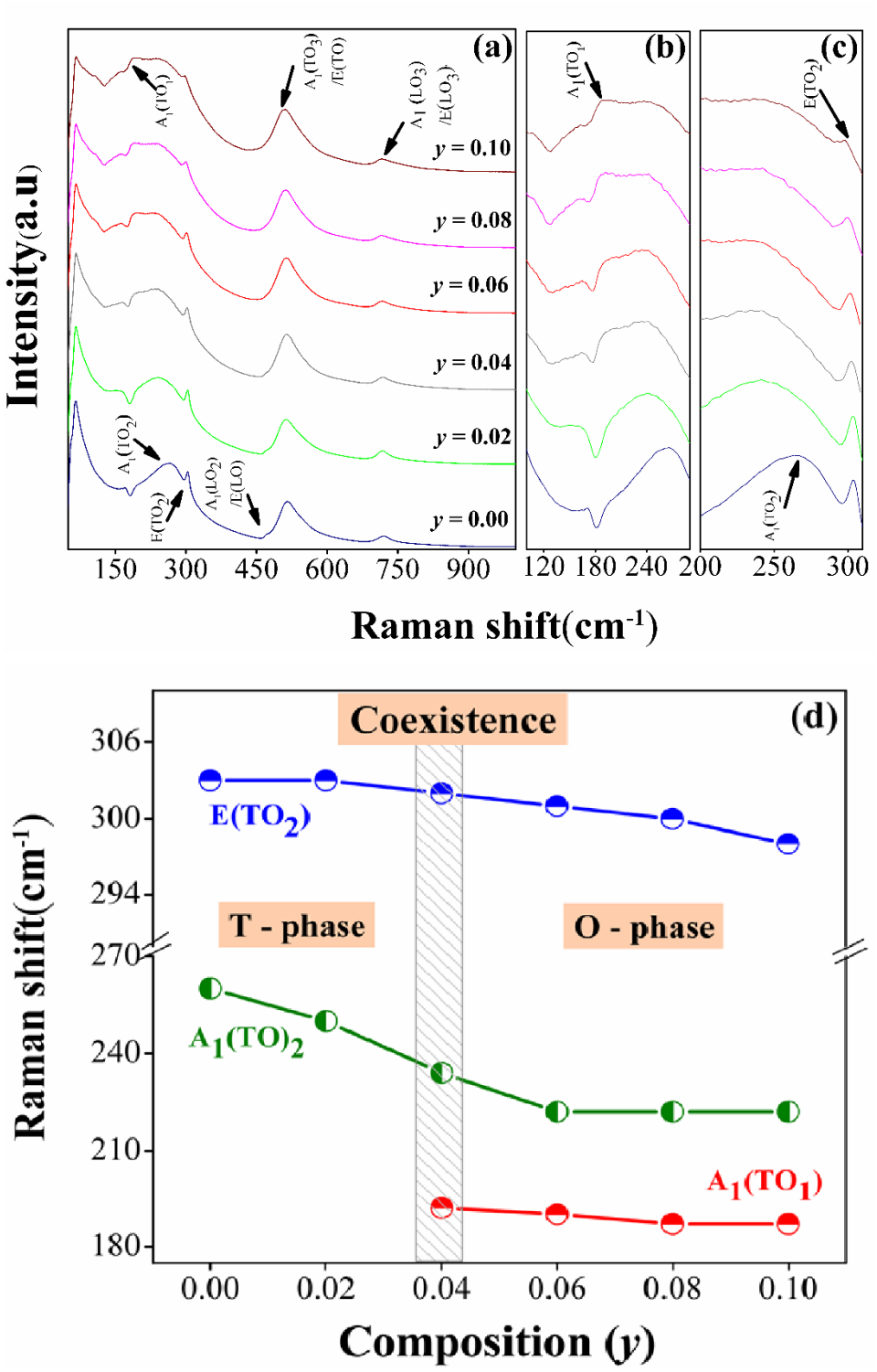

Figure 4.3 (a) Raman spectra of (0.975-*y*)$BaTiO_3$–0.025$SrTiO_3$–*y*$BaSnO_3$ ceramic at room temperature with the compositions, $0.00 \leq y \leq 0.10$, in the wave number range from 100 to 1,000 cm^{-1}, (b) enlarged Raman shift range from 100 to 290 cm^{-1}, (c) enlarged Raman shift range from 200 to 310 cm^{-1}, and (d) the relative plot between wave number cm^{-1} and composition *y*.

Figure 4.4 presents the temperature dependence of relative permittivity (ε_r) and dielectric loss ($tan\delta$) of BT–ST–*y*BS systems with *y* = 0.00, 0.02, 0.04, 0.06, 0.08 and 0.10 compositions at frequencies 1, 10 and 100 kHz. The relative permittivity curves for the composition, y = 0.00 and 0.02, exhibit one sharp peak at 110 and 97°C, respectively, with this transition being related to the transition from tetragonal (P4mm) ferroelectric to cubic (Pm3m) paraelectric phase. Nevertheless, the relative permittivity curves for the compositions, $0.04 \leq y \leq 0.08$, presented two anomalous peaks. A higher temperature was associated with the ferro-to-paraelectric phase transition, while a lower temperature suggested the phase transition from orthorhombic to tetragonal phase. The O–T phase transition temperature shifted slightly with increasing Sn content to a high temperature from 32°C for y = 0.04 – 41°C for *y* = 0.08. Furthermore, the transition temperature decreases with increasing Sn content (Fig. 4.5). The temperature range width of the tetragonal phase decreases continuously with increasing Sn content. The permittivity at room temperature is seen to increase continuously from *y* = 0.00 – 0.04 with increasing Sn content. This result is due to the shift of O–T phase transition temperature that is close to room temperature. It is known that the relative permittivity of a normal ferroelectric phase, which is above the maximum relative permittivity temperature, can be described by the Curie – Weiss law [7, 22];

$$\frac{1}{\varepsilon_r} = \frac{C}{T - T_0}\ ;\ (T > T_0) \tag{4.1}$$

where T_0 is the Curie – Weiss temperature and *C* is the Curie – Weiss constant. The relative permittivity of pure BT obeys the Curie – Weiss law, which is $T_0 \sim 383$ K and *C* $\sim 1.56 \times 10^5$ K [14]. However, further characterization of broad relative permittivity and diffuseness of the phase transition followed a modified Curie-Weiss law, as described below [23, 24]:

$$\frac{\varepsilon_m}{\varepsilon} = 1 + \frac{(T - T_m)^\gamma}{2\delta_\gamma^2}\ ;\ (T > T_m) \tag{4.2}$$

where γ is constant and ε_m is the maximum value of relative permittivity at phase transition temperature (T_m). The parameter γexpresses information on the character of the phase transition, and when γ = 1, the equation follows the Curie – Weiss law, which indicates normal ferroelectrics; while γ = 2 describes a complete diffuse phase transition. The δ value can be applied to gauge the degree of diffuseness in the phase

transition. Figure 4.6 illustrates the plot of ln $(\frac{1}{\varepsilon} - \frac{1}{\varepsilon_m})$ as a ln$(T - T_m)$ function of (0.975-*y*)$BaTiO_3$–0.025$SrTiO_3$–*y*$BaSnO_3$ systems at 1 kHz. The value of parameter γ and δ is presented in Table 1. It can be seen that parameter γ tends to increase from 1.20 to 1.37 with increasing Sn content. The δ value has a similar tendency of an increase from 12.47 to 13.40 with increasing Sn content, thus confirming that a diffuse phase transition appears in the BT–ST–*y*BS system. This result occurs when at least two cations dominate the same crystallographic site, a or b, which is found in many complex perovskite structures such as lead-free $BaZrO_3$–$CaTiO_3$–$BaTiO_3$ [11], $K_{0.5}Na_{0.5}NbO_3$–$LiSbO_3$ [25] and $(Ba_{0.85}Ca_{0.15})(Zr_{0.1}Ti_{0.9})O_3$–$Bi(Mg_{0.5}Ti_{0.5})O_3$ [26].

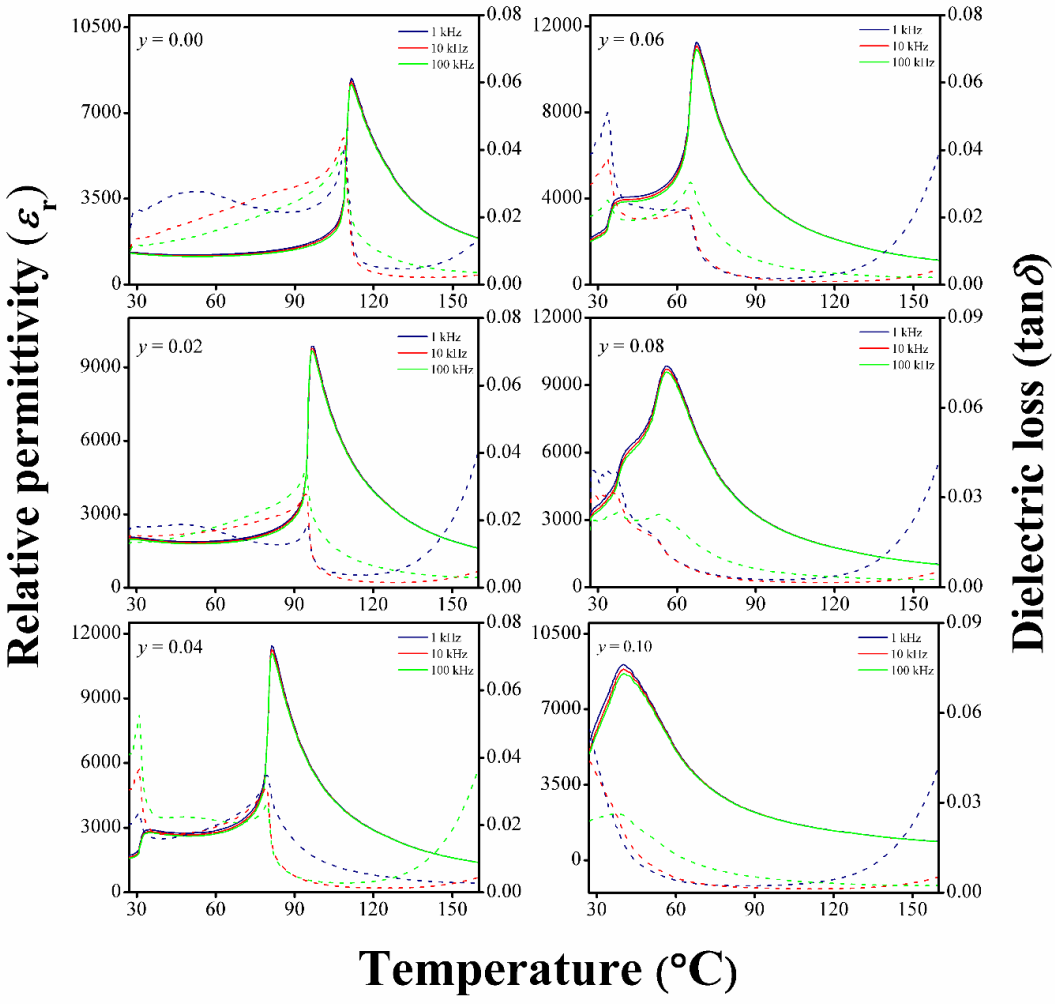

Figure 4.4 Relative permittivity (ε_r) and dielectric loss (tanδ) as temperature dependent (0.975-*y*)$BaTiO_3$–0.025$SrTiO_3$–*y*$BaSnO_3$ ceramic with compositions, $0.00 \leq y \leq 0.10$.

Table 4.1 The dielectric ferroelectric and piezoelectric properties of (0.975-*y*)$BaTiO_3$ 0.025$SrTiO_3$–*y*$BaSnO_3$ ceramic with the composition, $0.00 \leq y \leq 0.10$.

y	T_C (℃)	$\varepsilon_{r\,max}$ at 1 kHz	$\tan\delta_{\,room}$ at 1 kHz	γ	δ_γ	P_r (μC/cm^2)	E_c (kV/cm)	R_{sq}	d_{33}^* (pm/V)	d_{33} (pC/N)
0.00	110	8400	0.02	1.20	12.5	12.9	7.0	0.80	702	260
0.02	97	9850	0.02	1.21	12.6	12.5	6.4	0.80	835	320
0.04	81	11430	0.02	1.24	12.8	13.1	5.4	0.77	1280	450
0.06	68	11250	0.04	1.25	12.8	10.5	4.4	0.83	840	370
0.08	56	9850	0.04	1.30	13.1	7.5	3.2	0.73	830	200
0.10	41	11000	0.05	1.37	13.4	6.9	3.1	0.72	740	120

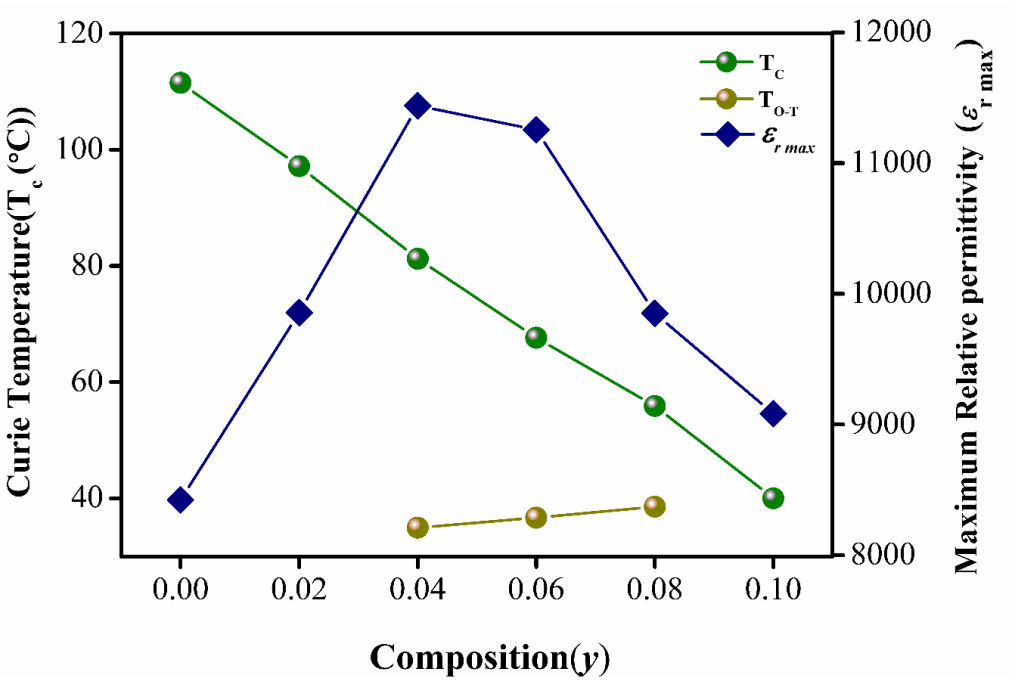

Figure 4.5 The relative plot between Curie temperature (T_C) and maximum relative permittivity ($\varepsilon_{r\,max}$) at 1 kHz of (0.975-*y*)$BaTiO_3$–0.025$SrTiO_3$–*y*$BaSnO_3$ ceramic as a function of composition *y*.

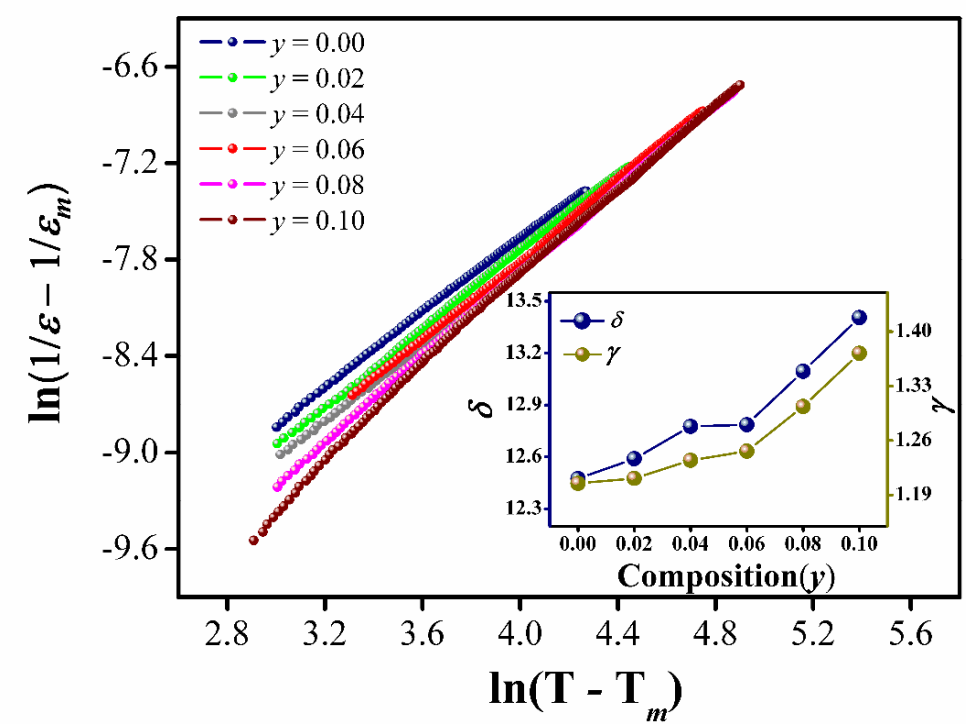

Figure 4.6 The relative plot between ln $\left(\frac{1}{\varepsilon}-\frac{1}{\varepsilon_m}\right)$ and ln$(\boldsymbol{T}-\boldsymbol{T_m})$.

In order to investigate the ferroelectric behavior in BT–ST–*y*BS ceramics, the electrical polarization hysteresis loop of each composition was measured at room temperature with an electric field of 60 kV/cm. Figure 4.7a illustrates the polarization–electric field hysteresis loop for all compositions of *y* at a frequency of 4 Hz. All BT–ST–*y*BS ceramics with *y* = 0.00–0.10 compositions exhibit symmetry in shape and well-saturated hysteresis loops and result in domain switching in an electric field. The plot of P_r and E_c value as a function of composition *y* is presented in Fig. 4.7b. It can be seen that the P_r initially tends to increase from 12.93 μC/cm^2 at *y* = 0.00 to a maximum value of 13.14 μC/cm^2 at *y* = 0.04, and then it decreases gradually from 10.48 μC/cm^2 at *y* = 0.06 – 6.95 μC/cm^2 at *y* = 0.10. In addition, the E_c values decrease clearly from 7.00 to 3.08 kV/cm with increasing Sn content, as shown in Fig. 4.7b. The decrease in E_c indicates that ceramics become ‘‘softer’’ with increasing Sn content, regarding the electric field, because the free energy profile for polarized rotation is flattened anisotropically at the two phases and multiphase coexistence [12, 27]. In order to investigate the changes in hysteresis loop behavior, the empirical relationship between P_r, P_s and polarization at fields above E_c was proposed by Haertling and Zimmer for calculating squareness of the hysteresis loop as follows [28]:

$$R_{sq} = \frac{P_r}{P_s} + \frac{P_{1.1E_C}}{P_r} \tag{4.3}$$

where *R*sq is the squareness of the hysteresis loop, and P_r and P_s are remanent and saturated polarization, respectively. $P_{1.1Ec}$ is polarization at an increasing electric field of 1.1 times the coercive field (E_c). The squareness parameter investigates the quantification of changes in P–E hysteresis loops. The *R*sq is equal to 2 for an ideal P–E hysteresis loop. The calculated *R*sq values of all ceramics are inferred in Table 4.1. It was found that the *R*sq parameter tended to decrease from 0.80 to 0.72 with increasing Sn content, which implies that the P – E hysteresis loop becomes more slanted.

Figure 4.8a displays the unipolar electric field induced strain curve for the BT–ST–*y*BS ceramic, with y = 0.00 – 0.10 compositions, measured at 10 kV/cm. It can be observed that with increasing Sn content, the unipolar strain increases with increasing *y* of up to 0.04 and reaches the maximum electrostrain value of 0.13%. On increasing *y* further to 0.1, the unipolar strain decreases to 0.074%. Figure 4.8b illustrates the

direct piezoelectric coefficient (d_{33}) and a normalized strain or converse piezoelectric coefficient (d_{33}^{*} = S_{max}/E_{max}) at the electric field of 10 kV/cm as a function of composition. It can be observed that the d_{33}^{*} value tends to increase with increasing composition *y* and reaches its maximum at about 1280 pm/V at *y* = 0.04, before decreasing with increasing composition *y*. The d_{33} values also have a similar trend and maximum d_{33} values of 450 pC/N, as y increases to 0.04. As a result, ceramic at the composition, *y* = 0.04, exhibits the highest normalized strain and piezoelectric constant in the systematic series studied, due to the coexistence of orthorhombic and tetragonal phase near room temperature. The enhanced d_{33} and d_{33}^{*} values are considered to be reasonably consistent with the multiphase coexistence of the orthorhombic and tetragonal phase that occurs near ambient temperature at *y* = 0.04. In the point view of crystallographic symmetry, there are 18 domain orientation states (6 domain states along 100c direction for tetragonal symmetry and 12 along 110c direction for orthorhombic symmetry) near the O–T phase transitions. In general, a large number of thermodynamically equivalent states near O–T phase transitions allow a high degree of ferroelectric dipole alignment. This causes instability, multiple polarization and strain variants, so that the direction of polarization is rotated easily by external stress or the electric field, thus making it much easier for different grains to coordinate in a collective response.

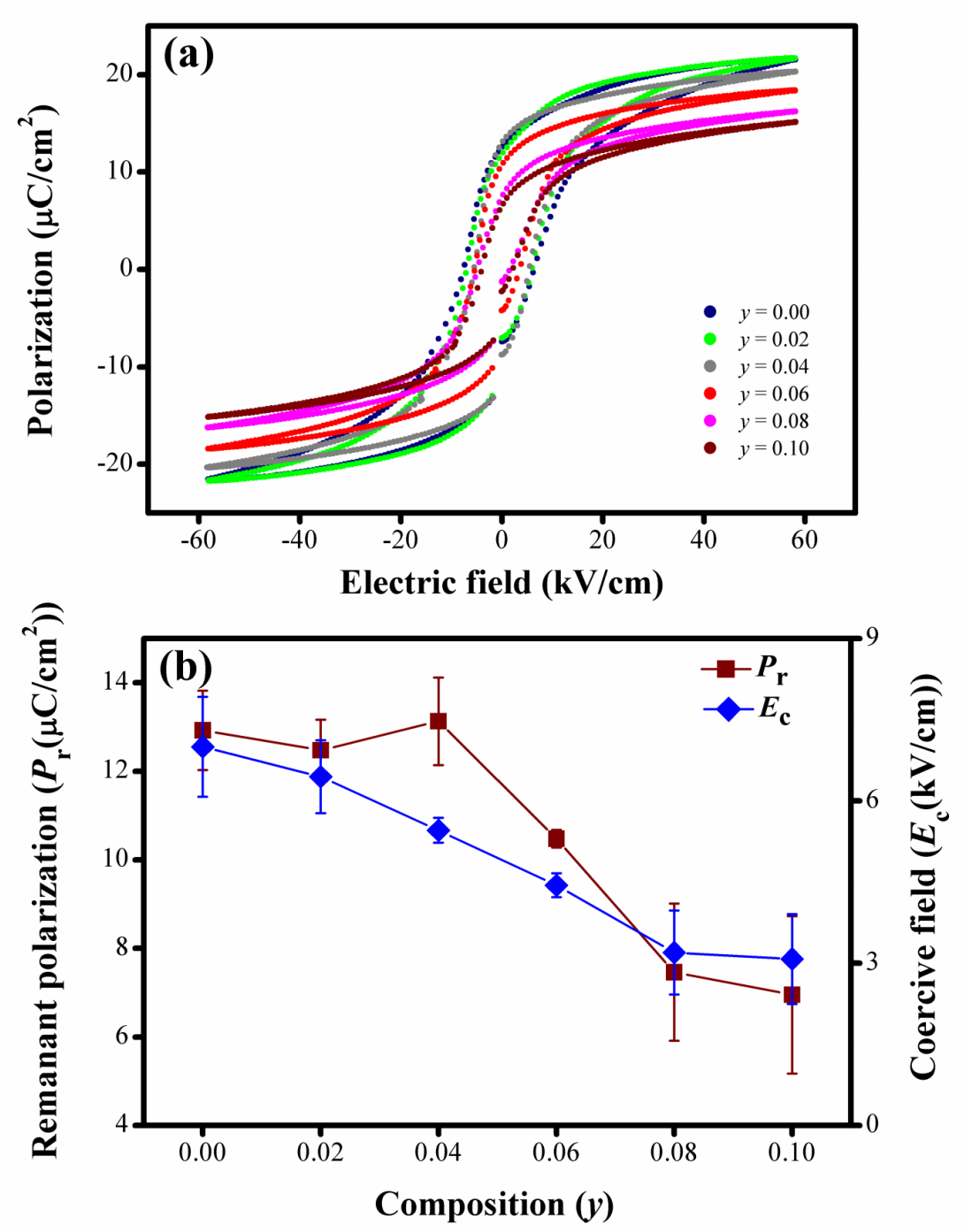

Figure 4.7 (a) The plot between polarization (μC/cm^2) and electric field (kV/cm) as a function of composition *y*, and (b) the plot of remanant polarization (μC/cm^2) and coercive field (kV/cm) value as a function of composition *y*.

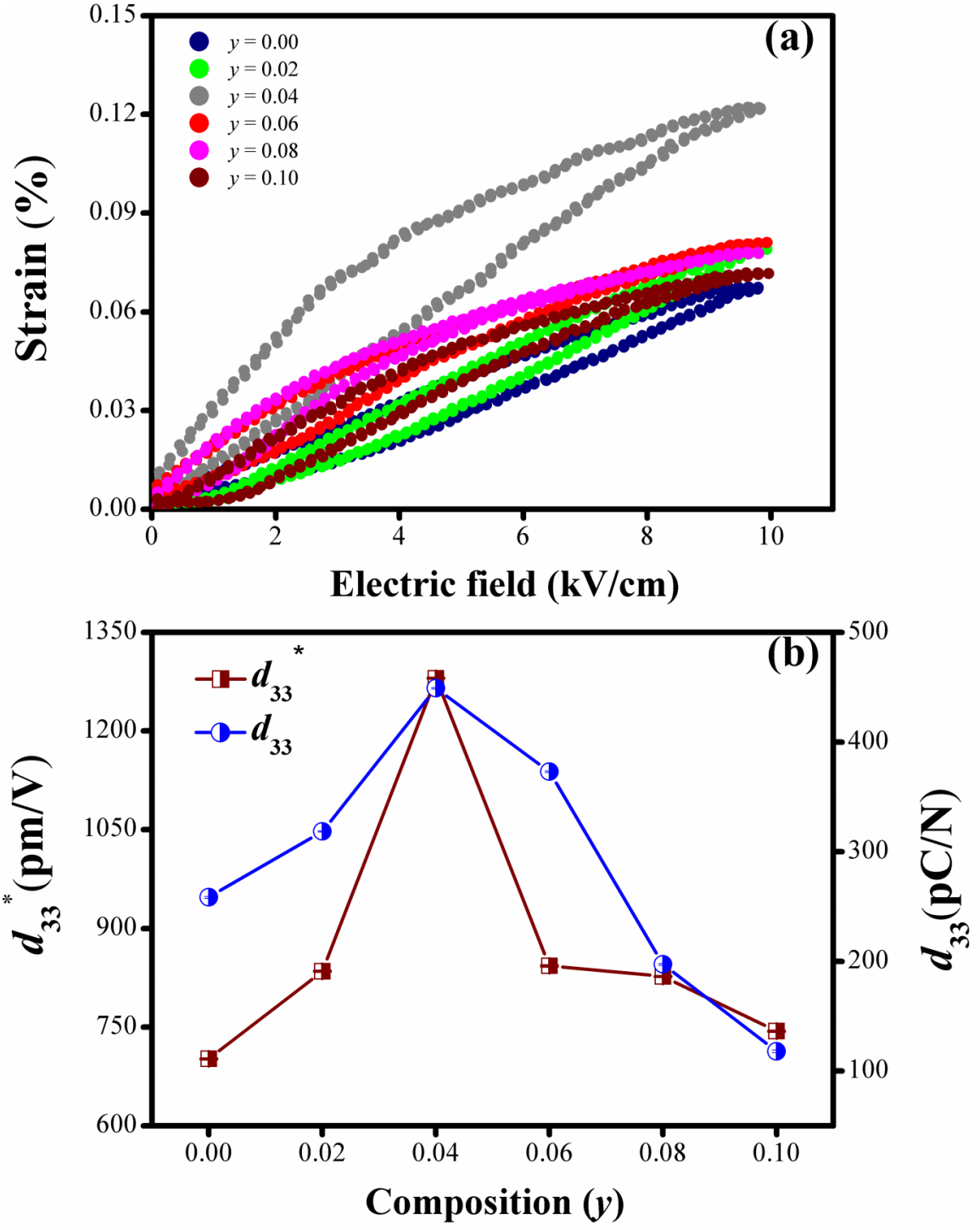

Figure 4.8 (a) The relative plot between unipolar strain (%) and electric field (kV/cm) as a function of composition, and (b) the plot of normalized strain (d_{33}^{*}(pm/V)) and piezoelectric constant (d_{33}(pC/N)) value as a function of composition *y*.

4.4 Conclusion

BT–ST–*y*BS ceramic was fabricated by the conventional solid – state reaction method. Raman and XRD study indicates that the orthorhombic and tetragonal phases coexist near ambient temperature at y = 0.04. Enhanced dielectric, ferroelectric and piezoelectric properties of $\varepsilon_{\mathbf{r\,max}} \sim$ 11500, $P_r \sim$ 13.14 μC/cm^2, $d_{33}^{*} \sim$ 1280 pm/V and $d_{33} \sim$ 450 pC/N were obtained as samples at y = 0.04. This observation indicated that the BT–ST–*y*BSn system is a promising candidate for lead–free piezoelectric ceramics.

4.5 References

[1] Zhang, S., Xia, R., and Shrout, TR. 2007. "Lead-free piezoelectric ceramics vs. PZT?" **J. Electroceram**. 19(4) : 251–257.

[2] Rodel, J., Jo, W., Seifert, KTP., Anton, EM., Granzow, T., and Damjanovic, D. 2009. "Perspective on the development of lead free piezoceramics." **J. Am. Ceram. Soc.** 92(6): 1153–1177

[3] Panda, PK. 2009 "Review: environmental friendly lead-free piezoelectric materials." **J. Mater. Sci.** 44(19): 5049–5062. doi: 10.1007/s10853-009-3643-0.

[4] Takenaka, T., and Nagata, H. 2005 "Current status and prospects of lead-free piezoelectric ceramics." J. Eur. Ceram. Soc. 25(12): 2693–2700.

[5] Beuerlein, MA., Kumar, N., Usher, TM., Brown-Shaklee, HJ., Raengthon, N., Reaney, IM., Cann, DP., Jones, JL., and Brennecka, GL. 2016. "Current understanding of structure–processing–property relationships in $BaTiO_3$–$Bi(M)O_3$ dielectrics." **J. Am. Ceram. Soc.** 99: 2849–2870.

[6] Randall, CA, Newnham, RE, Cross LE (2004) History of the first ferroelectric oxide, $BaTiO_3$.https://ceramics.org/wpcontent/uploads/2009/.../first_ferroelectric _oxide_ba_tio3.pdf. Accessed 10 Mar 2017.

[7] Moulson, AJ. and Herbert, JM. 2003. "Electroceramics: materials, properties, applications." Wiley, New York.

[8] Bechmann, R. 1956. "Elastic, Piezoelectric, and Dielectric Constants of Polarized Barium Titanate Ceramics and Some Applications of the Piezoelectric Equations" **J. Acoust. Soc. Am.** 28(3): 347-350.

[9] Li, W., Xu, ., Chu, R., Fu, P., and Zang, G. 2010. "Piezoelectric and dielectric properties of $(Ba_{1-x}Ca_x)(Ti_{0.95}Zr0.0_5)O_3$ leadfree ceramics. **J. Am. Ceram. Soc.** 93(10): 2942–2944.

[10] Sutapun, M., Vittayakorn, W., Muanghlua, R., and Vittayakorn, N. 2015. "High piezoelectric response in the new coexistent phase boundary of $0.87BaTiO_3$–$(0.13\text{-}x)BaZrO_3$–$xCaTiO_3$" **Mater. Design** 86: 564–574.

[11] Chaiyo, N., Cann, DP., Vittayakorn, N. 2015. "Phase transitions, ferroelectric, and piezoelectric properties of lead-free piezoelectric $xBaZrO_3$–$(0.25\text{-}x)CaTiO_3$–0.75 $BaTiO_3$ ceramics." **J. Mater. Sci.** 50(18): 6171–6179. doi:10.1007/s10853-015-9174y.

4.5 References (II)

[12] Yao, Y., Zhou, C., Duchao, LV., Wang, D., Wu, H., Yang, Y., and Ren, X. 2012. "Large piezoelectricity and dielectric permittivity in BaTiO – $xBaSnO_3$ systems: The role of phase coexisting" **EPL.** 98(2): 27008.

[13] Wang, X., Yamada, H., and Xu, C-N. 2005. "Large electrostriction near the solubility limit in $BaTiO_3$ – $CaTiO_3$ ceramics" **Appl. Phys. Lett.** 86(2): 022905-1-022905-3.

[14] Zhang, S-W., Zhang, H., Zhang, B-P., and Yang, S. 2010. "Phase-transition behavior and piezoelectric properties of lead-free $(Ba_{0.95}Ca_{0.05})(Ti_{1-x}Zr_x)O_3$ ceramics" **J. Alloy Compd.** 506(1) : 131–135.

[15] Zhu, L-F., Zhang, B-P., Zhao, X-K., Zhao, L., Zhou, P-F., and Li, J-F. 2013. "Enhanced Piezoelectric Properties of $(Ba_{1-x}Ca_x)(Ti_{0.92}Sn_{0.08})O_3$ Lead-Free Ceramics" **J. Am. Ceram. Soc.** 96(1) : 241–245.

[16] Zhu, L-F., Zhang, B-P., Zhao, X-K., Zhao, L., Yao, F-Z., Han, X., Zhou, P-F., and Li J-F. 2013. "Phase transition and high piezoelectricity in $(Ba,Ca)(Ti_{1-x}Sn_x)O_3$ lead-free ceramics" **Appl. Phys. Lett.** 103(7): 072905.

[17] Li, H-R., Chen, C-X., and Zheng, R-K. 2015. "Effects of Sr substitution on the structural, dielectric, ferroelectric, and piezoelectric properties of $Ba(Zr,Ti)O_3$ lead free ceramics" **J. Mater. Sci. – Mater. El.** 26(5): 3057–3063. doi: 10.1007/s10854-015-2797-6**.**

[18] Lee, C-E., Randall, CA., Kim, D-Y., Kim, SH. 2014. "Multi-site and multi-ionization of Sn in the doping of $BaTiO_3$". **J. Am. Ceram. Soc.** 97(2): 513–518.

[19] Shoichiro, S., Toshikazu, T., Akira, A., Takashi, O., Nobuyuki, W., Hideaki, N., and Hiroshi. T, 2010. "Effect of Sn^{2+} ion substitution on dielectric properties of (Ba, Ca)TiO_3 ferroelectric ceramics." **Jpn. J. Appl. Phys.** 49(9S): 09MC04–09MC05**.**

[20] Karan, N., Katiyar, R., Maiti, T., Guo, R., and Bhalla, A. 2009. "Raman spectral studies of Zr^{4+}-rich $BaZr_xTi_{1-x}O_3$ ($0.5 \leq x \leq 1.00$) phase diagram." **J. Raman Spectrosc.** 40(4): 370–375**.**

[21] Dobal, P., Dixit, A., Katiyar, R., Yu, Z., Guo, R., and Bhalla, A. 2001. "Micro-Raman scattering and dielectric investigations of phase transition behavior in the $BaTiO_3$–$BaZrO_3$ system." **J. Appl. Phys.** 89(12): 8085–8091

4.5 References (III)

[22] Vittayakorn, N., Rujijanagul, G., Tan, X., Marquardt, MA., and Cann, DP. 2004. "The morphotropic phase boundary and dielectric properties of the $xPb(Zr_{1/2}Ti_{1/2})O_3$-$(1 - x)Pb(Ni_{1/3}Nb_{2/3})O_3$ perovskite solid solution." **J. Appl. Phys.** 96(9): 5103–5109.

[23] Jaffe, B., Cook, WR., and Jaffe, H. 1971. "Piezoelectric Ceramics" Academic Press, London.

[24] Cross, LE. 1987. "Relaxor ferroelectrics." **Ferroelectrics** 76(1): 241–267.

[25] Palei, P., Sonia, and Kumar, SP. 2012. "Dielectric, ferroelectric and piezoelectric properties of (1 – x)[K0.5Na0.5NbO3] – x[LiSbO3] ceramics" **J. Phys. Chem. Solids** 73(7) : 827 – 833.

[26] Bai, W., Hao, J., Shen, B., and Zhai, J. 2013. "Dielectric properties and relaxor behavior of high Curie temperature $(Ba_{0.85}Ca_{0.15})(Zr_{0.1}Ti_{0.9})O_3$ – $Bi(Mg_{0.5}Ti_{0.5})O_3$ Lead – free ceramics" **Ceram. Int.** 39: 19 – 23.

[27] Liu, W., Ren X (2009) Large piezoelectric effect in Pb–free ceramics. **Phys. Rev. Lett.** 103(25): 257602.

[28] Haertling, GH., and Zimmer, W. 1966. "An analysis of hot-pressing parameters for lead zirconate – lead titanate ceramics containing two atom percent bismuth." **Am. Ceram. Soc. Bull.** 45(12): 1084 – 1089.

CHAPTER 5

DIELECTRIC, FERROELECTRIC AND PIEZOELECTRIC PROPERTIES OF THE LEAD FREE $0.9BaTiO_3$–$(0.1-x)Bi_{0.5}Na_{0.5}TiO_3$–$xBi(Mg_{0.5}Ti_{0.5})O_3$ SOLID SOLUTION

Based on article published in Ferroelectrics

Solid solution of $0.9BaTiO_3$–$(0.1-x)Bi_{0.5}Na_{0.5}TiO_3$–$xBi(Mg_{0.5}Ti_{0.5})O_3$ (BT–BNT–*x*BMT) system, where x = 0.00, 0.02, 0.04, 0.06, 0.08, 0.10, was synthesized by the solid state reaction. Dense BT–BNT–*x*BMT ceramics were obtained by sintering at 1,150–1,250°C for 4 h. The effect of BMT on crystal structure and electrical property of BT-BNT ceramics was investigated as a function of composition, x, using X-ray diffraction, dielectric spectroscopy, hysteresis and strain measurements. The crystal structure of solid solution BT–BNT–*x*BMT, where x = 0.00-0.10, successively transforms from tetragonal to pseudocubic symmetry, with increased BMT concentration. Temperature dependence of dielectric constant (ε_r) and dielectric loss ($tan\delta$) for BT–BNT–*x*BMT at various frequencies showed that phase transition of ceramics changed from ferroelectric to relaxor-like behavior as BMT content increased. Furthermore, remanent polarization (P_r), coercive field (E_c) and the normalized strain (d_{33}^*) of BT–BNT–*x*BMT ceramics tend to decrease with increasing BMT concentration.

5.1 Introduction

Lead zirconate titanate (PZT) ceramics have been used widely in many electronic devices such as piezoelectric sensor, actuators and transducers because of their excellence piezoelectric properties [1]. However, PZT–based piezoelectric ceramics are not environmental friendly because more than 60% wt of these ceramics contains the lead toxicity. Furthermore, the EU legislation forced draft directives including Waste from Electrical and Electronic Equipment (WEEE) and Restriction of Hazardous Substances (RoHS). According to the environmental issues, lead free friendly

piezoelectric ceramics have been received considerable attentions to replace lead-based piezoelectric materials.

Although no real lead free materials can be replaced the common use in lead-based ceramics for various applications, many potentially promising lead free materials have been developed. Among the lead free materials, Barium titanate ($BaTiO_3$; BT) has perovskite structure and good electrical properties such as ferroelectric and piezoelectric properties but low Curie temperature (T_C) [2]. In recent years, there are many researches about BT-base for example $Ba_{0.85}Ca_{0.15}Ti_{0.90}Zr_{0.10}O_3$ [3] and (1-x)$Ba_{0.98}Ca_{0.02}Ti_{0.94}Sn_{0.06}O_3$–x$Ba_{0.85}Ca_{0.15}Ti_{0.90}$-$Zr_{0.10}O_3$ [4]. Jiagang Wu *et al.* [4] found that BT-base ceramic by combining (1-x)$Ba_{0.98}Ca_{0.02}Ti_{0.94}Sn_{0.06}O_3$–*x*$Ba_{0.85}Ca_{0.15}Ti_{0.90}Zr_{0.10}O_3$((1-x)BCTS–*x*BCTZ) system has a phase boundary coexistence of orthorhombic and tetragonal phase at around 4 mol% BCTZ which show good dielectric and piezoelectric properties of dielectric constant ($\varepsilon_r \sim$ 5500), dielectric loss ($tan\delta \sim$ 0.3%) and piezoelectric constant ($d_{33} \sim$ 407 pC/N). The binary system of $Bi_{0.5}Na_{0.5}TiO_3$–$BaTiO_3$ (BNT-BT) is an important candidate for replacing lead-based piezoelectric. In a few decades, BNT–BT solid solution was studied by various research groups [2,5,6]. Takenaka *et al.* [5] found that BNT-BT system has a morphotrobic phase boundary (MPB) between rhombohedral and tetragonal phases at around 6-7 mol% BT which shows the excellent properties including $\varepsilon_{33}^T/\varepsilon_0$ = 580, piezoelectric constant (d_{33} = 125 pC/N), Curie temperature (T_C =288°C), dielectric loss ($tan\delta$ = 1.3 %) and planar coupling coefficient (k_{33} = 55.0%). Afterwards, researchers focused to develop BNT–BT binary material on the composition range of MPB by doing ternary solid solution such as KNN-modified BNT–BT [7,8] and BZr–modified BNT–BT [9]. Also, the BNT–BT based systems on the BNT–rich side have been investigated extensively for example (0.94-*x*)BNT–0.06BT–*x*KNN [7], 0.865BNT–0.350BT–0.100BKT [8] and BZr–modified BNT–BT [9]. However, few works have investigated and developed BNT–BT on the BT–rich side. Recently, Wada et al. studied on the combination between $BaTiO_3$ and $Bi(Mg_{0.5}Ti_{0.5})O_3$ (BMT) and found that BMT can enhance Curie temperature (T_C) of BT with the highest T_C (about 360°C) for 0.5$BaTiO_3$–0.5BMT ceramics [10]. Moreover, Qi Wang et al. have studied lead free $Bi_{0.5}Na_{0.5}TiO_3$–$Bi(Mg_{0.5}Ti_{0.5})O_3$ systems and reported that BMT can improve piezoelectric properties and enhance T_C of BNT ceramic. The 0.95BNT–0.05BMT ceramic showed the highest d_{33} about 110 pC/N and high T_C at 352°C [11].

This work dealt with the new ternary system of $0.9BaTiO_3$–$(0.1\text{-}x)Bi_{0.5}Na_{0.5}TiO_3$–$xBi(Mg_{0.5}Ti_{0.5})O_3$ in order to get more information of BT–BNT-based on BT–rich side. BT–BNT–*x*BMT ceramics were prepared by the solid state reaction. The effect of BMT on crystal structure, phase transition and electrical properties were studied as a function of composition, *x*.

5.2 Experimental procedure

Lead free $0.9BaTiO_3$–$(0.1\text{-}x)Bi_{0.5}Na_{0.5}TiO_3$–$xBi(Mg_{0.5}Ti_{0.5})O_3$ (BT–BNT–*x*BMT) ceramics, where x = 0.00, 0.02, 0.04, 0.06, 0.08, 0.10, were synthesized by the solid state reaction. Bi_2O_3 (99.9%, Sigma-Aldrich), $BaCO_3$ (98.5%, Fluka), Na_2CO_3 (99.8%, Riedel-deHaen), TiO_2 (99.9%, Sigma-Aldrich) and MgO (99%, Fluka) powders were used raw materials. First, stoichiometric amounts of raw materials were weighted and ball-milled with yttrium-stabilized zirconia in ethanol media for 18 hours. After drying the mixture for 24 hours in an oven, the mixed powder was calcined at 900 for 4 hours with heating/cooling rate 10°C/min. In order to obtain fine particles prior to making a pellet, the calcined powders were ground and sieved. The fine powders were pressed into disks with 15 mm diameter. 5 wt% polyvinyl alcohol as a binder was used as binder. The disks were sintered at 1150 – 1250°C for 4 hours with heating/cooling rate 5°C/min. The crystal structure of ceramics was characterized using X–ray diffraction (Bruker – AXS D 8 Advance) with Cu(K_α) radiation in the 2θ scan range of 20 – 80°. For electrical measurements, the samples were polished for both sides and made parallel before electrode coating with silver paste (C1000, Heraeus) on both surfaces. Silver paste was heated on at 750°C for 20 mins with heating/cooling rate 5°C/min. The relative permittivity (ε_r) and dielectric loss ($tan\delta$) were determined as a function of frequency (1 – 100 kHz) and temperature (room temperature to 250°C) using LCR meter (HP4284A, Hewlett-Packard, Palo Alto, CA). Polarization-electric field (P – E) hysteresis loop were determined at room temperature using Radiant Technologies, Inc (RT66A). The strain-electric field (S – E) curves were determined using MTI-2100 Fotonic sensor combined with Radiant Technologies. The peak field for P – E hysteresis loop and S – E curve measurements was maintained at 60 kV/cm during measurement. The surface morphology of ceramics was observed using scanning electron microscope (EVO®MA10).

5.3 Results and discussion

The X-ray diffraction patterns of BT–BNT–*x*BMT ceramics, where x = 0.00, 0.02, 0.04, 0.06, 0.08, 0.1, are shown in Figure 5.1(a). It indicates that all samples are a single phase with the perovskite structure. The secondary and other phases were not observed in the XRD patterns, which indicates that all compositions in the BT–BNT–*x*BMT system can completely form solid solution with a perovskite structure. A (111) peak at around 39° was chosen to identify the crystal structure of BT-BNT-*x*BMT ceramics as shown in figure 5.1(b). In the compositions, $0.00 \leq x \leq 0.08$, the crystal structure has a tetragonal symmetry, identified by a splitting of the (002) and (200) peaks. At the higher BMT content of x = 0.1, the doublet of (002) and (200) peaks become a single peak of (200) and the (111) peak still exhibits a single peak. These results indicated that the crystal structure changed to a pseudocubic symmetry.

The average ionic radius of A – site and B – site, calculated lattice parameters, the tetragonality c/a ratio and tolerance factor of each composition are listed in Table 5.1. The tetragonality c/a ratio is the important factor representing the lattice distortion of the tetragonal symmetry. It is seen that the c/a ratio decreases significantly with increasing BMT content. The ionic radii of Bi^{3+} (CN = 12, 1.40 Å) are smaller than the ionic radii of Ba^{2+} (CN = 12, 1.61 Å) resulting in the decreasing of average ionic radii at A-site [12]. Also, the substitution of Ti^{4+} ions (CN = 6, 0.605 Å) by Mg^{2+} (CN = 6, 0.72 Å) results in the increasing of average ionic radii at B-site as shown in Table 5.1. Then, it is reasonable to assume that the substitution of BMT into BT–BNT leads to the distortion and deformation of tetragonal structure. Furthermore, the tolerance factor (t) is important factor that reflecting the perovskite structure distortion, rotation and tilt of the BO_6 octahedra [13]. Generally, the perovskite structure is stable in the range of $0.880 < t < 1.090$ region [14] and the symmetry is higher as the t value is approach to 1. It is also noticed that the t for BT–BNT–*x*BMT ceramics tends to decrease with increasing BMT which corresponds well with the phase transition from tetragonal to pseudocubic symmetry.

Based on the XRD data, it could be said that the combination between BT–BNT and BMT could form completely crystalline solid solution of perovskite structure but the existence of BMT caused the tetragonality of BT–BNT decrease.

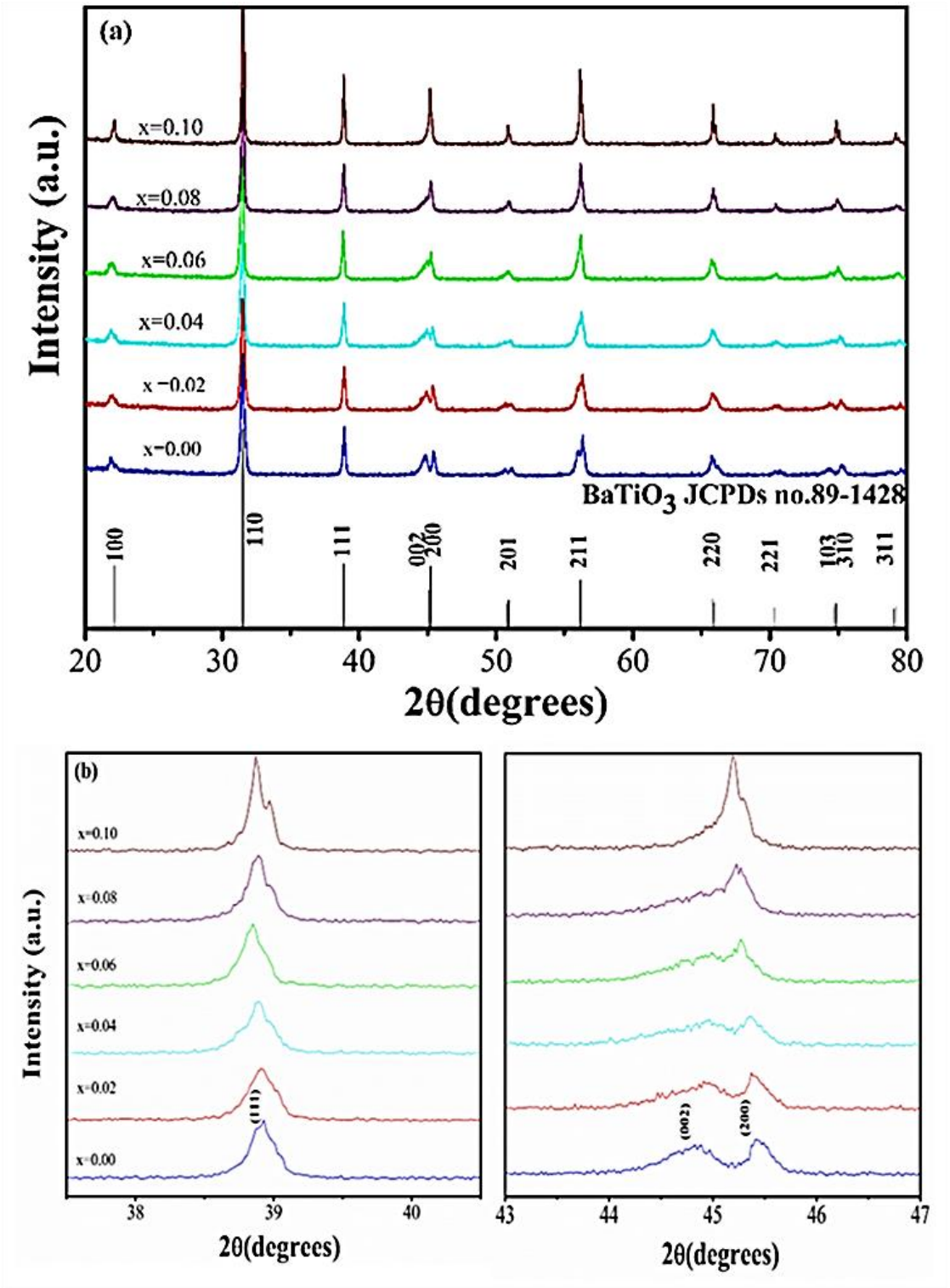

Figure 5.1 (a) X-ray diffraction patterns of BT–BNT–*x*BMT ceramics with the composition $0.00 \leq x \leq 0.10$ (b) X-ray diffraction patterns for (111), (002) and (200) peaks of BT–BNT–*x*BMT ceramics with the composition $0.00 \leq x \leq 0.10$.

Table 5.1 Lattice parameters and lattice anisotropy of BT–BNT–*x*BMT ceramics with the composition $0.00 \leq x \leq 0.10$.

x	Crystal Structure	Ionic radii (Å)		Tolerance factor (*t*)	Lattice parameter(Å)		c/a
		A - site	B - site		a	c	
0.00	T	1.5910	0.6050	1.0548	3.9590 ± 0.0792	4.1086 ± 0.2924	1.0378
0.02	T	1.5906	0.6062	1.0541	3.9847 ± 0.0518	4.0619 ± 0.1678	1.0194
0.04	T	1.5902	0.6073	1.0534	3.9792 ± 0.0500	4.0675 ± 0.1641	1.0222
0.06	T	1.5898	0.6085	1.0526	3.9969 ± 0.0421	4.0282 ± 0.0456	1.0078
0.08	T	1.5894	0.6096	1.0519	4.0017 ± 0.0159	4.0131 ± 0.0118	1.0029
0.10	PC	1.5890	0.6107	1.0511	4.0066 ± 0.0049	-	-

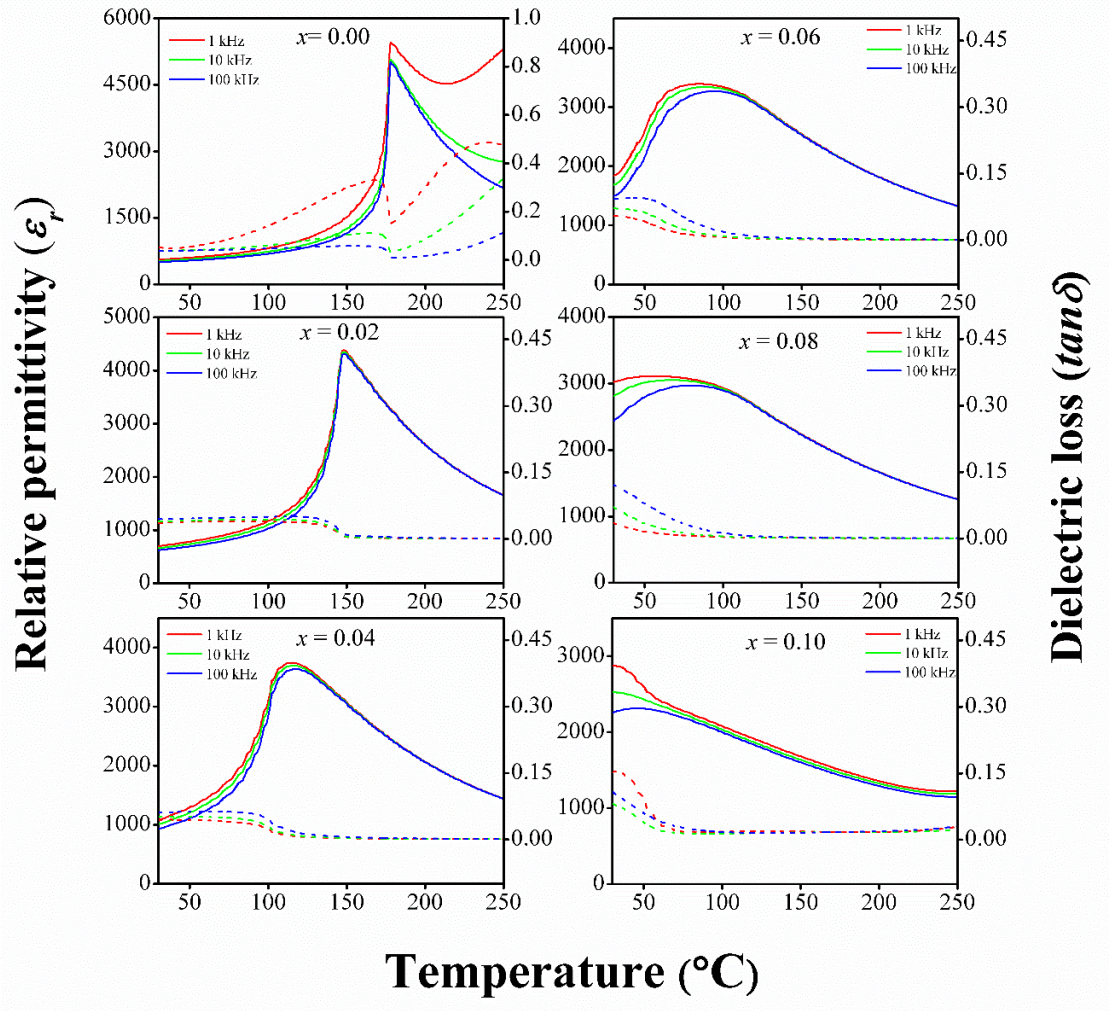

Figure 5.2 Relative permittivity (ε_r) and dielectric loss ($tan\delta$) as a temperature dependence of BT–BNT–*x*BMT ceramics with the composition $0.00 \leq x \leq 0.10$.

Figure 5.2 illustrates the temperature dependence of the relative permittivity (ε_r) and dielectric loss ($tan\delta$) of BT–BNT–*x*BMT ceramics measured at various frequencies between 1 and 100 kHz. Regarding the composition, x = 0.00, the relative permittivity of 0.9BT-0.1BNT increased slowly until the temperature approached transition temperature, then it abruptly increased and passed through a maximum of about 178°C. This discontinuity of dielectric constant at phase transition is characteristic of the first order phase transition [15] and occurs from the change of the tetragonal ferroelectric (FE) phase into the cubic paraelectric (PE) phase, in agreement with previous reports [2]. The relative permittivity curves at the compositions, $0.02 \leq x \leq 0.10$, showed only one phase transition. The composition, x = 0.02, showed a

broadening dielectric peak which much like the characteristic of relaxor ferroelectric, however the position of the peaks keep unchanged at various applied frequency. At higher composition, $0.04 \leq x \leq 0.10$, the diffuse phase transition behaviour with broad maximum and frequency dispersion became more self–evident when BMT concentration increased. Also, the transition temperature is dependent of frequency and increases with increasing frequency. These results indicated that BT–BNT–*x*BMT progressively change from normal ferroelectric to relaxor ferroelectric when BMT concentration increases. This phenomenon of BT–BNT–*x*BMT system resulted from the substitutions of Bi^{3+} ions for Na^{+} ions and Mg^{2+} ions for Ti^{4+}, which distort the unit cell and change dipole moment. For complex perovskite compound, the more cations occupy the equivalent crystallographic site of A or B, the more the chemical fluctuation and structural disorder in arrangement of cations are inhomogeneous at the nanometre scale, then the relaxation characteristic becomes more distinctly [16, 17].

In order to further characterize the relaxor behavior, a modified Curie – Weiss law in equation (1) was used for description a broad relative permittivity and diffuseness of phase transition [18, 19].

$$\frac{\varepsilon_m}{\varepsilon} = 1 + \frac{(T-T_m)^{\gamma}}{2\delta_{\gamma}^{2}} \tag{5.1}$$

Where, ε_m is the maximum value of relative permittivity and T_m is the temperature of dielectric maximum. The γ value expresses the degree of dielectric relaxation in relaxor ferroelectric material which this value is in the range of $1 \leq \gamma \leq 2$. When γ value is equal 1, Eq. (1) becomes the classic Curie Weiss law valid in the case of normal ferroelectric. When γ value is equal 5.1, the ideal relaxor behavior with quadratic dependence is described. The parameter δ_{γ} is the diffuse parameter which can be used to determine the degree of diffuseness in the phase transition. The δ_{γ} value can be observed from the slope of $\varepsilon_m'/\varepsilon'$ versus $(T - T_m)^2$, which should be linear. Plot of $\ln\left(\frac{1}{\varepsilon} - \frac{1}{\varepsilon_m}\right)$ as function of $\ln(T - T_m)$ at 100 kHz of BT–BNT–*x*BMT ceramics are displayed in figure 5.3. By plotting $\ln\left(\frac{1}{\varepsilon} - \frac{1}{\varepsilon_m}\right)$ versus $\ln(T - T_m)$, the γ value can be determined directly from the gradient. The γ and δ_{γ} values are determined and shown in Table 5.2. It is clearly seen that both δ_{γ} and γ values tend to increase with increasing

of the BMT content, confirming the relaxor behavior in these solid solution. Based on the dielectric data, a slim P-E hysteresis loop in BT–BNT–*x*BMT ceramic at high BMT content is expected to observe at room temperature.

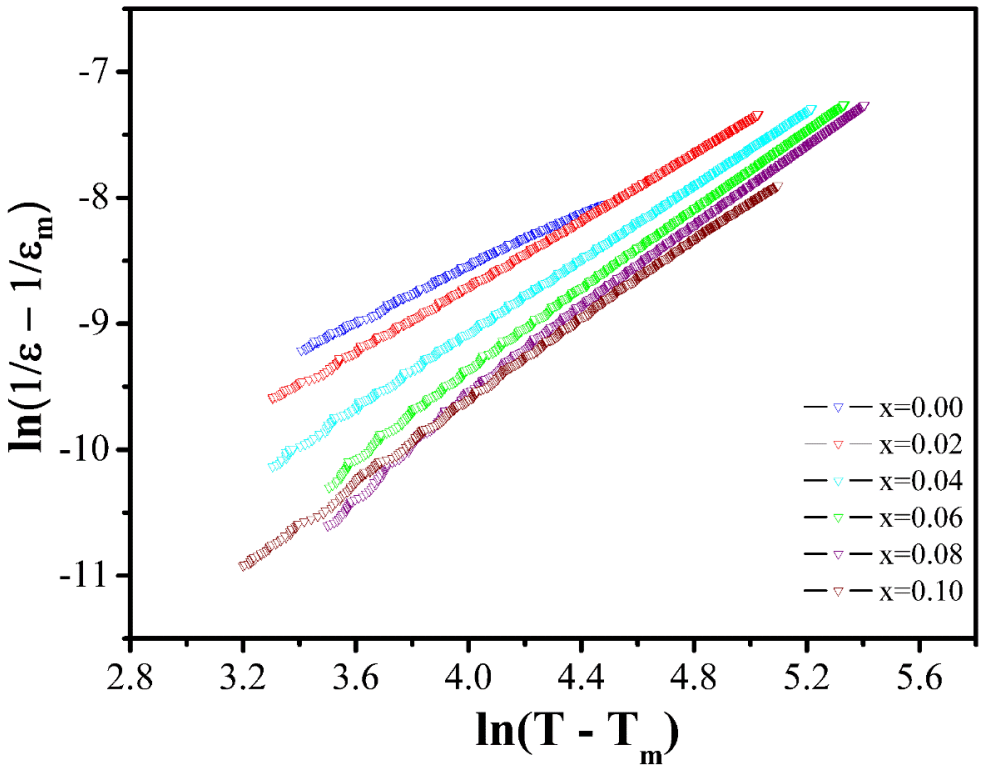

Figure 5.3 The relative plot between $\ln\left(\frac{1}{\varepsilon}-\frac{1}{\varepsilon_m}\right)$ versus $\ln(T-T_m)$

Curie temperature and maximum relative permittivity ($\varepsilon_{r\ max}$) at 100 kHz of BT–BNT–*x*BMT ceramics are determined and plotted as a function of composition in figure 5.4(a). It was observed that Curie temperature decreased rapidly with further increase of BMT. As the previous works have reported that the rapidly decrease in transition can be caused by valence mismatch [20, 21]. In BT–BNT–*x*BMT system, the differences in valence of ions at A-site (Ba^{2+}, Na^{+}, Bi^{3+}) and B-site (Mg^{2+}, Ti^{4+}) might be result in valance mismatch, thus Curie temperature decrease with increasing BMT content. Similar behavior is also observed for the substitution of BMT in KNN structure [22]. Moreover, the maximum relative permittivity ($\varepsilon_{r\ max}$) of BT–BNT–*x*BMT ceramics tends to decrease with increasing BMT concentration. However, at room temperature the relative permittivity ($\varepsilon_{r\ room}$) tends to abruptly increase with increasing BMT,

excepting the composition, x = 0.10. While, dielectric loss ($tan\delta$) tend to gradually increase with BMT increase as shown in figure 5.4(b). The smooth increase of $\varepsilon_{r\ room}$ for the compositions, $0.02 \leq x \leq 0.08$, might be attributed to the decreasing of Curie temperature to room temperature. While, the $\varepsilon_{r\ room}$ of composition, x = 0.10 is decrease might be the Curie temperature being below room temperature.

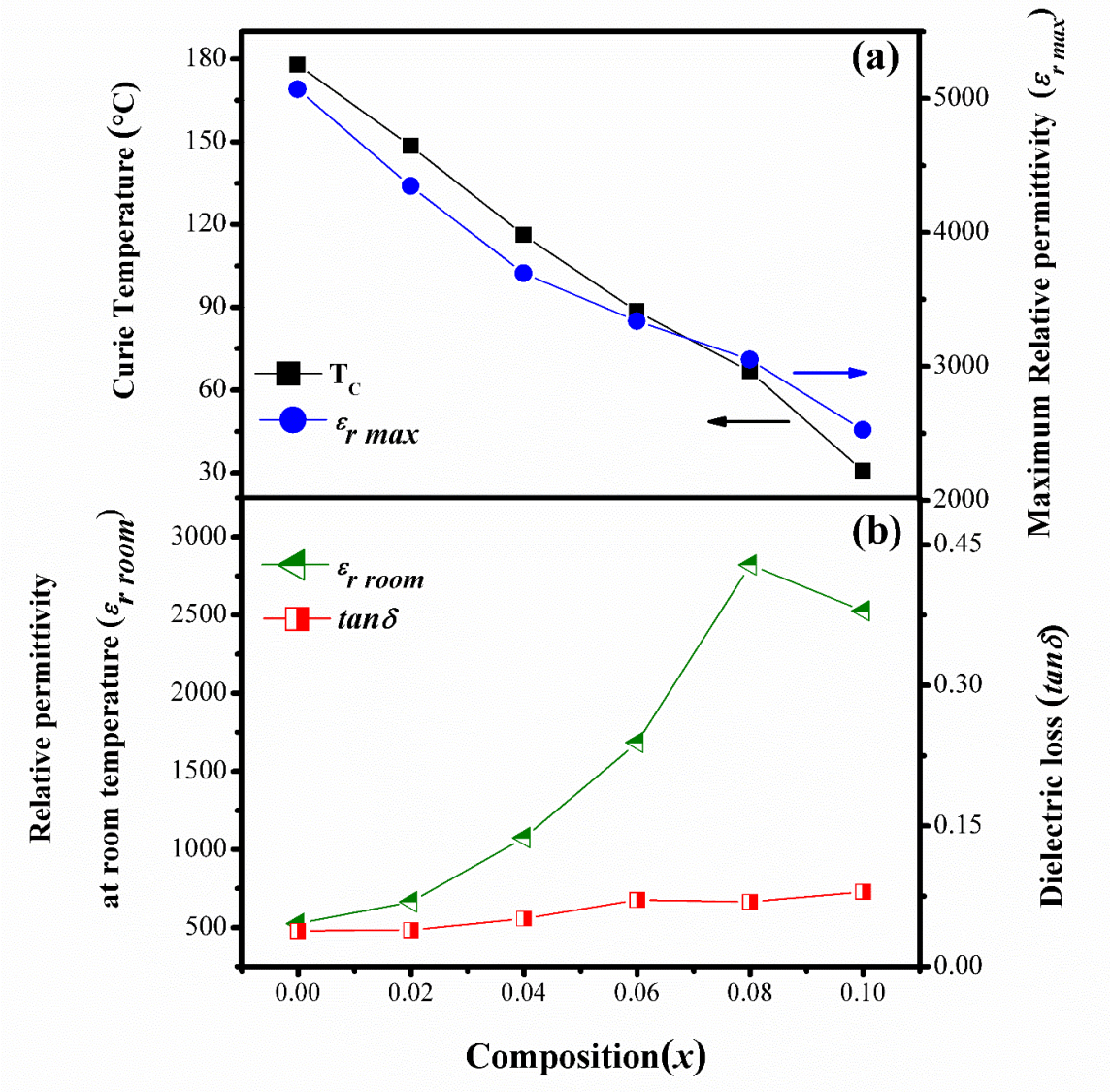

Figure 5.4 (a) The relative plot between Curie temperature and maximum relative permittivity($\varepsilon_{r\ max}$) as a function of composition(x) (b) The relative plot between relative permittivity at room temperature($\varepsilon_{r\ room}$) and dielectric loss ($tan\delta$) as a function of composition(x).

Table 5.2 The dielectric and ferroelectric properties of BT–BNT–*x*BMT ceramics with the composition $0.00 \leq x \leq 0.10$

x	$\varepsilon_{r\,max}$ at 100 kHz	$\tan\delta$ at 100 kHz	γ	δ_γ	P_r ($\mu C/cm^2$)	P_S ($\mu C/cm^2$)	E_c (kV/cm)	Squareness hysteresis loop(R_{sq})
0.00	524	0.038	1.08	12.88	15.52	19.72	29.47	1.56
0.02	663	0.039	1.32	13.98	12.87	18.04	24.31	1.38
0.04	1075	0.051	1.47	14.94	11.26	17.74	20.41	1.20
0.06	1684	0.071	1.60	15.77	8.30	17.30	13.64	0.88
0.08	2820	0.069	1.67	16.26	2.55	15.96	4.24	0.37
0.10	2526	0.080	1.59	15.97	1.63	11.77	3.48	0.33

The composition dependence of polarization-electric field (P-E) hysteresis loops for BT–BNT–*x*BMT system was measured at room temperature with electric field of 60 kV/ cm, as shown in figure 5.5. It is evident that all ceramics display the saturated P-E hysteresis loops. For 0.9BT-0.1BNT, a shape of hysteresis loop displays typically normal ferroelectric behavior with remanent polarization (P_r) and coercive field (E_c) of 15.52 μC/cm^2 and 29.47 kV/cm, respectively, which in good agreement with previous work [2]. Normal ferroelectric contains a long-range interaction between dipoles in the ferroelectric micro-domain state, giving a typical square hysteresis loops with high P_r and E_c. As expected for BT–BNT–*x*BMT ceramics, the substitution of BMT has significantly effect on the hysteresis loops shape and polarization and coercive field values. The more BMT concentration increases, the more the hysteresis loop shape becomes slim, identified the gradually drop of P_r, P_s and E_c values as summarized in Table 5.2. This result suggests that the long-range order of polarization in ferroelectric micro-domain was significantly broken down to polar nano-regions by adding BMT. Then, at high content of BMT, normal ferroelectric BT–BNT–*x*BMT ceramics become relaxor–like behavior exhibiting a slim P-E hysteresis loop with low P_r and E_c. For low content of BMT, the decreasing of P_r and E_c might be due to an easier of domain switching and domain wall motions [23] as well as tetragonality decreasing of crystal structure in this system [24]. The plots of P_r and E_c values against composition are given in figure 5.6. Again, a clearly smooth trend of decrease was seen in P_r and E_c with respect to BMT content, confirming the completely solid solution formation in BT–BNT–*x*BMT system.

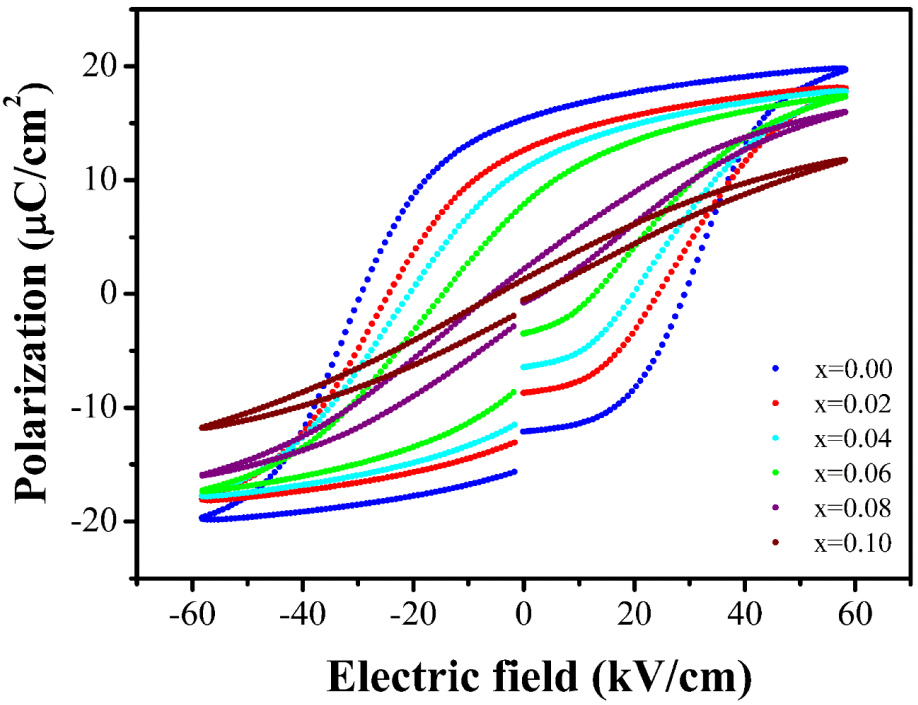

Figure 5.5 The relative plot of polarization (μC/cm^2) with electric field (kV/cm) of BT–BNT–*x*BMT (*x* = 0.00-0.10) ceramics.

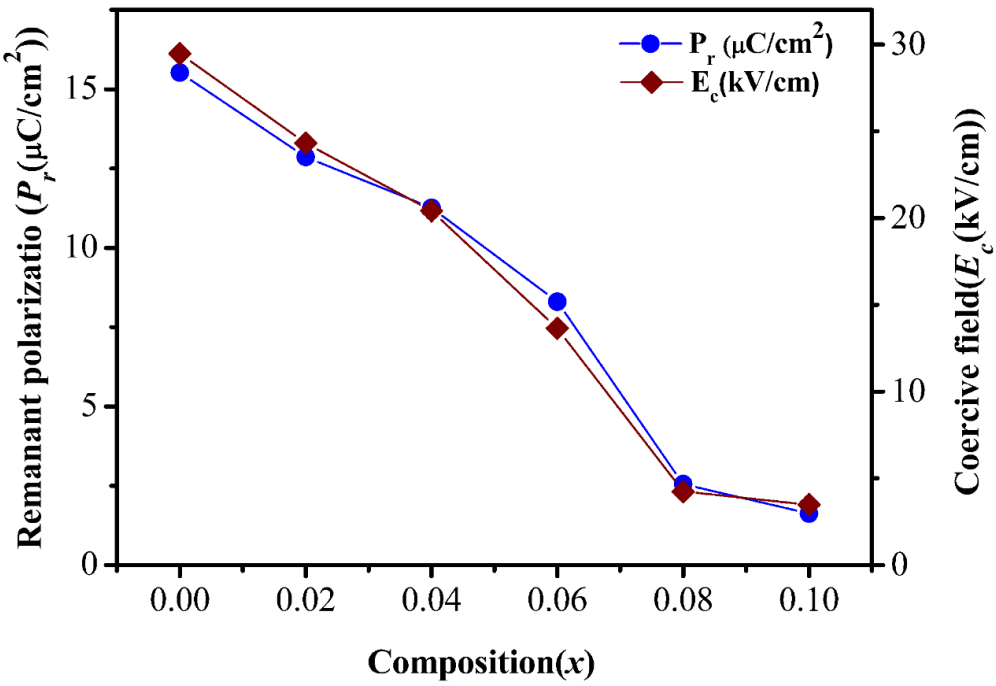

Figure 5.6 The composition (*x*) dependence of Remanent polarization (P_r(μC/cm^2)) and coercive field (E_c(kV/cm)) in BT–BNT–*x*BMT ceramics.

To confirm the changes in hysteresis behavior, the empirical relationship between P_r, P_s and polarization at fields above the E_c proposed by Haertling and Zimmer was used for calculated the squareness of hysteresis loop [25]

$$R_{sq} = \frac{P_r}{P_s} + \frac{P_{1.1E_C}}{P_r} \quad (5.2)$$

where, R_{sq}, P_r and P_s are squareness of hysteresis loop, remanent polarization and saturation polarization, respectively. $P_{1.1Ec}$ is the polarization at an electric field equal to 1.1 times the coercive field (E_c). The squareness parameter reflects the quantification of changes P-E hysteresis loops. For an ideal P-E hysteresis loop, the R_{sq} is equal to 5.2. The calculated R_{sq} for all ceramics is listed in Table 5.2. It is clearly found that, as BMT content increase, the R_{sq} parameter decreases from 1.56 to 0.33 which implies that P – E hysteresis loop becomes more slanted. On the other words, the P – E loops changes from normal ferroelectric to relaxor behavior with increasing BMT concentration which is consistent with the dielectric result.

Combined with the ferroelectric, the dielectric and XRD results of BT–BNT–*x*BMT ceramic, all of changes such as the transformation of crystal structure, the decreasing of transition temperature and remanent polarization and ferroelectric– relaxor ferroelectric phase transition are so smooth. Therefore, it could be said that BT–BNT and BMT can completely form solid solution throughout the whole composition range.

Figure 5.7 illustrates the unipolar strain curves of BT–BNT–*x*BMT ceramics measured at room temperature with an external electric field of 60 kV/cm. It is clearly found the decreasing of unipolar strain of BT–BNT–*x*BMT ceramics from 0.2% to 0.09% when the composition of *x* was increased from 0.00 to 0.10. The normalized strain (d_{33}^*) value of BT-BNT-XBMT ceramics was calculated from the S_{max}/E_{max} ratio for each composition. The composition dependence of normalized strain tends to decrease from 328 pC/N to 153 pC/N when composition of BMT increases, as represented in figure 5.8. This result has caused the approaching to the relaxor-like behavior with increasing of BMT [26]. The composition dependence of the level of induce strain is similar to result observation of BT–$Bi(Ni_{1/2}Ti_{1/2})O_3$ system [27].

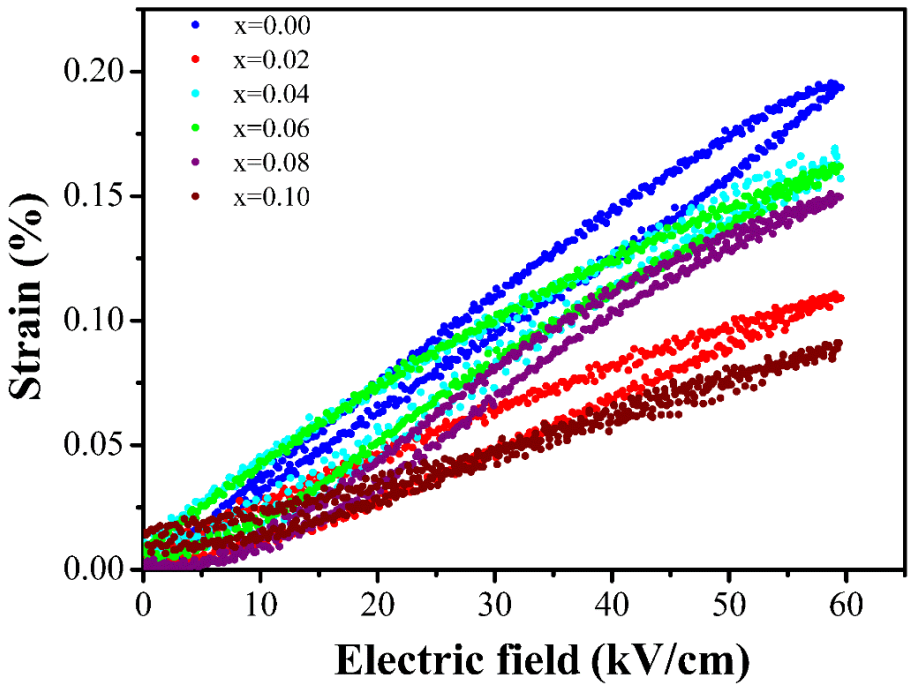

Figure 5.7 The relative plot of unipolar strain (%) as a function of electric field (kV/cm) in BT–BNT–*x*BMT (x = 0.00 – 0.10) ceramics.

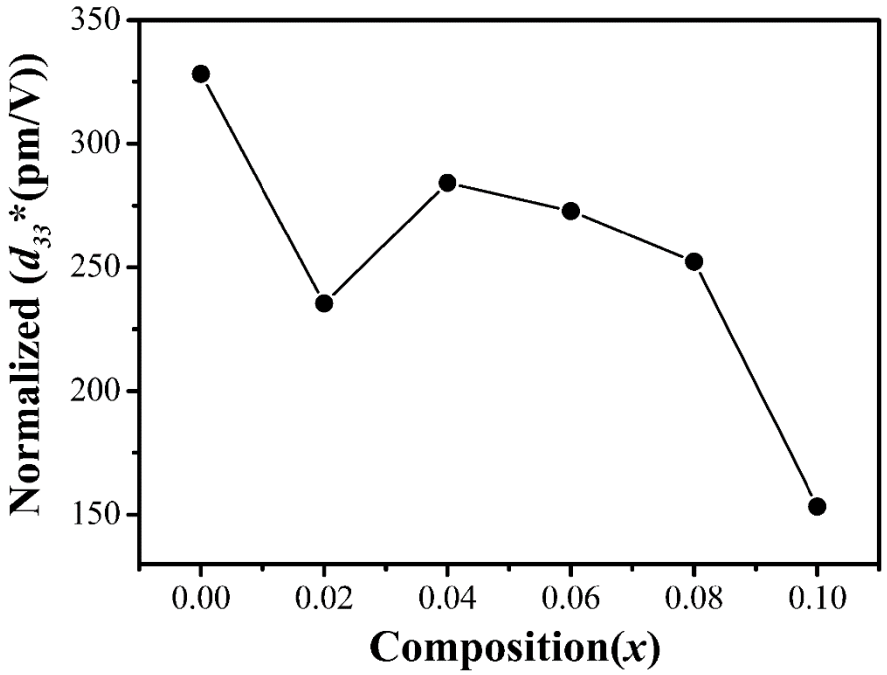

Figure 5.8 Normalized strain (d_{33}^{*} (pm/V)) value of BT–BNT–*x*BMT ceramics with the composition $0.00 \leq x \leq 0.10$.

Figure 5.9 displays SEM micrograph of the sintered surfaces of BT–BNT–*x*BMT ceramics at x = 0.00, 0.02, 0.04 and 0.10. The substitution of BMT directly effects on the average grain size of BT–BNT–*x*BMT ceramics. For the composition x = 0.00, the grain morphology shows and the average grain size is about 1.01 ± 0.14 μm. Homogeneous and uniformity feature microstructures were observed in the composition x = 0.00. The wide grain size distributions was observed in the composition x = 0.02 and 0.04. For the composition x = 0.10, more disorderly and unsystematic shaped grains are observed. A dramatic grain growth inhibition was founded with increasing BMT composition. The average grain size decreased significantly with increasing the composition x. The average grain size are about 0.72 ± 0.09 μm, 0.54 ± 0.09 μm, and 0.49 ± 0.07 μm for the composition x = 0.02, 0.04 and 0.10 respectively. This should be attributed to the effects arisen from the donor–type nature of BMT on inhibiting the grain growth [22]. The decreasing in piezoelectric properties in BNT–BT–xBMT system may be attributed to the inhibiting of the grain growth coursed by substitution of BMT in the BNT–BT system. The detailed mechanisms of the diminution in piezoelectric properties of BT–BNT–*x*BMT system are unclear and demands further study.

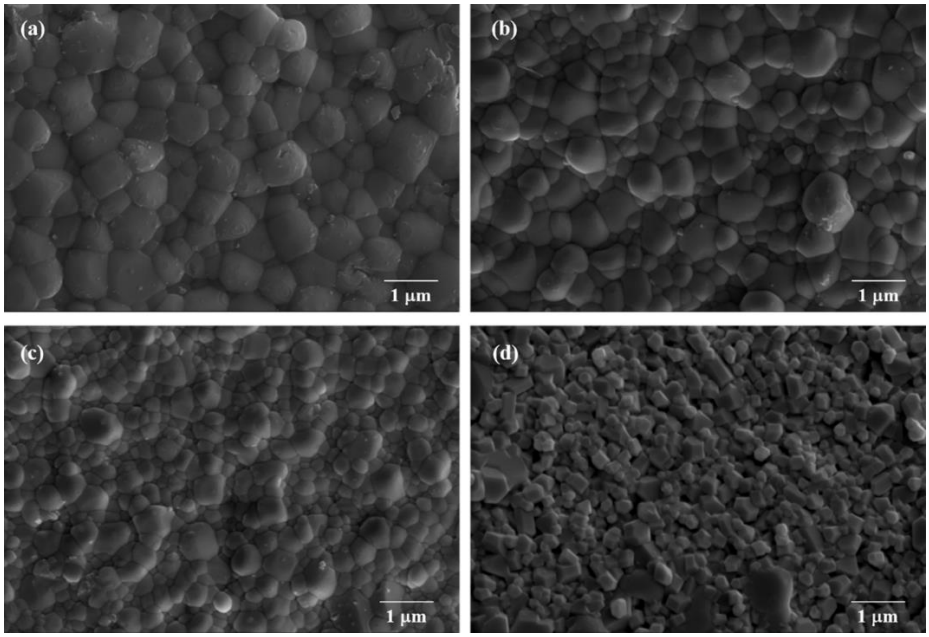

Figure 5.9 SEM micrographs of BT–BNT–*x*BMT ceramics with various compositions (a) x = 0.00, (b) x = 0.02, (c) x = 0.04, and (d) x = 0.10.

5.4 Conclusion

Lead free $0.9BaTiO_3$–$(0.1\text{-}x)Bi_{0.5}Na_{0.5}TiO_3$–$xBi(Mg_{0.5}Ti_{0.5})O_3$ (BT–BNT–*x*BMT; x = 0.00 – 0.10) piezoelectric ceramics were synthesized successfully by the solid state reaction. The crystal structure of BT–BNT–*x*BMT solid solution transforms from tetragonal to pseudocubic symmetry with increasing of BMT content. Combined with the ferroelectric and the dielectric results of BT–BNT–*x*BMT ceramic, phase transition of ceramics gradually changed from ferroelectric to relaxor–like behavior as BMT content increased. Also, BT-BNT and BMT can completely form solid solution throughout the whole composition range.

5.5 References

[1] Rödel, J., Jo, W., Seifert, KTP., Anton, EM., Granzow, T., and Damjanovic, D. 2009. "Perspective on the development of lead-free piezoceramics" **J. Am. Ceram. Soc.** 92 : 1153-1177.

[2] Rawat, M., and Yadav, KL. 2013. "Structural, dielectric and ferroelectric properties of $Ba_{(1-x)}(Bi_{0.5}Na_{0.5})xTiO_3$ ceramics" **Ceram. Int.** 39 : 3627-3633.

[3] Wu, J., Xiao, D., Wu, W., Chen, Q., Zhu, Q., Yang, Z., and Wang, J. 2011. "Role of room-temperature phase transition in the electrical properties of (Ba, Ca)(Ti, Zr)O3 ceramics" **Scripta Mater.** 65 : 771-774.

[4] Wu., J, Habibul, A., Cheng, X., Wang, X., and Zhang, B. 2013. "Orthorhombic–tetragonal phase coexistence and piezoelectric behavior in (1-x)(Ba,Ca)(Ti,Sn)O_3–x(Ba,Ca)(Ti,Zr)O_3 lead-free ceramics" **Mater. Res. Bull.** 48(10) : 4411-4414.

[5] Takenaka, T., Maruyama, K., and Sakata, K. 1991. "$(Bi_{1/2}Na_{1/2})TiO_3$–$BaTiO_3$ System for Lead Free Piezoelectric Ceramics" **Jpn. J. Appl. Phys.** 30 : 2236-2239.

[6] Gao, L., Huang, L., Hu, Y., and Du, H. 2007. "Dielectric and ferroelectric properties of (1-x)$BaTiO_3$–x$Bi_{0.5}Na_{0.5}TiO_3$ ceramics" **Ceram Int.** 33 : 1041-1046.

[7] Zhang, S., Kounga, AB., Aulbach, E., Granzow, T., Jo, W., Kleebe, H., and Rödel, J. 2008. "Lead-free piezoceramics with giant strain in the system $Bi_{0.5}Na_{0.5}TiO_3$–$BaTiO_3$–$K_{0.5}Na_{0.5}NbO_3$. I. Structure and room temperature properties" **J. Appl. Phys.** 103 : 034107.

[8] Trelca, JF., Courtois, C., Rguiti, M., Leriche, A., Duvigneaud, PH., and Segato, T. 2012. "Morphotropic phase boundary in the BNT–BT–BKT system" **Ceram. Int.** 38 : 2823–2827.

[9] Rahman, JU., Hussain, A., Maqbool, A., Ryu, GH., Song, TK., Kim, W., and Kim, M.H. 2014. "Field induced strain response of lead-free $BaZrO_3$–modified $Bi_{0.5}Na_{0.5}TiO_3$–$BaTiO_3$ ceramics" **J. Alloy Compd.** 593 : 97-102.

[10] Wadda, S., Yamato, K., Pulpan, P., Kumada, N., Lee, BY., Iijima, T., Moriyoshi, C., and Kuroiwa, Y. 2010. "Preparation of barium titanate–bismuth magnesium titanate ceramics with high Curie temperature and their piezoelectric properties" **J. Ceram. Soc. Jpn.** 118(8) : 683-687.

5.5 References(II)

[11] Wang, Q., Chen, J., Fan, L., Liu, L., Fang, L., and Xing, X. 2013 "Preparation and Electric Properties of $Bi_{0.5}Na_{0.5}TiO_3$–$Bi(Mg_{0.5}Ti_{0.5})O_3$ Lead-Free Piezoceramics" **J. Am. Ceram. Soc.** 96(4) : 1171–1175.

[12] Shannon, RD. 1976. "Revised effective ionic radii and systematic studies of interatomic distances in halides and chalcogenides" **Acta. Crystallogr. A.** 32 : 751–767.

[13] Bhalla, AS., Guo, R., and Roy, R. 2000. "The perovskite structure–a review of its role in ceramic science and technology" **Mater. Res. Innov.** 4 : 3–26.

[14] Muller, O., and Roy, R. 1974. "The major ternary structural families" Springer–Verlag Berlin–Heidelberg–New York.

[15] Jaffe, B., and Cook, WR. 1971. "Piezoelectric ceramics" Academic Press, New York.

[16] Smolenskii, GA. 1970. "Physical phenomena in ferroelectrics with diffuse phase transition" **Jpn. J. Phys. Soc.** 28 : 26–37.

[17] Rout, SK., Sinha, E., and Panigrahi, S. 2007. "Dielectric properties and diffuse phase transition in $Ba_{(1-x)}Mg_xTi_{0.6}Zr_{0.4}O_3$ solid solutions" **Mater. Chem. Phys.** 101 : 428–432.

[18] Uchino, K., and Nomura, S. 1982. "Critical exponent of the dielectric constant in diffused-phase-transition crystals" **Ferroelectrics Lett.** 44 : 55.

[19] Clarke, R., and Burfoot, JC. 1974 "The diffuse phase transition in potassium strontium niobate" **Ferroelectrics.** 48 : 505.

[20] Isupov, VA. 2000 "Nonlinearity of the concentration dependence of the Curie temperature in ferroelectric perovskite solid solutions" **Phys. Stat. Sol.** 181 : 21.

[21] Bratton, RJ., and Tien, TY. 1967 "Phase Transitions in the System $BaTiO_3$–$KNbO_3$" **J. Am. Ceram. Soc.** 50 : 90–93.

[22] He, F., Chen, X., Chen, J., Wang, Y., Zhou, H., and Fang, L. 2013. "$(K_{0.5}Na_{0.5})NbO_3$–$Bi(Mg_{0.5}Ti_{0.5})O_3$ solid solution: phase evolution, microstructure and electrical properties" **J. Mater. Sci. – Mater. El.** 24 : 4346–4350.

[23] Bai, W., Bian, Y., Hao, J., Shen, B., and Zhai, J. 2013. "The Composition and Temperature-Dependent Structure Evolution and Large Strain Response in (1-*x*)$(Bi_{0.5}Na_{0.5})TiO_3$–*x*$Ba(Al_{0.5}Ta_{0.5})O_3$ Ceramics" **J. Am. Ceram. Soc.** 96 (1) : 246–252.

5.5 References(III)

[24] Xu, D., Li, WL., Wang, LD., Wang, W., Cao, WP., and Fei, WD. 2014. “Large piezoelectric properties induced by doping ionic pairs in $BaTiO_3$ ceramics” **Acta mater.** 79 : 84–92.

[25] Haertling, GH., and Zimmer, WJ. 1966. “Analysis of hot-pressing parameters for lead zirconate-lead titanate ceramics containing two atom percent bismuth” **Am. Ceram. Soc. Bull.** 45 : 1084-1089.

[26] Xu, D., Li, WL., Wang, LD., Wang, W., Cao, WP., and Fei, WD. 2014. “Large piezoelectric properties induced by doping ionic pairs in $BaTiO_3$ ceramics” **Acta mater.** 79 : 84–92.

[27] Fujit, I., Nakashima, K., Kumada, N., and Wada, S. 2012. “Structural, Dielectric and piezoelectric properties of $BaTiO_3$–$Bi(Ni_{1/2}Ti_{1/2})O_3$ ceramics” **J. Ceram. Soc. Jpn.**; 120 : 30–34.

CHAPTER 6

CONCLUSIONS AND SUGGESTION FOR FURTHER WORK

6.1 Conclusions

The barium titanium-based ternary system in two systems: $BaTiO_3$–$SrTiO_3$–$y$$BaSnO_3$ and $BaTiO_3$–$Bi_{0.5}Na_{0.5}TiO_3$–$Bi(Mg_{0.5}Ti_{0.5})O_3$ ceramics were selected, to design the multi-phase composition. All ceramics samples in both systems were prepared by conventional solid state method. The structure-properties relationship was explored.

The first ternary system was (0.975-y)$BaTiO_3$–0.025$SrTiO_3$–$y$$BaSnO_3$, where y = 0.00, 0.02, 0.04, 0.06, 0.08 and 0.10. The effect of Sn substitution on the ferroelectric phase transition and piezoelectric properties was explored to achieve high-performance piezoelectric properties. All of the ceramics exhibited pure perovskite structures. The coexistent tetragonal and orthorhombic phases were exhibited at the composition, y = 0.04, and showed an outstanding dielectric and piezoelectric properties, relative permittivity (ε_r) of 11,500 and piezoelectric coefficient (d_{33}) of 449 pC/N. An outstanding reversible strain of about 0.12%, with a normalized piezoelectric coefficient (S_{max}/E_{max}) of 1,280 pm/V at a low electric field (10 kV/cm), was observed clearly at the composition of the coexistent phase. This result indicated that the (0.975-y)$BaTiO_3$–0.025$SrTiO_3$–$y$$BaSnO_3$ ceramics are one promising candidate system for lead-free piezoelectric materials.

The second system was 0.9$BaTiO_3$–(0.1-x)$Bi_{0.5}Na_{0.5}TiO_3$–$x$$Bi(Mg_{0.5}Ti_{0.5})O_3$ system, where x = 0.00, 0.02, 0.04, 0.06, 0.08, 0.10. The effect of BMT on crystal structure and electrical property of BT–BNT ceramics was investigated as a function of composition, x. The crystal structure of solid solution BT–BNT–xBMT, where x = 0.00 – 0.10, successively transforms from tetragonal to pseudocubic symmetry, with increased BMT concentration. Temperature dependence of dielectric constant (ε_r) and dielectric loss ($tan\delta$) for BT–BNT–xBMT at various frequencies showed that phase transition of ceramics changed from ferroelectric to relaxor-like behavior as BMT content increased. Furthermore, remanent polarization (P_r), coercive field (E_c) and the

normalized strain (d_{33}^{*}) of BT-BNT-BMT ceramics tend to decrease with increasing BMT concentration.

6.2 Suggestions for further work

In part of structural characterization in X-ray diffraction result, it can seen that the diffraction peak of coexisting orthorhombic and tetragonal phases is not clearly because the relatively low resolution of the traditional X-ray diffractometer. In the future work, we suggest the following X-ray diffractometer from synchrotron radiation that have better line resolution to clarify the structure of ceramics.

VITA

Name–Surname	Jitkasem Mayamae
Date of birth	6 June 1990
Province	Pattani
Education	**B.S.** (Industrial Chemistry – Analytical Instrumentation) King Mongkut's Institute of Technology Ladkrabang, Bangkok (2012)
	M.S. (Nanoscience and Nanotechnology) King Mongkut's Institute of Technology Ladkrabang, Bangkok (2013 - present)

Conferences

1. **Jitkasem Mayamae**, Usa Sukkha, Surasak Niemchareon, Rangson Muanghlua and Naratip Vittayakorn "Dielectric, ferroelectric and piezoelectric properties of the lead free $0.9BaTiO_3$-$(0.1-x)Bi_{0.5}Na_{0.5}TiO_3$-$xBi(Mg_{0.5}Ti_{0.5})O_3$ solid solution" The 9th Asian Meeting on Ferroelectrics and Asian Meeting on Electroceramics (AMF-AMEC-2014), Shanghai, China, October 26-30, 2014. (Poster Presentation)
2. **Jitkasem Mayamae**, Usa Sukkha, Surasak Niemchareon, Rangson Muanghlua and Naratip Vittayakorn "Dielectric, ferroelectric and piezoelectric properties of the lead free $0.9BaTiO_3$-$(0.1-x)Bi_{0.5}Na_{0.5}TiO_3$-$xBi(Mg_{0.5}Ti_{0.5})O_3$ ceramics system". The 40th Congress on Science and Technology of Thailand (STT 40), December 2-4, 2014 (Oral Presentation)
3. **Jitkasem Mayamae**, Wanwilai Vittayakorn, Surasak Niemchareon, Rangson Muanghlua, Soodkhet Pojprapai, Somsak Woramongkolchai and Naratip Vittayakorn "Effect of Sn^{4+} content on dielectric and piezoelectric properties for ternary systems of $(0.975-y)BaTiO_3$–$0.025SrTiO_3$–$yBaSnO_3$ ceramics" The 3rd International Congress on Advanced Materials (AM 2016) (Poster Presentation)

International publications

1) **Jitkasem Mayamae**, Usa Sukkha, Surasak Niemchareon, Rangson Muanghlua and Naratip Vittayakorn "Dielectric, ferroelectric and piezoelectric properties of the lead free $0.9BaTiO_3$-$(0.1-x)Bi_{0.5}Na_{0.5}TiO_3$-$xBi(Mg_{0.5}Ti_{0.5})O_3$ solid solution" *Ferroelectrics,* 490: 23-35 (2016).

2) **Jitkasem Mayamae**, Wanwilai Vittayakorn, Rangson Muanghlua, Somsak Woramongkolchai and Naratip Vittayakorn "Effect of Sn content on the dielectric and piezoelectric properties of the ternary system $(0.975-y)BaTiO_3$–$0.025SrTiO_3$–$yBaSnO_3$". *Journal of Materials science*, 52(12): 6928-6936 (2017).

J Mater Sci

Effect of Sn content on the dielectric and piezoelectric properties of the ternary system (0.975-y)$BaTiO_3$–0.025$SrTiO_3$–$y$$BaSnO_3$

Jitkasem Mayamae[1], Wanwilai Vittayakorn[1,5], Rangson Muanghlua[2], Somsak Woramongkolchai[3,4], and Naratip Vittayakorn[1,3,4,5,*]

[1] Electroceramic Research Laboratory, College of Nanotechnology, King Mongkut's Institute of Technology Ladkrabang, Bangkok 10520, Thailand
[2] Department of Electronics Engineering, Faculty of Engineering, King Mongkut's Institute of Technology Ladkrabang, Bangkok 10520, Thailand
[3] Department of Chemistry, Faculty of Science, King Mongkut's Institute of Technology Ladkrabang, Bangkok 10520, Thailand
[4] Advanced Materials Research Unit, Faculty of Science, King Mongkut's Institute of Technology Ladkrabang, Bangkok 10520, Thailand
[5] Nano-KMITL Center of Excellence on Nanoelectronic Devices, King Mongkut's Institute of Technology Ladkrabang, Bangkok 10520, Thailand

Received: 7 December 2016
Accepted: 8 February 2017

ABSTRACT

Design of the polymorphic phase composition in the (0.975-y)$BaTiO_3$–0.025$SrTiO_3$–$y$$BaSnO_3$; BT-ST-$y$BSn ternary system was based on the ferroelectric phase diagram. The dense ceramic of BT-ST-yBSn, with $y = 0.00$, 0.02, 0.04, 0.06, 0.08 and 0.10 compositions, was fabricated successfully via the solid-state reaction method. The effect of Sn substitution on the ferroelectric phase transition and piezoelectric properties was explored in order to achieve high-performance piezoelectric properties. All of the ceramics exhibited pure perovskite structures. Orthorhombic to tetragonal phase transition was evidenced clearly as a function of Sn content. The orthorhombic to tetragonal phase transition shifted close to ambient temperature by increasing the Sn content. The coexistent tetragonal and orthorhombic phases were exhibited at the composition, $y = 0.04$, and showed outstanding dielectric and piezoelectric properties, maximum relative permittivity ($\varepsilon_{r\ max}$) of 11500 and piezoelectric coefficient (d_{33}) of 450 pC/N. An outstanding reversible strain of about 0.12%, with a normalized piezoelectric coefficient (S_{max}/E_{max}) of 1280 pm/V at a low electric field (10 kV/cm), was observed clearly at the composition of the coexistent phase. The BT-ST-BSn ceramics are the most promising candidate for lead-free piezoelectric materials.

Address correspondence to E-mail: naratip.vi@kmitl.ac.th; naratipcmu@yahoo.com

DOI 10.1007/s10853-017-0906-z

Published online: 17 March 2017

Introduction

Lead-based piezoelectric ceramics such as lead zirconate titanate [$Pb(Zr_{1-x}Ti_x)O_3$; PZT] have been used most widely in actuator and sensor devices, due to their excellent piezoelectric properties [1]. Nevertheless, PZT ceramics are environmentally unfriendly and dangerous to human health, due to the toxicity of lead in fabrication processing [2, 3]. Therefore, attention has been drawn to lead-free piezoelectric materials with a performance comparable to that in lead-based materials. Consequently, in recent years diverse systems have been explored, including bismuth-alkaline metal titanates and niobates, and especially $BaTiO_3$; BT solid solution [2–5].

Ferroelectric behavior was discovered in Barium titanate ($BaTiO_3$; BT) by Wul and Goldman in 1946 [6], which led to the widespread use of BT in capacitors and electromechanical devices [6, 7]. BT has a tetragonal perovskite structure at room temperature, and pure BT exhibits a piezoelectric constant (d_{33}) of about 191 pC/N) [8] that is relatively low when compared to PZT-based ($d_{33} = 300$–600 pC/N) [8]. Therefore, BT has been modified by doping with A and/or B site substitutions [9–11]. The binary system of $BaTiO_3$–$BaSnO_3$; BT-BSn recently showed high dielectric permittivity (ε_r) ~75000 and excellent piezoelectric coefficient (d_{33}) ~697 pC/N at the quasi-quadruple point, which exhibited coexistent Cubic–Tetragonal–Orthorhombic–Rhombohedral phases in BT-BSn [12]. Wang et al. [13] reported a high electrostriction strain of ~0.22% in the binary systems of $BaTiO_3$–$CaTiO_3$; BT-CT. Excellent piezoelectric properties also were obtained in the coexistent phase composition in the $BaTiO_3$–$BaZrO_3$–$CaTiO_3$; BT-BZ-CT and $BaTiO_3$–$BaZrO_3$–$CaTiO_3$; BT-BS-CT system [9, 14]. The $(Ba_{1-x}Ca_x)(Ti_{0.92}Sn_{0.08})O_3$ ceramics recently displayed high $d_{33} = 568$ pC/N, $k_p = 47.7\%$, $\varepsilon_r = 23{,}000$ and normalized strain (dS/dE) = 1013 pm/V at the orthorhombic/tetragonal coexistent phase composition [15]. The coexistent phase composition in the Sn dope BT-CT system also exhibited ultra-high d_{33} (670 pC/N) and electrostrain (0.061%) [16]. Li et al. [17] recently reported a high piezoelectric coefficient (d_{33}) of about 380 pC/N and k_p of about 38% in the Sr dope Ba(Zr,Ti)O_3; BZT system. The Sr substitute BZT, not only enhanced piezoelectric properties by shifting the ferroelectric phase transition close to room temperature, but also decreased the sintering temperature of the ceramic. In order to find new BT-based ceramics with excellent piezoelectric properties, Sn cation was selected to substitute the Sr-doped $BaTiO_3$ in this work. Sr-doped BT was used as a base composition, due to Sr being able to enhance piezoelectric properties and slightly decrease the sintering temperature of the ceramic. Systematic study of how the Sn substitution affects crystal structure, and dielectric and piezoelectric behavior of $(0.975\text{-}y)BaTiO_3$–$0.025SrTiO_3$–$yBaSnO_3$; BT-ST-yBSn ceramics, is still rare. The BT-ST-yBSn ceramic, with $y = 0.00$, 0.02, 0.04, 0.06, 0.08 and 0.10 compositions, is designated in this study as a lead-free composition that explores the compositional dependence of structure and piezoelectric behavior in Sn content. The development of piezoelectric properties by optimizing Sn content in BT-ST-yBSn ceramics has been established.

Experimental procedure

The $(0.975\text{-}y)BaTiO_3$–$0.025SrTiO_3$–$yBaSnO_3$; BT-ST-yBSn ceramic, with $y = 0.00$, 0.02, 0.04, 0.06, 0.08 and 0.10 compositions, was fabricated via the solid-state reaction technique. The metal carbonate and oxide powder of $BaCO_3$ (99.9%, Inframal Advance Materials), $SrCO_3$ (99.5%, Inframal Advance Materials), TiO_2 (99.9%, Sigma-Aldrich) and SnO_2 (99.9%, Inframal Advance Materials) were used as raw materials. The stoichiometric amount of starting materials was mixed in ethanol with yttrium-stabilized zirconia in the first step and then vibro-milled for 6 h. The mixtures were dried and calcined at temperatures between 1200 and 1300 °C for 4 h, with a heating/cooling rate of 5 °C/min. The calcined powders were ground and sieved. Finally, the calcined powders were pressed into pellets of 10–20 mm diameter and a thickness of about 1–1.5 mm, using 5 wt% polyvinyl alcohol (PVA) as a binder. The pellets were sintered at between 1375 and 1450 °C for 4 h with a heating/cooling rate of 5 °C/min. Ceramics with more than 94% theoretical density were selected for investigating electrical properties. The crystal structure of ceramics was carried out with X-ray diffraction (Bruker-AXS D 8 Advance) using CuK_α radiation in the 2θ scan range of 20°–80°. In order to support crystal structure identification of the ceramics, Raman spectra were measured in the 100–1000 cm^{-1} wave number range with a Thermo Scientific DXR Raman microscope, using the 532 nm exciting line of

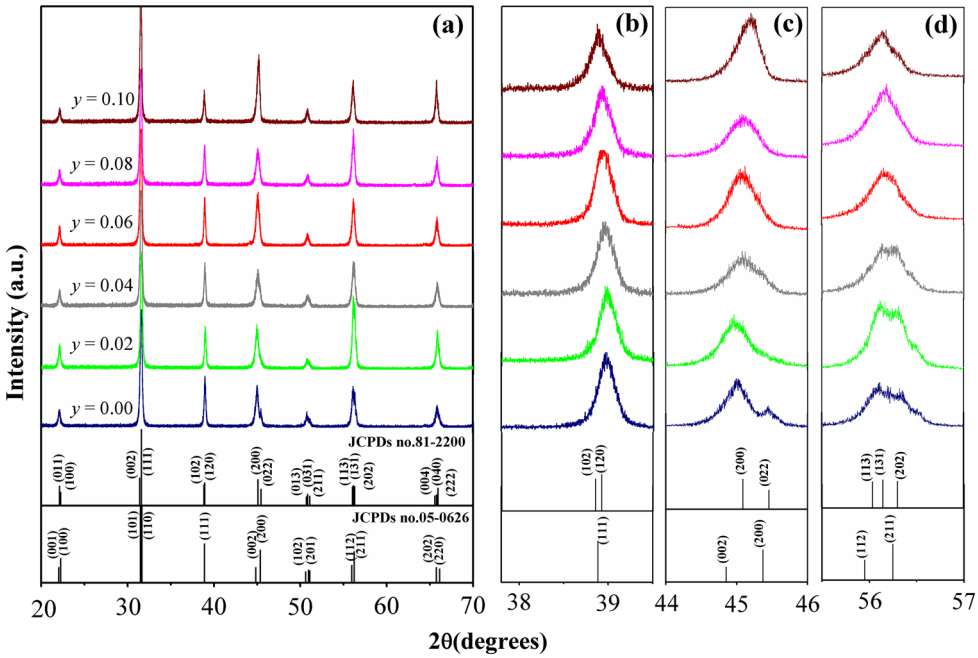

Figure 1 **a** X-ray diffraction patterns of BT-ST-*y*BSn ceramic between the 2θ range of 20°–80°, **b** expanded range of 38°–40°, **c** expanded range of 44°–46° and **d** expanded range of 55°–57°.

a He–Ne laser. In order to obtain electrical measurement, both sides of the samples were polished and paralleled for electrical measurements. Then, the pellets were coated on both surfaces with silver electrodes (C1000, Heraeus) and heated at 750 °C for 20 min, with a heating/cooling rate of 5 °C/min. The frequency (1, 10, 100 kHz) and temperature (room temperature to 160 °C) dependence of relative permittivity (ε_r) and dielectric loss (tan δ) were obtained by using an LCR analyzer (HP4284A, Hewlett-Packard, Palo Alto, CA, USA). Ferroelectric hysteresis loops were determined at room temperature by using a ferroelectric tester (RT66A, Radiant Technologies, Inc.), and the strain-electric field (*S*–*E*) loop was measured by unipolar driving at 4 Hz using an MTI-2100 Fotonic sensor combined with a ferroelectric tester. The pellets of 10 mm diameter and 0.6 mm thickness were poled under a DC field at 35–40 kV/cm for 30 min at room temperature and aged for 24 h before piezoelectric measurements. The piezoelectric coefficient, d_{33}, was characterized using a quasi-static $d_{33\ m}$ (YE2730A, APC International Ltd.).

Results and discussion

The characteristics of crystal structured ceramics were examined by X-ray diffraction (XRD). XRD patterns of the BT-ST-*y*BSn system, with compositions of $y = 0.00$, 0.02, 0.04, 0.06, 0.08 and 0.10, are shown in Fig. 1a–d. All of the samples demonstrated a single phase with the perovskite structure, and the secondary or impure phase was not observed in the XRD patterns, which indicates that both Sr and Sn ions are fully diffused into the $BaTiO_3$ lattice to form solid solution. The crystal structure of BT-ST-*y*BSn at the compositions, $0.00 \leq y \leq 0.02$, has a tetragonal symmetry, identified by a single peak at 2θ of 38.7° (Fig. 1b) and splitting of (002) and (200) peaks at 2θ of 44.8°–45.6° (Fig. 1c). At higher compositions of $0.06 \leq y \leq 0.10$, the XRD pattern exhibits splitting of two peaks [(102)/(120)] at around 38°–39.5° and splitting of three peaks [(113)/(131)/(202)] at around 55.8°–56.3°, which indicates an orthorhombic symmetry (Fig. 1d). Therefore, the results indicated that the crystal structure changed from tetragonal to orthorhombic phase with increasing Sn content. Meanwhile, it is anticipated that the tetragonal and orthorhombic phases for $y = 0.04$ coexist, which is confirmed by dielectric and piezoelectric measurements. It is seen clearly that the diffraction pattern of all compositions shifts gradually to low angles with increasing Sn content, which should induce expansion of the host lattice. Lattice parameter (Å) and unit cell volume (Å^3) were calculated and plotted as a function of Sn content, as shown in Fig. 2a, b. Regarding the compositions, $0.00 \leq y \leq 0.02$, with tetragonal symmetry, the unit cell a and c increase slightly with increasing Sn content, which corresponds with increased unit cell volume. The

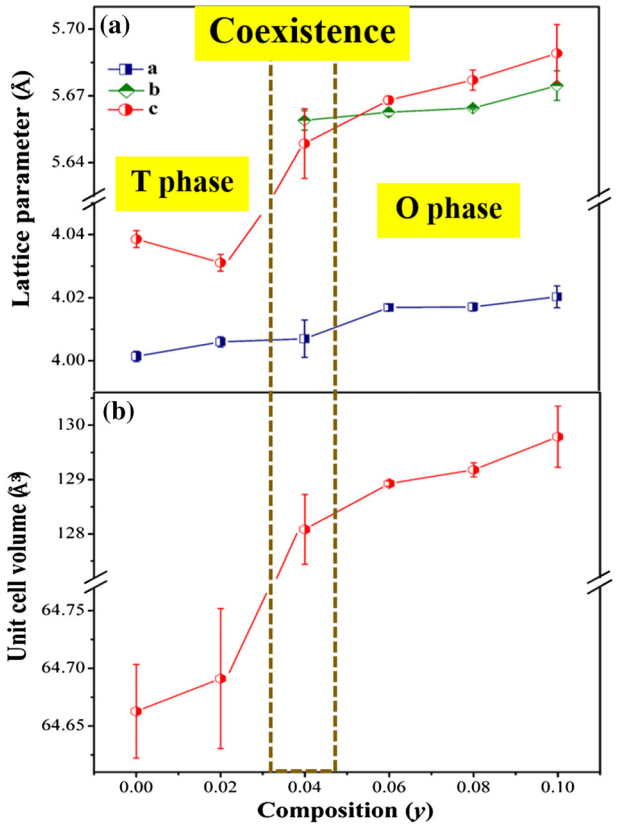

Figure 2 Relative plot between the **a** lattice parameter (Å), and **b** cell volume (Å^3) and composition y in BT-ST-yBSn ceramic.

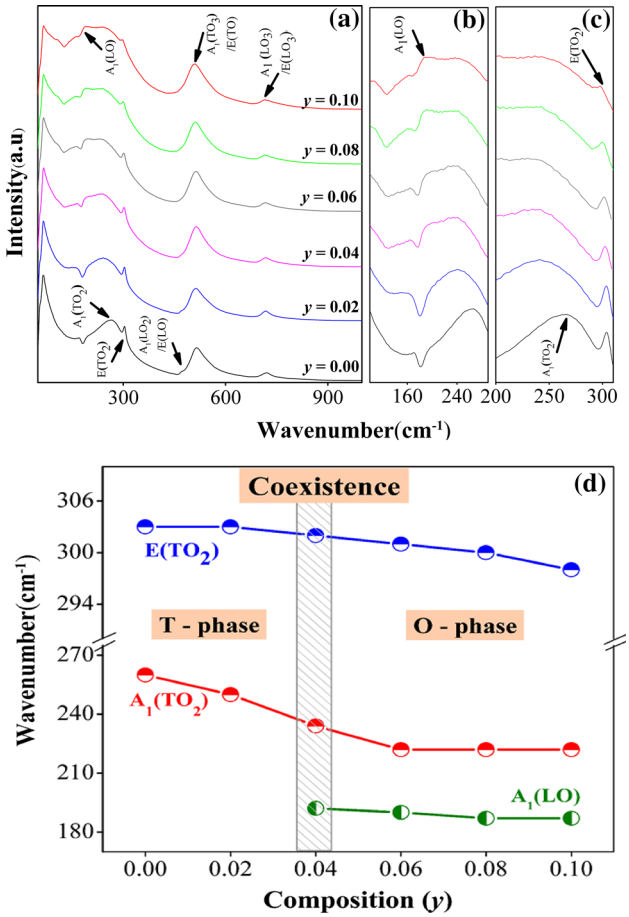

Figure 3 **a** Raman spectra of BT-ST-yBSn ceramic at room temperature with the compositions, $0.00 \leq y \leq 0.10$, in the wave number range from 100 to 1000 cm^{-1}, **b** enlarged Raman shift range from 100 to 290 cm^{-1}, **c** enlarged Raman shift range from 200 to 310 cm^{-1} and **d** the relative plot between wave number cm^{-1} and composition y.

ostensibly discontinuous changes are noticed at $0.02 < y < 0.06$ when the tetragonal and orthorhombic phases coexist. The orthorhombic lattice parameters (a, b and c) and unit cell volume slightly increase for the compositions, $0.06 \leq y \leq 0.10$. This is consistent with the result reported by Zhu et al. [16]. The increase in the lattice parameter is caused mainly by the majority of Sn ions substitute Ti^{4+} ions the B site of the perovskite structure with Sn^{4+} state. However, it should be noted that the valency of the Sn ion is very sensitive and allowed to adapt to a divalent, trivalent and tetravalent state in oxide ceramics [18]. Suzuki et al. [19] reported that under sintering conditions of reducing atmosphere, the Sn ions can substitute Ba^{2+} ions at the A-site of the perovskite structure with Sn^{2+} state. The oxidation states of the Sn ion in BT-ST-yBSn ceramics must be considered for future investigation. Dependence on the composition of Raman spectra for BT-ST-yBSn systems was investigated at room temperature in the frequency range of 100–1000 cm^{-1}, as shown in Fig. 3a–d. The ferroelectric phase with tetragonal symmetry corresponds with group theory analysis in normal optical mode, with each F_{1u} mode transforming into A_1 and E modes, whereas the F_{2u} mode gives rise to B_1 (silent) and E modes. All spectra generally display Raman-active modes of ferroelectric material. The interference dips at around 180 cm^{-1}, due to antiresonance between sharp $A_1(TO_1)$ and broad $A_1(TO_2)$ modes, such as a broad peak of $A_1(TO_2)$ mode near 257 cm^{-1}; sharp peak of $E(TO_2)$ mode at 295 cm^{-1}; broad peak of $A_1(TO_3)$ and E(TO) mode at around 515 cm^{-1}, which is a bending and stretching vibration of symmetric Ti–O in $[TiO_6]^{2-}$; and a broad peak of $A_1(LO_3)/E(LO_3)$ mode at around 712 cm^{-1} [20]. Therefore, Raman spectra of all compositions are observed at a broad peak of $A_1(TO_2)$, $E(TO_2)$, $A_1(TO_3)/E(TO)$, $A_1(LO_3)/E(LO_3)$ and interference

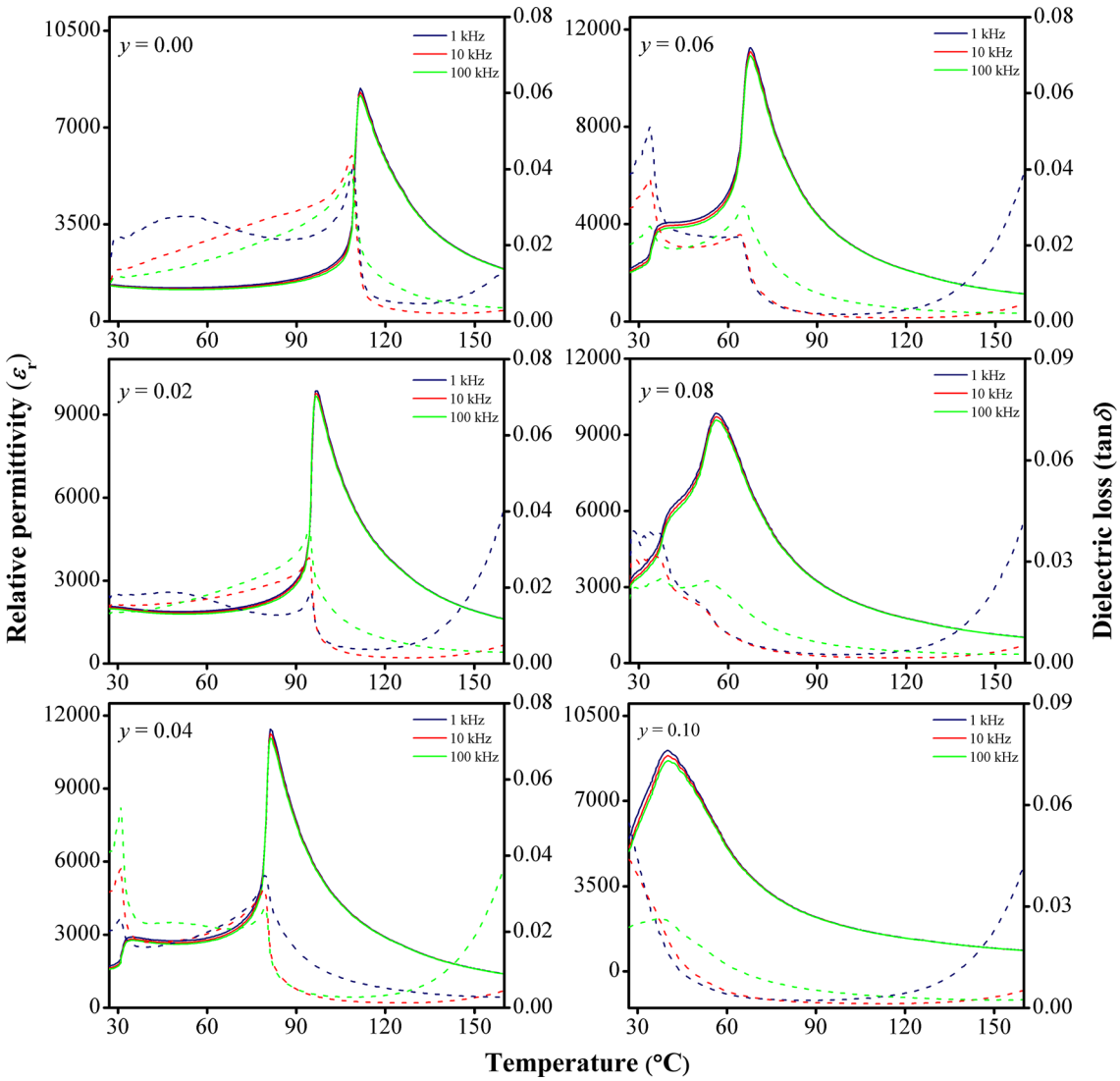

Figure 4 Relative permittivity (ε_r) and dielectric loss (tan δ) as temperature dependent BT-ST-yBSn ceramic with compositions, $0.00 \leq y \leq 0.10$.

dip mode (Fig. 3a), which indicates that all compositions exhibit ferroelectric phase. The signature Raman mode of tetragonal phase for BT is generally a broad $A_1(TO_2)$ mode, sharp $E(TO_2)$ mode, broad $A_1(TO_3)$/$E(TO)$ mode, swelling $A_1(LO_2)$/$E(LO)$ mode and broad $A_1(LO_3)$/$E(LO_3)$ mode [21]. Also, the mode of orthorhombic phase is a broad $A_1(TO_1)$, $A_1(TO_2)$, $A_1(TO_3)$/$E(TO)$ and $A_1(LO_3)$/$E(LO_3)$ peak and sharp $E(TO_2)$ peak [21]. In the compositions, $0.00 \leq y \leq 0.02$, all of the Raman patterns show $A_1(TO_2)$, $E(TO_2)$, $A_1(LO_2)$/$E(LO)$, $A_1(TO_3)$/$E(TO)$ and $A_1(LO_3)$/$E(LO_3)$ at around 260, 303, 472, 517 and 720 cm^{-1}, respectively, which indicates a ferroelectric tetragonal phase. At the higher compositions, $0.04 \leq y \leq 0.10$, the $A_1(TO_1)$ mode appeared gradually at 190 cm^{-1} and $A_1(LO_2)$/$E(LO)$ mode at 472 cm^{-1}, but both were absent in the Raman spectrum. Therefore, the compositions, $0.06 \leq y \leq 0.10$, were considered as a signature of the ferroelectric orthorhombic phase by the presence of $A_1(TO_1)$, $A_1(TO_2)$, $E(TO_2)$, $A_1(TO_3)$/$E(TO)$ and $A_1(LO_3)$/$E(LO_3)$ mode near 190, 222, 301, 514 and 716 cm^{-1}, respectively. A weak $A_1(TO_1)$, $A_1(TO_2)$, $E(TO_2)$, $A_1(TO_3)$/$E(TO)$ and $A_1(LO_3)$/$E(LO_3)$ peak at the composition, $y = 0.04$, showed coexistence of the ferroelectric tetragonal and orthorhombic phase. These results identified that the phase transition changed from tetragonal to orthorhombic phase, which corresponds well with the XRD pattern.

Table 1 Dielectric, ferroelectric and piezoelectric properties of $(0.975\text{-}y)BaTiO_3$–$0.025SrTiO_3$–$yBaSnO_3$ ceramic with the composition, $0.00 \leq y \leq 0.10$

y	T_m (°C)	$\varepsilon_{r\ max}$ at 1 (kHz)	tan δ at 1 (kHz)	γ	δ_γ	P_r (μC/cm^2)	E_c (kV/cm)	R_{sq}	d^*_{33} (pm/V)	d_{33} (pC/N)
0.00	110	8400	0.02	1.20	12.5	12.9	7.0	0.80	702	260
0.02	97	9850	0.02	1.21	12.6	12.5	6.4	0.80	835	320
0.04	81	11430	0.02	1.24	12.8	13.1	5.4	0.77	1280	450
0.06	68	11250	0.04	1.25	12.8	10.5	4.4	0.83	840	370
0.08	56	9850	0.04	1.30	13.1	7.5	3.2	0.73	830	200
0.10	41	11000	0.05	1.37	13.4	6.9	3.1	0.72	740	120

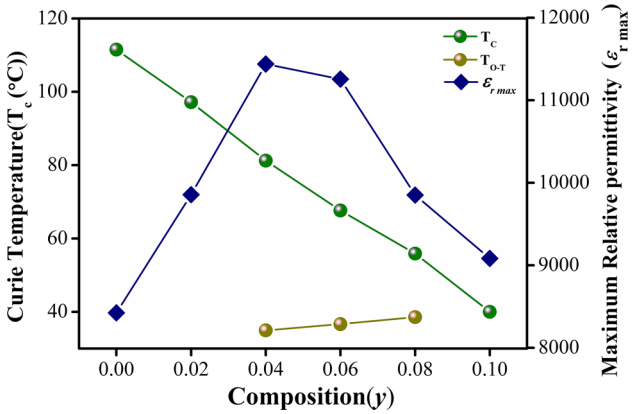

Figure 5 Relative plot between transition temperature (T_m) and maximum relative permittivity ($\varepsilon_{r\ max}$) at 1 kHz of BT-ST-yBSn ceramic as a function of composition y.

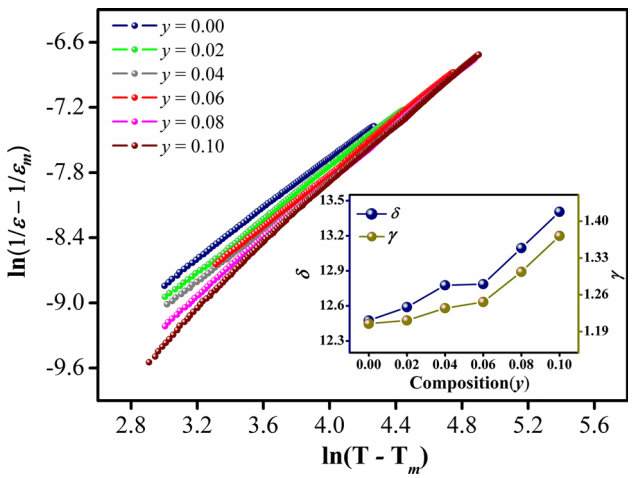

Figure 6 Relative plot between $\ln(1/\varepsilon - 1/\varepsilon_m)$ and $\ln(T - T_m)$.

Figure 4 presents the temperature dependence of relative permittivity (ε_r) and dielectric loss (tan δ) of BT-ST-yBSn systems with $y = 0.00$, 0.02, 0.04, 0.06, 0.08 and 0.10 compositions at frequencies 1, 10 and 100 kHz. The relative permittivity curves for the composition, $y = 0.00$ and 0.02, exhibit one sharp peak at 110 and 97 °C, respectively, with this transition being related to the transition from tetragonal (P4 mm) ferroelectric to cubic (Pm3m) paraelectric phase. Nevertheless, the relative permittivity curves for the compositions, $0.04 \leq y \leq 0.08$, presented two anomalous peaks. A higher temperature was associated with the ferro-to-paraelectric phase transition, while a lower temperature suggested the phase transition from orthorhombic to tetragonal phase. The O–T phase transition temperature shifted slightly with increasing Sn content to a high temperature from 32 °C for $y = 0.04$–41 °C for $y = 0.08$. Furthermore, the transition temperature decreases with increasing Sn content (Fig. 5). The temperature range width of the tetragonal phase decreases continuously with increasing Sn content. The permittivity at room temperature is seen to increase continuously from $y = 0.00$–0.04 with increasing Sn content. This result is due to the shift of O–T phase transition temperature that is close to room temperature. It is known that the relative permittivity of a normal ferroelectric phase, which is above the maximum relative permittivity temperature, can be described by the Curie–Weiss law [7, 22];

$$\frac{1}{\varepsilon_r} = \frac{C}{T - T_0}, \quad (T > T_c) \tag{1}$$

where T_0 is the Curie–Weiss temperature and C is the Curie–Weiss constant. The relative permittivity of pure BT obeys the Curie–Weiss law, which is $T_0 \sim 383$ K and $C \sim 1.56 \times 10^5$ K [14]. However, further characterization of broad relative permittivity and diffuseness of the phase transition followed a modified Curie–Weiss law, as described below [23, 24]:

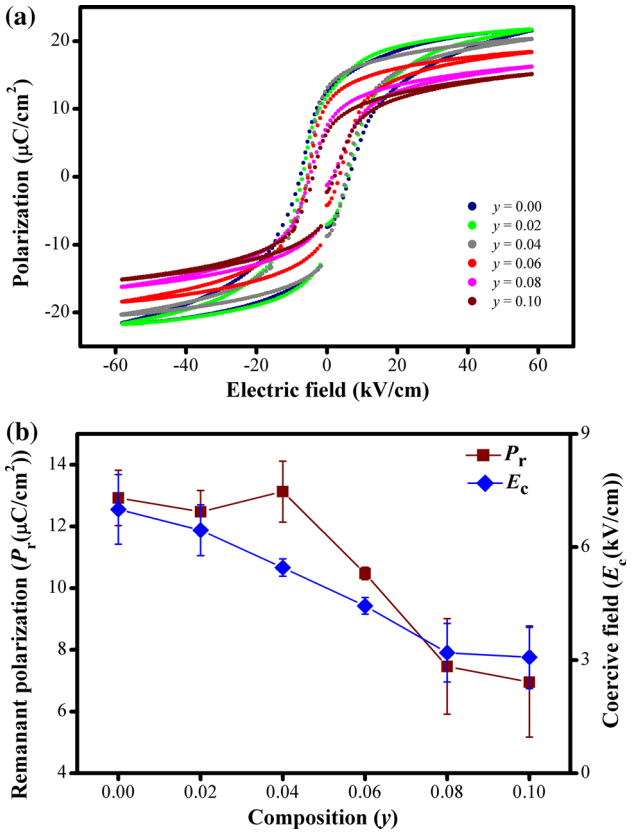

Figure 7 **a** Plot between polarization (μ C/cm^2) and electric field (kV/cm) as a function of composition y, and **b** the plot of remanent polarization (μ C/cm^2) and coercive field (kV/cm) value as a function of composition y.

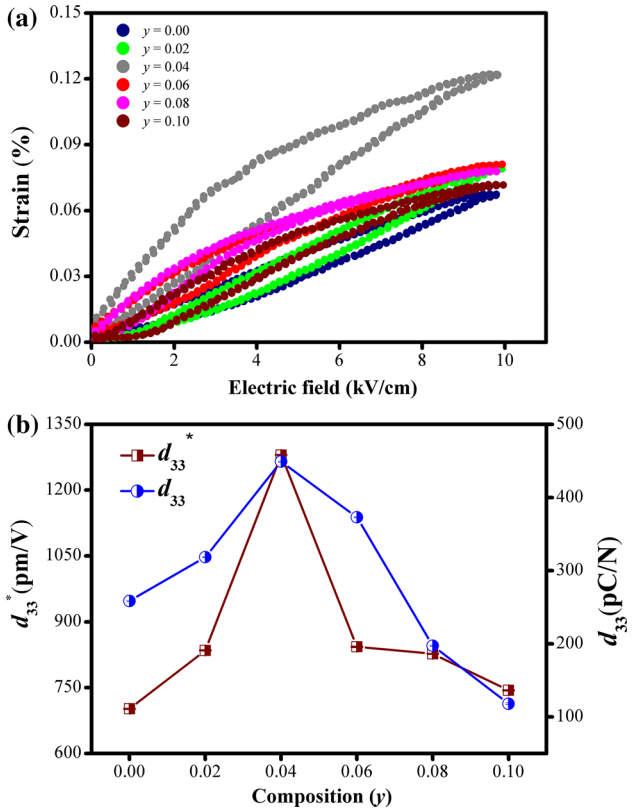

Figure 8 **a** Relative plot between unipolar strain (%) and electric field (kV/cm) as a function of composition, and **b** the plot of normalized strain [d^*_{33} (pm/V)] and piezoelectric constant [d_{33} (pC/N)] value as a function of composition y.

$$\frac{\varepsilon_m}{\varepsilon} = 1 + \frac{(T - T_m)^\gamma}{2^2}, \quad (\text{at } T > T_m), \tag{2}$$

where γ is constant and ε_m is the maximum value of relative permittivity at phase transition temperature (T_m). The parameter γ expresses information on the character of the phase transition, and when $\gamma = 1$, the equation follows the Curie–Weiss law, which indicates normal ferroelectrics, while $\gamma = 2$ describes a complete diffuse phase transition. The δ value can be applied to gauge the degree of diffuseness in the phase transition. Figure 6 illustrates the plot of $\ln\left(\frac{1}{\varepsilon} - \frac{1}{\varepsilon_m}\right)$ as a $\ln(T - T_m)$ function of BT-ST-yBSn systems at 1 kHz. The value of parameter γ and δ is presented in Table 1. It can be seen that parameter γ tends to increase from 1.20 to 1.37 with increasing Sn content. The δ value has a similar tendency to increase from 12.47 to 13.40 with increasing Sn content, thus confirming that a diffuse phase transition appears in the BT-ST-yBSn system. This result occurs when at least two cations dominate the same crystallographic site, a or b, which is found in many complex perovskite structures such as lead-free $BaZrO_3$–$CaTiO_3$–$BaTiO_3$ [11], $K_{0.5}Na_{0.5}NbO_3$–$LiSbO_3$ [25] and $(Ba_{0.85}Ca_{0.15})(Zr_{0.1}Ti_{0.9})O_3$–$Bi(Mg_{0.5}Ti_{0.5})O_3$ [26].

In order to investigate the ferroelectric behavior in BT-ST-yBSn ceramics, the electrical polarization hysteresis loop of each composition was measured at room temperature with an electric field of 60 kV/cm. Figure 7a illustrates the polarization–electric field hysteresis loop for all compositions of y at a frequency of 4 Hz. All BT-ST-yBSn ceramics with $y = 0.00$–0.10 compositions exhibit symmetry in shape and well-saturated hysteresis loops and result in domain switching in an electric field. The plot of P_r and E_c value as a function of composition y is presented in Fig. 7b. It can be seen that the P_r initially tends to increase from 12.93 μC/cm^2 at $y = 0.00$ to a maximum value of 13.14 μC/cm^2 at $y = 0.04$, and then it decreases gradually from 10.48 μC/cm^2 at $y = 0.06$–6.95 μC/cm^2 at $y = 0.10$. In addition, the E_c

values decrease clearly from 7.00 to 3.08 kV/cm with increasing Sn content, as shown in Fig. 7b. The decrease in E_c indicates that ceramics become "softer" with increasing Sn content, regarding the electric field, because the free energy profile for polarized rotation is flattened anisotropically at the two phases and multiphase coexistence [12, 27]. In order to investigate the changes in hysteresis loop behavior, the empirical relationship between P_r, P_s and polarization at fields above E_c was proposed by Haertling and Zimmer for calculating squareness of the hysteresis loop as follows [28]:

$$R_{sq} = \frac{P_r}{P_s} + \frac{P_{1.1E_C}}{P_r} \quad (3)$$

where R_{sq} is the squareness of the hysteresis loop, and P_r and P_s are remanent and saturated polarization, respectively. $P_{1.1Ec}$ is polarization at an increasing electric field of 1.1 times the coercive field (E_c). The squareness parameter investigates the quantification of changes in P–E hysteresis loops. The R_{sq} is equal to 2 for an ideal P–E hysteresis loop. The calculated R_{sq} values of all ceramics are inferred in Table 1. It was found that the R_{sq} parameter tended to decrease from 0.80 to 0.72 with increasing Sn content, which implies that the P–E hysteresis loop becomes more slanted. Figure 8a displays the unipolar electric field induced strain curve for the BT-ST-yBSn ceramic, with $y = 0.00$–0.10 compositions, measured at 10 kV/cm. It can be observed that with increasing Sn content, the unipolar strain increases with increasing y of up to 0.04 and reaches the maximum electrostrain value of 0.13%. On increasing y further to 0.1, the unipolar strain decreases to 0.074%. Figure 8b illustrates the direct piezoelectric coefficient (d_{33}) and a normalized strain or converse piezoelectric coefficient ($d^*_{33}=S_{max}/E_{max}$) at the electric field of 10 kV/cm as a function of composition. It can be observed that the d^*_{33} value tends to increase with increasing composition y and reaches its maximum at about 1280 pm/V at $y = 0.04$, before decreasing with increasing composition y. The d^*_{33} values also have a similar trend and maximum d_{33} values of 450 pC/N, as y increases to 0.04. As a result, ceramic at the composition, $y = 0.04$, exhibits the highest normalized strain and piezoelectric constant in the systematic series studied, due to the coexistence of orthorhombic and tetragonal phase near room temperature. The enhanced d_{33} and d^*_{33} values are considered to be reasonably consistent with the multiphase coexistence of the orthorhombic and tetragonal phase that occurs near ambient temperature at $y = 0.04$. In the point view of crystallographic symmetry, there are 18 domain orientation states (6 domain states along 100c direction for tetragonal symmetry and 12 along 110c direction for orthorhombic symmetry) near the O–T phase transitions. In general, a large number of thermodynamically equivalent states near O–T phase transitions allow a high degree of ferroelectric dipole alignment. This causes instability, multiple polarization and strain variants, so that the direction of polarization is rotated easily by external stress or the electric field, thus making it much easier for different grains to coordinate in a collective response.

Conclusion

BT-ST-yBSn ceramic was fabricated by the conventional solid-state reaction method. Raman and XRD study indicates that the orthorhombic and tetragonal phases coexist near ambient temperature at $y = 0.04$. Enhanced dielectric, ferroelectric and piezoelectric properties of $\varepsilon_{r\ max} \sim 11500$, $P_r \sim 13.14\ \mu C/cm^2$, $d^*_{33} \sim 1280$ pm/V and $d_{33} \sim 450$ pC/N were obtained as samples at $y = 0.04$. This observation indicated that the BT-ST-yBSn system is a promising candidate for lead-free piezoelectric ceramics.

Acknowledgements

This work was supported by King Mongkut's Institute of Technology Ladkrabang [Grant No. A118-59-047], the work of W. Vittayakorn was supported under Grant No KREF045801 and the work of R. Muanghlua was supported by Grant No. KREF045604.

References

[1] Zhang S, Xia R, Shrout TR (2007) Lead-free piezoelectric ceramics versus PZT? J Electroceram 19(4):251–257. doi:10.1007/s10832-007-9056-z

[2] Rödel J, Jo W, Seifert KTP, Anton EM, Granzow T, Damjanovic D (2009) Perspective on the development of lead-free piezoceramics. J Am Ceram Soc 92(6):1153–1177

[3] Panda PK (2009) Review: environmental friendly lead-free piezoelectric materials. J Mater Sci 44(19):5049–5062. doi:10.1007/s10853-009-3643-0

[4] Takenaka T, Nagata H (2005) Current status and prospects of lead-free piezoelectric ceramics. J Eur Ceram Soc 25(12):2693–2700

[5] Beuerlein MA, Kumar N, Usher TM, Brown-Shaklee HJ, Raengthon N, Reaney IM, Cann DP, Jones JL, Brennecka GL (2016) Current understanding of structure–processing–property relationships in $BaTiO_3$–Bi(M)O_3 dielectrics. J Am Ceram Soc 99:2849–2870

[6] Randall CA, Newnham RE, Cross LE (2004) History of the first ferroelectric oxide, $BaTiO_3$. https://ceramics.org/wp-content/uploads/2009/.../first_ferroelectric_oxide_ba_tio3.pdf. Accessed 10 Mar 2017

[7] Moulson AJ, Herbert JM (2003) Electroceramics: materials, properties, applications. Wiley, New York

[8] Bechmann R (1956) Elastic, piezoelectric, and dielectric constants of polarized barium titanate ceramics and some applications of the piezoelectric equations. J Acoust Soc Am 28(3):347–350

[9] Li W, Xu Z, Chu R, Fu P, Zang G (2010) Piezoelectric and dielectric properties of $(Ba_{1-x}Ca_x)(Ti0.95Zr0.05)O_3$ lead-free ceramics. J Am Ceram Soc 93(10):2942–2944

[10] Sutapun M, Vittayakorn W, Muanghlua R, Vittayakorn N (2015) High piezoelectric response in the new coexistent phase boundary of 0.87$BaTiO_3$–(0.13-x)$BaZrO_3$–$x$$CaTiO_3$. Mater Des 86:564–574

[11] Chaiyo N, Cann DP, Vittayakorn N (2015) Phase transitions, ferroelectric, and piezoelectric properties of lead-free piezoelectric $x$$BaZrO_3$–(0.25-$x$)$CaTiO_3$–0.75 $BaTiO_3$ ceramics. J Mater Sci 50(18):6171–6179. doi:10.1007/s10853-015-9174-y

[12] Yao Y, Zhou C, Lv D, Wang D, Wu H, Yang Y, Ren X (2012) Large piezoelectricity and dielectric permittivity in $BaTiO_3$_$x$$BaSnO_3$ system: the role of phase coexisting. EPL (Europhysics Letters) 98(2):27008

[13] Wang X, Yamada H, Xu C-N (2005) Large electrostriction near the solubility limit in $BaTiO_3$–$CaTiO_3$ ceramics. Appl Phys Lett 86(2):2905

[14] Zhang S-W, Zhang H, Zhang B-P, Yang S (2010) Phase-transition behavior and piezoelectric properties of lead-free $(Ba_{0.95}Ca_{0.05})(Ti_{1-x}Zr_x)O_3$ ceramics. J Alloy Compd 506(1):131–135

[15] Zhu LF, Zhang BP, Zhao XK, Zhao L, Zhou PF, Li JF (2013) Enhanced piezoelectric properties of $(Ba_{1-x}Ca_x)$ (Ti0.92Sn0.08)O_3 lead-free ceramics. J Am Ceram Soc 96(1):241–245

[16] Zhu L-F, Zhang B-P, Zhao X-K, Zhao L, Yao F-Z, Han X, Zhou P-F, Li J-F (2013) Phase transition and high piezoelectricity in (Ba, Ca)$(Ti_{1-x}Sn_x)O_3$ lead-free ceramics. Appl Phys Lett 103(7):072905

[17] Li H-R, Chen C-X, Zheng R-K (2015) Effects of Sr substitution on the structural, dielectric, ferroelectric, and piezoelectric properties of Ba (Zr, Ti) O_3 lead-free ceramics. J Mater Sci Mater Electron 26(5):3057–3063. doi:10.1007/s10854-015-2797-6

[18] Lee C-E, Randall CA, Kim D-Y, Kim SH (2014) Multi-site and multi-ionization of Sn in the doping of $BaTiO_3$. J Am Ceram Soc 97(2):513–518

[19] Shoichiro S, Toshikazu T, Akira A, Takashi O, Nobuyuki W, Hideaki N, Hiroshi T (2010) Effect of Sn^{2+} ion substitution on dielectric properties of (Ba, Ca)TiO_3 ferroelectric ceramics. Jpn J Appl Phys 49(9S):09MC04–09MC05

[20] Karan N, Katiyar R, Maiti T, Guo R, Bhalla A (2009) Raman spectral studies of Zr^{4+}-rich $BaZr_xTi_{1-x}O3$ ($0.5 < x < 1.00$) phase diagram. J Raman Spectrosc 40(4):370–375

[21] Dobal P, Dixit A, Katiyar R, Yu Z, Guo R, Bhalla A (2001) Micro-Raman scattering and dielectric investigations of phase transition behavior in the $BaTiO_3$–$BaZrO_3$ system. J Appl Phys 89(12):8085–8091

[22] Vittayakorn N, Rujijanagul G, Tan X, Marquardt MA, Cann DP (2004) The morphotropic phase boundary and dielectric properties of the $x$$Pb(Zr_{1/2}Ti_{1/2})O_3$-$(1-x)$$Pb(Ni_{1/3}Nb_{2/3})O_3$ perovskite solid solution. J Appl Phys 96(9):5103–5109

[23] Jaffe B, Cook WR, Jaffe H (1971) Piezoelectric ceramics. Academic Press, London

[24] Cross LE (1987) Relaxor ferroelectrics. Ferroelectrics 76(1):241–267

[25] Palei P, Kumar P (2012) Dielectric, ferroelectric and piezoelectric properties of $(1-x)[K_{0.5}Na_{0.5}NbO_3] - x[LiSbO_3]$ ceramics. J Phys Chem Solids 73(7):827–833

[26] Bai W, Hao J, Shen B, Zhai J (2013) Dielectric properties and relaxor behavior of high Curie temperature $(Ba_{0.85}Ca_{0.15})(Zr_{0.1}Ti_{0.9})O_3$–$Bi(Mg_{0.5}Ti_{0.5})O_3$ lead-free ceramics. Ceram Int 39:S19–S23

[27] Liu W, Ren X (2009) Large piezoelectric effect in Pb-free ceramics. Phys Rev Lett 103(25):257602

[28] Haertling GH, Zimmer W (1966) An analysis of hot-pressing parameters for lead zirconate—lead titanate ceramics containing two atom percent bismuth. Am Ceram Soc Bull 45(12):1084–1089

Ferroelectrics

ISSN: 0015-0193 (Print) 1563-5112 (Online) Journal homepage: http://www.tandfonline.com/loi/gfer20

Dielectric, Ferroelectric and Piezoelectric Properties of the Lead Free $0.9BaTiO_3$-$(0.1-x)Bi_{0.5}Na_{0.5}TiO_3$-$xBi(Mg_{0.5}Ti_{0.5})O_3$ Solid Solution

Jitkasem Mayamae, Usa Sukkha, Surasak Niemchareon, Rangson Muanghlua & Naratip Vittayakorn

To cite this article: Jitkasem Mayamae, Usa Sukkha, Surasak Niemchareon, Rangson Muanghlua & Naratip Vittayakorn (2016) Dielectric, Ferroelectric and Piezoelectric Properties of the Lead Free $0.9BaTiO_3$-$(0.1-x)Bi_{0.5}Na_{0.5}TiO_3$-$xBi(Mg_{0.5}Ti_{0.5})O_3$ Solid Solution, Ferroelectrics, 490:1, 23-35, DOI: 10.1080/00150193.2015.1070656

To link to this article: http://dx.doi.org/10.1080/00150193.2015.1070656

Published online: 29 Jan 2016.

Ferroelectrics, 490: 23–35, 2016

ISSN: 0015-0193 print / 1563-5112 online
DOI: 10.1080/00150193.2015.1070656

Taylor & Francis
Taylor & Francis Group

Dielectric, Ferroelectric and Piezoelectric Properties of the Lead Free $0.9BaTiO_3$-$(0.1\text{-}x)Bi_{0.5}Na_{0.5}TiO_3$-$xBi(Mg_{0.5}Ti_{0.5})O_3$ Solid Solution

JITKASEM MAYAMAE,[1] USA SUKKHA,[2] SURASAK NIEMCHAREON,[3] RANGSON MUANGHLUA,[3] AND NARATIP VITTAYAKORN[1,4,5,*]

[1]Electroceramic Research Laboratory, College of Nanotechnology, King Mongkut's Institute of Technology Ladkrabang, Bangkok 10520, Thailand
[2]Synchrotron Light Research Institute (Public Organization), 111 University Avenue, Muang District, Nakhon Ratchasima 30000, Thailand
[3]Department of Electronics Engineering, Faculty of Engineering, King Mongkut's Institute of Technology Ladkrabang, Bangkok 10520, Thailand
[4]Advanced Materials Research Unit, Faculty of Science, King Mongkut's Institute of Technology Ladkrabang, Bangkok 10520, Thailand
[5]Nano-KMITL Center of Excellence on Nanoelectronic Devices, KMITL, Ladkrabang, Bangkok 10520, Thailand

Solid solution of $0.9BaTiO_3$-$(0.1\text{-x})Bi_{0.5}Na_{0.5}TiO_3$-x$Bi(Mg_{0.5}Ti_{0.5})O_3$ (BT-BNT-xBMT) system, where x = 0.00, 0.02, 0.04, 0.06, 0.08, 0.10, was synthesized by the solid state reaction. Dense BT-BNT-xBMT ceramics were obtained by sintering at 1,150–1,250°C for 4 h. The effect of BMT on crystal structure and electrical property of BT-BNT ceramics was investigated as a function of composition, x, using X-ray diffraction, dielectric spectroscopy, hysteresis and strain measurements. The crystal structure of solid solution BT-BNT-xBMT, where x = 0.00-0.10, successively transforms from tetragonal to pseudocubic symmetry, with increased BMT concentration. Temperature dependence of dielectric constant (ε_r) and dielectric loss (tanδ) for BT-BNT-xBMT at various frequencies showed that phase transition of ceramics changed from ferroelectric to relaxor-like behavior as BMT content increased. Furthermore, remanent polarization (P_r), coercive field (E_c) and the normalized strain (d_{33}) of BT-BNT-xBMT ceramics tend to decrease with increasing BMT concentration.*

Keywords BT-BNT-*x*BMT; lead free piezoelectric; phase transition; electrical properties

1. Introduction

Lead zirconate titanate (PZT) ceramics have been used widely in many electronic devices such as piezoelectric sensor, actuators and transducers because of their excellence

Received October 26, 2014; in final form January 20, 2015.
*Corresponding author. E-mail: naratipcmu@yahoo.com
Color versions of one or more of the figures in this article can be found online at www.tandfonline.com/gfer.

piezoelectric properties [1]. However, PZT-based piezoelectric ceramics are not environmental friendly because more than 60% wt of these ceramics contains the lead toxicity. Furthermore, the EU legislation forced draft directives including Waste from Electrical and Electronic Equipment (WEEE) and Restriction of Hazardous Substances (RoHS). According to the environmental issues, lead free friendly piezoelectric ceramics have been received considerable attentions to replace lead-based piezoelectric materials.

Although no real lead free materials can be replaced the common use in lead-based ceramics for various applications, many potentially promising lead free materials have been developed. Among the lead free materials, Barium titanate ($BaTiO_3$; BT) has perovskite structure and good electrical properties such as ferroelectric and piezoelectric properties but low Curie temperature (T_c) [2]. In recent years, there are many researches about BT-base for example $Ba_{0.85}Ca_{0.15}Ti_{0.90}Zr_{0.10}O_3$ [3] and (1-x)$Ba_{0.98}Ca_{0.02}Ti_{0.94}Sn_{0.06}O_3$-x$Ba_{0.85}$-$Ca_{0.15}Ti_{0.90}$ -$Zr_{0.10}O_3$ [4]. Jiagang Wu *et al.* [4] found that BT-base ceramic by combining (1-x)$Ba_{0.98}Ca_{0.02}Ti_{0.94}Sn_{0.06}O_3$-x$Ba_{0.85}Ca_{0.15}Ti_{0.90}Zr_{0.10}O_3$((1-x)BCTS-xBCTZ) system has a phase boundary coexistence of orthorhombic and tetragonal phase at around 4 mol% BCTZ which show good dielectric and piezoelectric properties of dielectric constant ($\varepsilon_r \sim 5500$), dielectric loss ($\tan\delta \sim 0.3\%$) and piezoelectric constant ($d_{33} \sim 407$ pC/N). The binary system of $Bi_{0.5}Na_{0.5}TiO_3$-$BaTiO_3$ (BNT-BT) is an important candidate for replacing lead-based piezoelectric. In a few decades, BNT-BT solid solution was studied by various research groups [2, 5, 6]. Takenaka *et al.* [5] found that BNT-BT system has a morphotrobic phase boundary (MPB) between rhombohedral and tetragonal phases at around 6-7 mol% BT which shows the excellent properties including $\varepsilon_{33}^T/\varepsilon_0 = 580$, piezoelectric constant ($d_{33} = 125$ pC/N), Curie temperature ($T_c = 288°C$), dielectric loss ($tan\delta = 1.3\%$) and planar coupling coefficient ($k_{33} = 55.0\%$). Afterwards, researchers focused to develop BNT-BT binary material on the composition range of MPB by doing ternary solid solution such as KNN-modified BNT-BT [7,8] and BZr-modified BNT-BT [9]. Also, the BNT-BT-based systems on the BNT-rich side have been investigated extensively for example (0.94-x)BNT-0.06BT-xKNN [7], 0.865BNT–0.350BT–0.100BKT [8] and BZr-modified BNT-BT [9]. However, few works have investigated and developed BNT-BT on the BT-rich side. Recently, Wada et al. studied on the combination between $BaTiO_3$ and Bi($Mg_{0.5}Ti_{0.5}$)O_3 (BMT) and found that BMT can enhance Curie temperature (T_C) of BT with the highest T_C (about 360°C) for 0.5$BaTiO_3$-0.5BMT ceramics [10]. Moreover, Qi Wang et al. have studied lead free $Bi_{0.5}Na_{0.5}TiO_3$–Bi($Mg_{0.5}Ti_{0.5}$)O_3 systems and reported that BMT can improve piezoelectric properties and enhance T_C of BNT ceramic. The 0.95BNT-0.05$BMTO_3$ ceramic showed the highest d_{33} about 110pC/N and high T_C at 352°C [11].

This work dealt with the new ternary system of 0.9$BaTiO_3$-(0.1-*x*)$Bi_{0.5}Na_{0.5}TiO_3$-*x*Bi($Mg_{0.5}Ti_{0.5}$) in order to get more information of BT-BNT-based on BT-rich side. BT-BNT-*x*BMT ceramics were prepared by the solid state reaction. The effect of BMT on crystal structure, phase transition and electrical properties were studied as a function of composition, *x*.

2. Experimental

Lead free 0.9$BaTiO_3$-(0.1-*x*)$Bi_{0.5}Na_{0.5}TiO_3$-*x*Bi($Mg_{0.5}Ti_{0.5}$)O_3 (BT-BNT-*x*BMT) ceramics, where $x = 0.00, 0.02, 0.04, 0.06, 0.08, 0.10$, were synthesized by the solid state reaction. Bi_2O_3 (99.9%, Sigma-Aldrich), $BaCO_3$ (98.5%, Fluka), Na_2CO_3 (99.8%, Riedel-deHaen), TiO_2 (99.9%, Sigma-Aldrich) and MgO (99%, Fluka) powders were used raw materials. First, stoichiometric amounts of raw materials were weighted and ball-milled with yttrium-stabilized zirconia in ethanol media for 18 hours. After drying the mixture for 24 h in an oven, the mixed

powder was calcined at 900°C for 4 hours with heating/cooling rate 10°C/min. In order to obtain fine particles prior to making a pellet, the calcined powders were ground and sieved. The fine powders were pressed into disks with 15 mm diameter. 5 wt% polyvinyl alcohol as a binder was used as binder. The disks were sintered at 1150-1250°C for 4 hours with heating/cooling rate 5°C/min. The crystal structure of ceramics was characterized using X-ray diffraction (Bruker-AXS D 8 Advance) with Cu(Kα) radiation in the 2θ scan range of 20°–80°. For electrical measurements, the samples were polished for both sides and made parallel before electrode coating with silver paste (C1000, Heraeus) on both surfaces. Silver paste was heated on at 750°C for 20 min with heating/cooling rate 5°C/min. The relative permittivity (ε_r) and dielectric loss (*tan*δ) were determined as a function of frequency (1-100 kHz) and temperature (room temperature to 250°C) using LCR meter (HP4284A, Hewlett-Packard, Palo Alto, CA). Polarization-electric field (P-E) hysteresis loop were determined at room temperature using Radiant Technologies, Inc (RT66A). The strain-electric field (S-E) curves were determined using MTI-2100 Fotonic sensor combined with Radiant Technologies. The peak field for P-E hysteresis loop and S-E curve measurements was maintained at 60 kV/cm during measurement. The surface morphology of ceramics was observed using scanning electron microscope (EVO®MA10).

3. Results and Discussion

The X-ray diffraction patterns of BT-BNT-*x*BMT ceramics, where $x = 0.00$, 0.02, 0.04, 0.06, 0.08, 0.1, are shown in Figure 1(a). It indicates that all samples are a single phase with the perovskite structure. The secondary and other phases were not observed in the XRD patterns, which indicating that all compositions in the BT-BNT-*x*BMT system can completely form solid solution with a perovskite structure. A (111) peak at around 39 was chosen to identify the crystal structure of BT-BNT-XBMT ceramics as shown in Figure 1(b). In the compositions, $0.00 \leq x \leq 0.08$, the crystal structure has a tetragonal symmetry, identified by a splitting of the (002) and (200) peaks. At the higher BMT content of $x = 0.1$, the doublet of (002) and (200) peaks become a single peak of (200) and the (111) peak still exhibits a single peak. These results indicated that the crystal structure changed to a pseudocubic symmetry.

The average ionic radius of A-site and B-site, calculated lattice parameters, the tetragonality c/a ratio and tolerance factor of each composition are listed in Table 1. The tetragonality c/a ratio is the important factor representing the lattice distortion of the tetragonal symmetry. It is seen that the c/a ratio decreases significantly with increasing BMT content. The ionic radii of Bi^{3+} (CN = 12, 1.40 Å) are smaller than the ionic radii of Ba^{2+} (CN = 12, 1.61 Å) resulting in the decreasing of average ionic radii at A-site [12]. Also, the substitution of Ti^{4+} ions (CN = 6, 0.605 Å) by Mg^{2+} (CN = 6, 0.72 Å) results in the increasing of average ionic radii at B-site as shown in Table 1. Then, it is reasonable to assume that the substitution of BMT into BT-BNT leads to the distortion and deformation of tetragonal structure. Furthermore, the tolerance factor (t) is important factor that reflecting the perovskite structure distortion, rotation and tilt of the BO_6 octahedra [13]. Generally, the perovskite structure is stable in the range of $0.880 < t < 1.090$ region [14] and the symmetry is higher as the t value is approach to 1. It is also noticed that the t for BT-BNT-*x*BMT ceramics tends to decrease with increasing BMT which corresponds well with the phase transition from tetragonal to pseudocubic symmetry.

Based on the XRD data, it could be said that the combination between BT-BNT and BMT could form completely crystalline solid solution of perovskite structure but the existence of BMT caused the tetragonality of BT-BNT decrease.

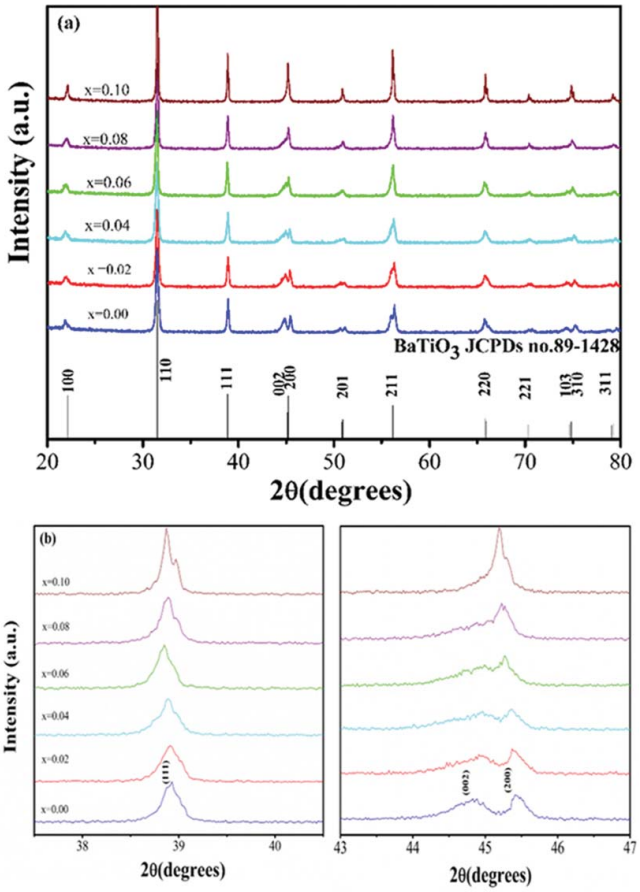

Figure 1. (a) X-ray diffraction patterns of 0.9BT-(0.1-x)BNT-(x)BMT ceramics with the composition $0.00 \leq x \leq 0.10$; (b) X-ray diffraction patterns for (111), (002) and (200) peaks of 0.9BT-(0.1-x)BNT-(x)BMT ceramics with the composition $0.00 \leq x \leq 0.10$.

Figure 2 illustrates the temperature dependence of the relative permittivity (ε_r) and dielectric loss ($tan\delta$) of BT-BNT-xBMT ceramics measured at various frequencies between 1 and 100 kHz. Regarding the composition, $x = 0.00$, the relative permittivity of 0.9BT-0.1BNT increased slowly until the temperature approached transition temperature, then it abruptly increased and passed through a maximum of about 178°C. This discontinuity of dielectric constant at phase transition is characteristic of the first order phase transition [15] and occurs from the change of the tetragonal ferroelectric (FE) phase into the cubic paraelectric (PE) phase, in agreement with previous reports [2]. The relative permittivity curves at the compositions, $0.02 \leq x \leq 0.10$, showed only one phase transition. The composition, $x = 0.02$, showed a broadening dielectric peak which much like the characteristic of relaxor ferroelectric, however the position of the peaks keep unchanged at various applied frequency. At higher composition, $0.04 \leq x \leq 0.10$, the diffuse phase transition behaviour with broad maximum and frequency dispersion became more self-evident when BMT concentration increased. Also, the transition temperature is dependent of frequency and increases with increasing frequency. These results indicated that BT-BNT-xBMT progressively change from normal ferroelectric to relaxor ferroelectric when

Table 1
Lattice parameters and lattice anisotropy of BT-BNT-XBMT ceramics with the composition $0.00 \leq x \leq 0.10$

		Ionic radii (Å)			Lattice parameter (Å)		
x	Crystal structure	A-site	B-site	Tolerance factor (t)	a	c	c/a
0.00	T	1.5910	0.605	1.0548	3.9590 ± 0.0792	4.1086 ± 0.2924	1.0378
0.02	T	1.5906	0.6062	1.0541	3.9847 ± 0.0518	4.0619 ± 0.1678	1.0194
0.04	T	1.5902	0.6073	1.0534	3.9792 ± 0.0500	4.0675 ± 0.1641	1.0222
0.06	T	1.5898	0.6085	1.0526	3.9969 ± 0.0421	4.0282 ± 0.0456	1.0078
0.08	T	1.5894	0.6096	1.0519	4.0017 ± 0.0159	4.0131 ± 0.0118	1.0029
0.10	PC	1.5890	0.6107	1.0511	4.0066 ± 0.0049	–	–

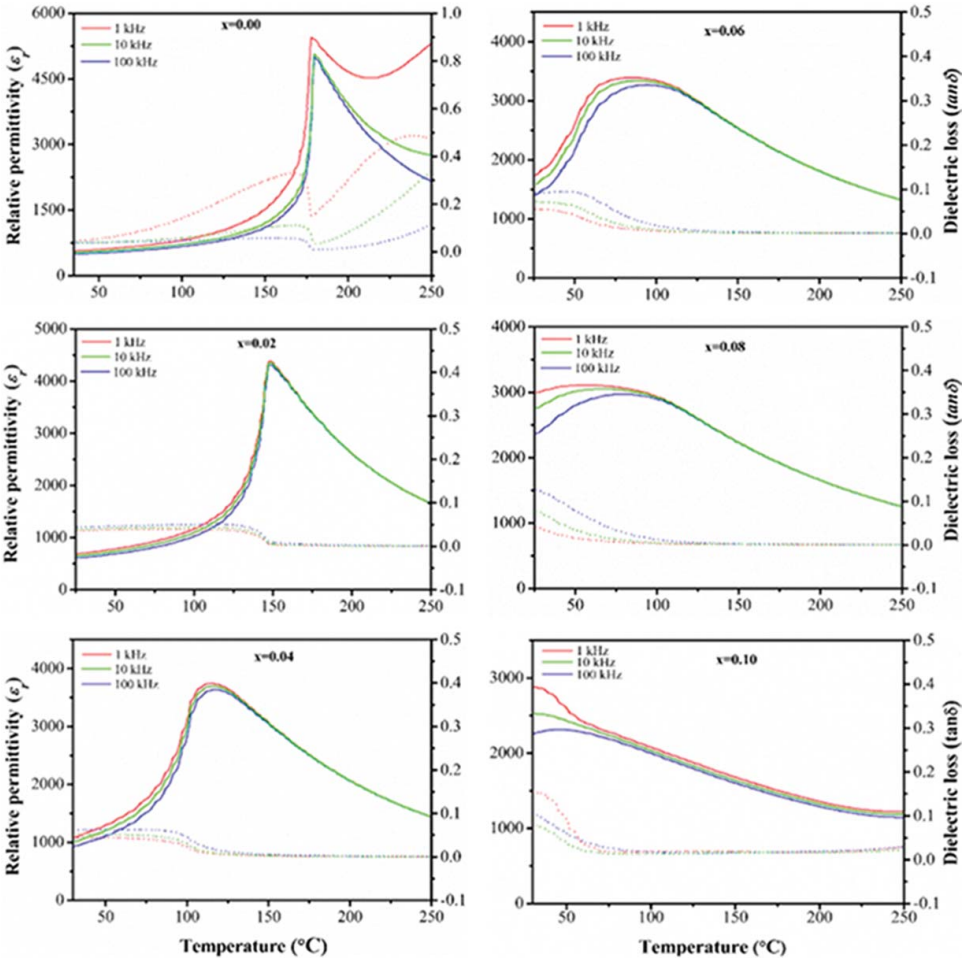

Figure 2. Relative permittivity (ε_r) and dielectric loss ($tan\delta$) as a temperature dependence of 0.9BT-(0.1-x)BNT-(x)BMT ceramics with the composition $0.00 \leq x \leq 0.10$.

BMT concentration increases. This phenomenon of BT-BNT-xBMT system resulted from the substitutions of Bi^{3+} ions for Na^{+} ions and Mg^{2+} ions for Ti^{4+}, which distort the unit cell and change dipole moment. For complex perovskite compound, the more cations occupy the equivalent crystallographic site of A or B, the more the chemical fluctuation and structural disorder in arrangement of cations are inhomogeneous at the nanometre scale, then the relaxation characteristic becomes more distinctly [16, 17].

In order to further characterize the relaxor behavior, a modified Curie–Weiss law in equation (1) was used for description a broad relative permittivity and diffuseness of phase transition [18, 19].

$$\frac{\varepsilon_m}{\varepsilon} = 1 + \frac{(T - T_m)^{\gamma}}{2\delta_{\gamma}} \tag{1}$$

where ε_m is the maximum value of relative permittivity and T_m is the temperature of dielectric maximum. The γ value expresses the degree of dielectric relaxation in relaxor

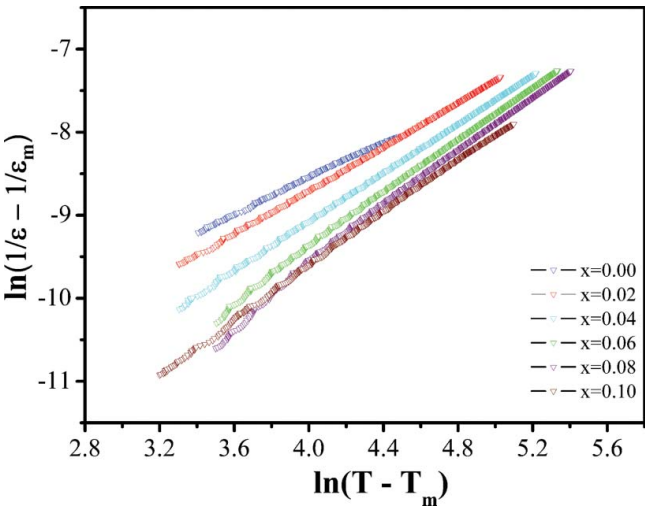

Figure 3. The relative plot between ln(1/ε–1/ε$_m$) and ln(T – T$_m$).

ferroelectric material which this value is in the range of $1 \leq \gamma \leq 2$. When γ value is equal 1, Eq. (1) becomes the classic Curie Weiss law valid in the case of normal ferroelectric. When γ value is equal 1, the ideal relaxor behavior with quadratic dependence is described. The parameter δ_γ is the diffuse parameter which can be used to determine the degree of diffuseness in the phase transition. The $\delta_{\boldsymbol{\gamma}}$ value can be observed from the slope of $\varepsilon'_m/\varepsilon'$ versus $(T\text{-}T_m)^2$, which should be linear. Plot of ln $(\frac{1}{\varepsilon} - \frac{1}{\varepsilon_m})$ as function of ln (T-T$_m$) at 100 kHz of BT-BNT-*x*BMT ceramics are displayed in figure 3. By plotting ln (1/ε–1/ε$_{max}$) versus ln(T-T$_m$), the γ value can be determined directly from the gradient. The γ and $\boldsymbol{\delta\gamma}$ values are determined and shown in Table 2. It is clearly seen that both δ_γ and γ values tend to increase with increasing of the BMT content, confirming the relaxor behavior in these solid solution. Based on the dielectric data, a slim P-E hysteresis loop in BT-BNT-*x*BMT ceramic at high BMT content is expected to observe at room temperature.

Curie temperature and maximum relative permittivity ($\varepsilon_{r\,max}$) at 100 kHz of BT-BNT-*x*BMT ceramics are determined and plotted as a function of composition in

Table 2
The dielectric and ferroelectric properties of BT-BNT-XBMT ceramics with the composition $0.00 \leq x \leq 0.10$

x	$\varepsilon_{r\ room}$ at 100 kHz	*tan*δ at 100 kHz	γ	δ_γ	P_r (μC/cm^2)	P_s (μC/cm^2)	E_c (kV/cm)	Squareness hysteresis loop (R_{sq})
0.00	524	0.038	1.08	12.88	15.52	19.72	29.47	1.56
0.02	663	0.039	1.32	13.98	12.87	18.04	24.31	1.38
0.04	1075	0.051	1.47	14.94	11.26	17.74	20.41	1.20
0.06	1684	0.071	1.60	15.77	8.30	17.30	13.64	0.88
0.08	2820	0.069	1.67	16.26	2.55	15.96	4.24	0.37
0.10	2526	0.080	1.59	15.97	1.63	11.77	3.48	0.33

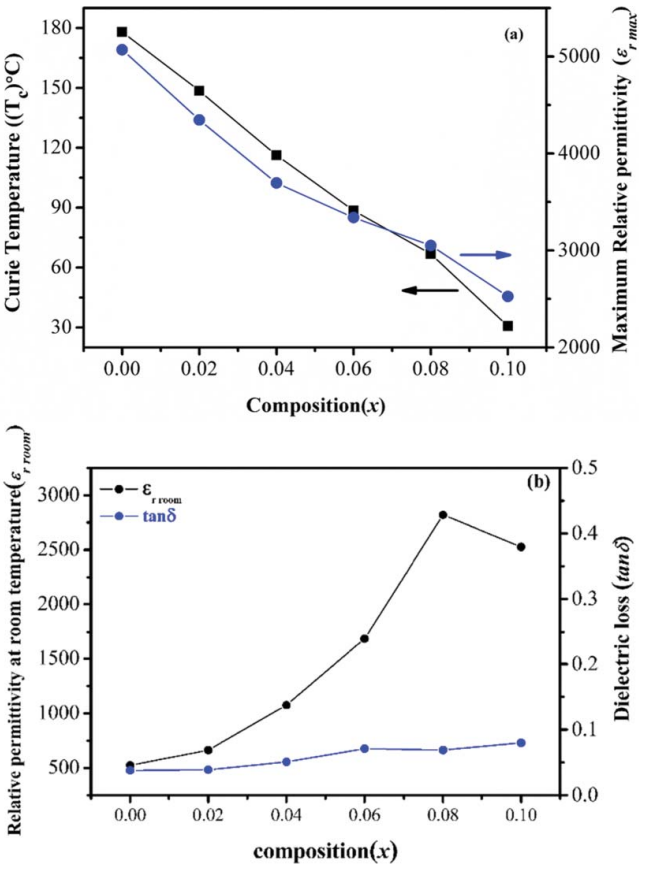

Figure 4. (a) The relative plot between Curie temperature and maximum relative permittivity ($\varepsilon_{r\,max}$) as a function of composition (x); (b) The relative plot between relative permittivity at room temperature ($\varepsilon_{r\ room}$) and dielectric loss ($tan\delta$) as a function of composition (x).

Figure 4(a). It was observed that Curie temperature decreased rapidly with further increase of BMT. As the previous works have reported that the rapidly decrease in transition can be caused by valence mismatch [20, 21]. In BT-BNT-xBMT system, the differences in valence of ions at A-site (Ba^{2+}, Na^{+}, Bi^{3+}) and B-site (Mg^{2+}, Ti^{4+}) might be result in valance mismatch, thus Curie temperature decrease with increasing BMT content. Similar behavior is also observed for the substitution of BMT in KNN structure [22]. Moreover, the maximum relative permittivity ($\varepsilon_{r\ max}$) of BT-BNT-XBMT ceramics tends to decrease with increasing BMT concentration. However, at room temperature the relative permittivity ($\varepsilon_{r\ room}$) tends to abruptly increase with increasing BMT, excepting the composition, x = 0.10. While, dielectric loss ($tan\delta$) tend to gradually increase with BMT increase as shown in Figure 4(b). The smooth increase of $\varepsilon_{r\ room}$ for the compositions, $0.02 \leq x \leq 0.08$, might be attributed to the decreasing of Curie temperature to room temperature. While, the $\varepsilon_{r\ \mathrm{room}}$ of composition, x = 0.10 is decrease might be the Curie temperature being below room temperature.

The composition dependence of polarization-electric field (P-E) hysteresis loops for BT-BNT-xBMT system was measured at room temperature with electric field of 60 kV/ cm, as shown in figure 5. It is evident that all ceramics display the saturated P-E

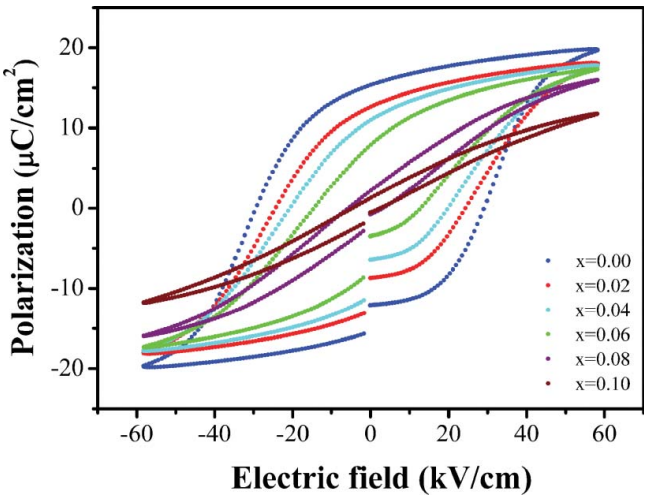

Figure 5. The relative plot of polarization (μC/cm^2) with electric field (kV/cm) of 0.9BT-(0.1-x) BNT-(x)BMT ($x = 0.00$-0.10) ceramics.

hysteresis loops. For 0.9BT-0.1BNT, a shape of hysteresis loop displays typically normal ferroelectric behavior with remanent polarization (P_r) and coercive field (E_c) of 15.52 μC/cm^2 and 29.47 kV/cm, respectively, which in good agreement with previous work [2]. Normal ferroelectric contains a long-range interaction between dipoles in the ferroelectric micro-domain state, giving a typical square hysteresis loops with high P_r and E_c. As expected for BT-BNT-xBMT ceramics, the substitution of BMT has significantly effect on the hysteresis loops shape and polarization and coercive field values. The more BMT concentration increases, the more the hysteresis loop shape becomes slim, identified the gradually drop of P_r, P_s and E_c values as summarized in Table 2. This result suggests that the long-range order of polarization in ferroelectric micro-domain was significantly broken down to polar nano-regions by adding BMT. Then, at high content of BMT, normal ferroelectric BT-BNT-xBMT ceramics become relaxor-like behavior exhibiting a slim P-E hysteresis loop with low P_r and E_c. For low content of BMT, the decreasing of P_r and E_c might be due to an easier of domain switching and domain wall motions [23] as well as tetragonality decreasing of crystal structure in this system [24]. The plots of P_r and E_c values against composition are given in figure 6. Again, a clearly smooth trend of decrease was seen in P_r and E_c with respect to BMT content, confirming the completely solid solution formation in BT-BNT-xBMT system.

To confirm the changes in hysteresis behavior, the empirical relationship between P_r, P_s and polarization at fields above the E_c proposed by Haertling and Zimmer was used for calculated the squareness of hysteresis loop [25]

$$R_{sq} = \frac{P_r}{P_s} + \frac{P_{1.1EC}}{P_r} \tag{2}$$

where R_{sq}, P_r and P_s are squareness of hysteresis loop, remanent polarization and saturation polarization, respectively. $P_{1.1Ec}$ is the polarization at an electric field equal to 1.1 times the coercive field (E_c). The squareness parameter reflects the quantification of changes P-E hysteresis loops. For an ideal P-E hysteresis loop, the R_{sq} is equal to 2. The calculated R_{sq} for all ceramics is listed in Table 2. It is clearly found that, as BMT content

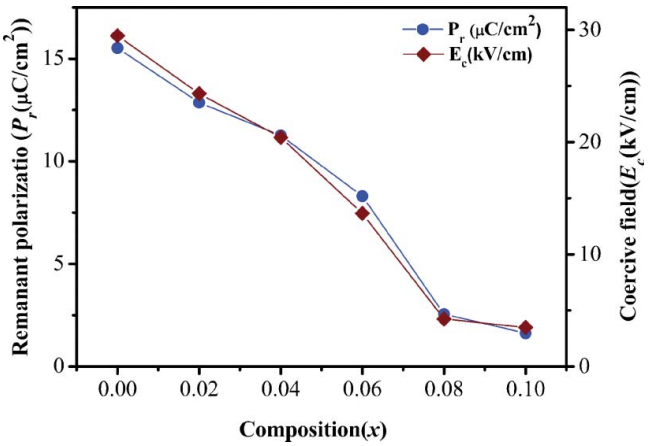

Figure 6. The composition (x) dependence of remanent polarization (P_r (μC/cm^2)) and coercive field (E_c(kV/cm)) in 0.9BT-(0.1-x)BNT-(x)BMT ceramics.

increase, the R_{sq} parameter decreases from 1.56 to 0.33 which implies that P-E hysteresis loop becomes more slanted. On the other words, the P-E loops changes from normal ferroelectric to relaxor behavior with increasing BMT concentration which is consistent with the dielectric result.

Combined with the ferroelectric, the dielectric and XRD results of BT-BNT-xBMT ceramic, all of changes such as the transformation of crystal structure, the decreasing of transition temperature and remanent polarization and ferroelectric – relaxor ferroelectric phase transition are so smooth. Therefore, it could be said that BT-BNT and BMT can completely form solid solution throughout the whole composition range.

Figure 7 illustrates the unipolar strain curves of BT-BNT-xBMT ceramics measured at room temperature with an external electric field of 60 kV/cm. It is clearly found the decreasing of unipolar strain of BT-BNT-xBMT ceramics from 0.2% to 0.09% when the

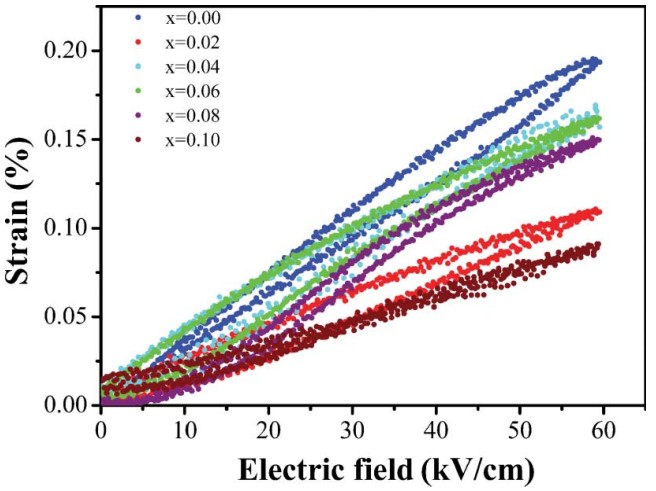

Figure 7. The relative plot of unipolar strain (%) as a function of electric field (kV/cm) in 0.9BT-(0.1-x)BNT-(x)BMT ($x = 0.00$-0.10) ceramics.

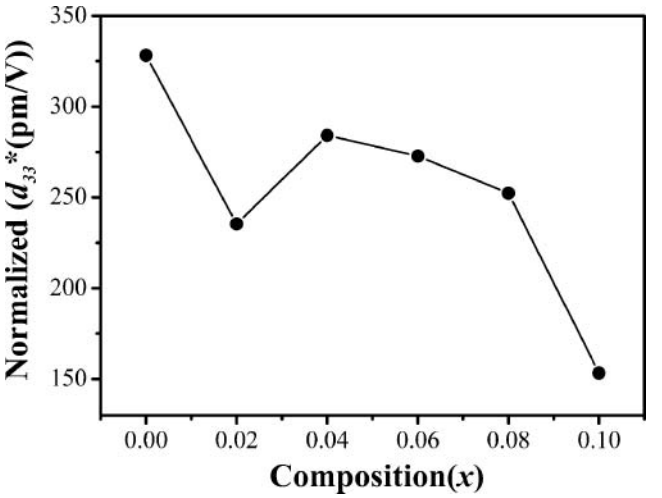

Figure 8. Normalized strain (d_{33} *(pm/V)) value of 0.9BT-(0.1-x)BNT-(x)BMT ceramics with the composition $0.00 \leq x \leq 0.10$.

composition of x was increased from 0.00 to 0.10. The normalized strain (d_{33}*) value of BT-BNT-XBMT ceramics was calculated from the S_{max}/E_{max} ratio for each composition. The composition dependence of normalized strain tends to decrease from 328 pm/V to 153 pm/V when composition of BMT increases, as represented in figure 8. This result has caused the approaching to the relaxor-like behavior with increasing of BMT [26].

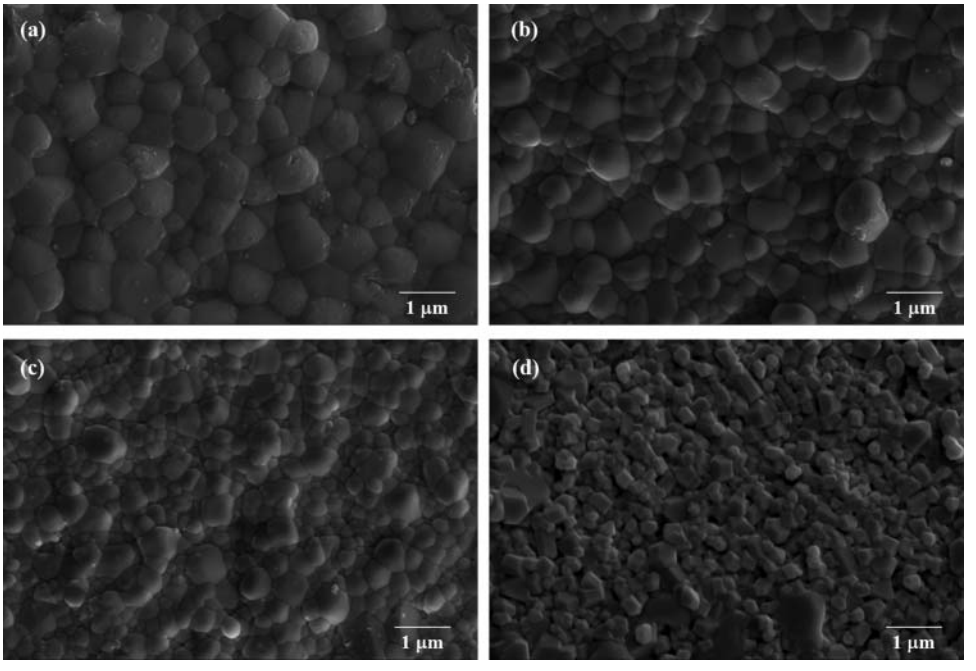

Figure 9. SEM micrographs of 0.9BT-(0.1-x)BNT-(x)BMT ceramics with various compositons (a) x = 0.00, (b) x = 0.02, (c) x = 0.04, and (d) x = 0.10.

The composition dependence of the level of induce strain is similar to result observation of BT-Bi($Ni_{1/2}Ti_{1/2}$)O_3 system [27].

Figure 9 displays SEM micrograph of the sintered surfaces of BT-BNT-*x*BMT ceramics at $x = 0.00$, 0.02, 0.04 and 0.10. The substitution of BMT directly effects on the average grain size of BT-BNT-*x*BMT ceramics. For the composition $x = 0.00$, the grain morphology shows and the average grain size is about 1.01 ± 0.14 μm. Homogeneous and uniformity feature microstructures were observed in the composition $x = 0.00$. The wide grain size distributions was observed in the composition $x = 0.02$ and 0.04. For the composition $x = 0.10$, more disorderly and unsystematic shaped grains are observed. A dramatic grain growth inhibition was founded with increasing BMT composition. The average grain size decreased significantly with increasing the composition *x*. The average grain size are about 0.72 ± 0.09 μm, 0.54 ± 0.09 μm, and 0.49 ± 0.07 μm for the composition $x = 0.02$, 0.04 and 0.10 respectively. This should be attributed to the effects arisen from the donor-type nature of BMT on inhibiting the grain growth [22]. The decreasing in piezoelectric properties in BNT-BT-xBMT system may be attributed to the inhibiting of the grain growth coursed by substitution of BMT in the BNT-BT system. The detailed mechanisms of the diminution in piezoelectric properties of BNT-BT-xBMT system are unclear and demands further study.

4. Conclusion

Lead free 0.9$BaTiO_3$-(0.1-*x*)$Bi_{0.5}Na_{0.5}TiO_3$-*x*Bi($Mg_{0.5}Ti_{0.5}$)O_3 (BT-BNT-*x*BMT; $x = 0.00 - 0.10$) piezoelectric ceramics were synthesized successfully by the solid state reaction. The crystal structure of BT-BNT-*x*BMT solid solution transforms from tetragonal to pseudocubic symmetry with increasing of BMT content. Combined with the ferroelectric and the dielectric results of BT-BNT-*x*BMT ceramic, phase transition of ceramics gradually changed from ferroelectric to relaxor-like behavior as BMT content increased. Also, BT-BNT and BMT can completely form solid solution throughout the whole composition range.

Funding

This work was supported by the Thailand Research Fund (TRF), under Grant No. BRG5680006.

References

1. J. Rödel, W. Jo, K. T. P. Seifert, E. M. Anton, and T. Granzow, D. Damjanovic, Perspective on the development of lead-free piezoceramics. *J Am Ceram Soc.* **92**, 1153–1177 (2009).
2. M. Rawat, and K. L. Yadav, Structural, dielectric and ferroelectric properties of $Ba_{(1-x)}(Bi_{0.5}Na_{0.5})xTiO_3$ ceramics. *Ceram Int.* **39**, 3627–3633 (2013).
3. J. Wu, D. Xiao, W. Wu, Q. Chen, Q. Zhu, Z. Yang, and J. Wang, Role of room-temperature phase transition in the electrical properties of (Ba, Ca)(Ti, Zr)O_3 ceramics. *Scripta Mater.* **65**, 771–774 (2011).
4. J. Wu, A. Habibul, X. Cheng, X. Wang, and B. Zhang, Orthorhombic–tetragonal phase coexistence and piezoelectric behavior in (1-x)(Ba,Ca)(Ti,Sn)O_3–x(Ba,Ca)(Ti,Zr)O_3 lead-free ceramics
5. T. Takenaka, K. Maruyama, and K. Sakata, ($Bi_{1/2}Na_{1/2}$)TiO_3-$BaTiO_3$ System for Lead Free Piezoelectric Ceramics. *Jpn J Appl Phys.* **30**, 2236–2239 (1991).

6. L. Gao, L. Huang, Y. Hu, and H. Du, Dielectric and ferroelectric properties of (1-x)$BaTiO_3$–x$Bi_{0.5}Na_{0.5}TiO_3$ ceramics. *Ceram Int.* **33**, 1041–1046 (2007).
7. S. Zhang, A. B. Kounga, E. Aulbach, T. Granzow, W. Jo, and H. Kleebe, Rödel J: Lead-free piezoceramics with giant strain in the system $Bi_{0.5}Na_{0.5}TiO_3$-$BaTiO_3$ - K $_{0.5}Na_{0.5}NbO_3$. I. Structure and room temperature properties. *J Appl Phys.* **103**, 034107 (2008).
8. J. F. Trelca, C. Courtois, M. Rguiti, A. Leriche, P. H. Duvigneaud, and T. Segato, Morphotropic phase boundary in the BNT–BT–BKT system. *Ceram Int.* **38**, 2823–2827 (2012).
9. J. U. Rahman, A. Hussain, A. Maqbool, G. H. Ryu, T K Song, W. Kim, and M. H. Kim, Field induced strain response of lead-free $BaZrO_3$-modified $Bi_{0.5}Na_{0.5}TiO_3$-$BaTiO_3$ ceramics. *J. Alloy Compd.* **593**, 97–102 (2014).
10. S. Wadda, K. Yamato, P. Pulpan, N. Kumada, B. Y. Lee, T. Iijima, C. Moriyoshi, and Y. Kuroiwa, Preparation of barium titanate–bismuth magnesium titanate ceramics with high Curie temperature and their piezoelectric properties. *J. Ceram Soc Jpn.* **118**(8), 683–687 (2010).
11. Q. Wang, J. Chen, L. Fan, L. Liu, L. Fang, and X. Xing, Preparation and Electric Properties of $Bi_{0.5}Na_{0.5}TiO_3$–$Bi(Mg_{0.5}Ti_{0.5})O_3$ Lead-Free Piezoceramics. *J. Am. Ceram. Soc.* **96**(4), 1171–1175 (2013).
12. R. D. Shannon, Revised effective ionic radii and systematic studies of interatomic distances in halides and chalcogenides. *Acta Crystallogr.,Sect. A: Cryst. Phys.,Diffr.,Theor. Gen. Crystallogr.* **A 32**, 751–767 (1976).
13. A. S. Bhalla, R. Guo, and R. Roy, The perovskite structure - a review of its role in ceramic science and technology. *Mater Res Innov.* **4**, 3–26 (2000).
14. O. Muller, and R. Roy, *The major ternary structural families.* (Springer-Verlag Berlin-Heidelberg-New/sYork (1974).
15. B. Jaffe, and W. R. Cook, *Piezoelectric ceramics.* (Academic Press, New York, (1971).
16. G. A. Smolenskii, Physical phenomena in ferroelectrics with diffuse phase transition. *Jpn. J. Phys. Soc.* **28**, 26–37 (1970).
17. S. K. Rout, E. Sinha, and S. Panigrahi, Dielectric properties and diffuse phase transition in $Ba_{(1-x)}Mg_xTi_{0.6}Zr_{0.4}O_3$ solid solutions. *Mater.Chem.Phys.* **101**, 428–432 (2007).
18. K. Uchino, and S. Nomura, Critical exponent of the dielectric constant in diffused-phase-transition crystals. *Ferroelectrics Lett.* **44**, 55 (1982).
19. R. Clarke, and J. C. Burfoot, The diffuse phase transition in potassium strontium niobate. *Ferroelectrics.* **48**, 505 (1974).
20. V. A. Isupov, Nonlinearity of the concentration dependence of the Curie temperature in ferroelectric perovskite solid solutions. *Phys Stat. Sol. (a).* **181**, 21 (2000).
21. R. J. Bratton, and T. Y. Tien, Phase Transitions in the System $BaTiO_3$—$KNbO_3$. *J Am Ceram Soc.* **50**, 90–93 (1967).
22. F. He, X. Chen, J. Chen, Y. Wang, H. Zhou, and L. Fang, $(K_{0.5}Na_{0.5})NbO_3$-$Bi(Mg_{0.5}Ti_{0.5})O_3$ solid solution: phase evolution, microstructure and electrical properties. *J Mater Sci-Mater El.* **24**, 4346–4350 (2013).
23. W. Bai, Y. Bian, J. Hao, B. Shen, and J. Zhai, The Composition and Temperature-Dependent Structure Evolution and Large Strain Response in (1-x)$(Bi_{0.5}Na_{0.5})TiO_3$-x$Ba(Al_{0.5}Ta_{0.5})O_3$ Ceramics. *J. Am. Ceram. Soc.* **96**(1), 246–252 (2013).
24. D. Xu, W. L. Li, L. D. Wang, W. Wang, W. P. Cao, and W. D. Fei, Large piezoelectric properties induced by doping ionic pairs in BaTiO3 ceramics. *Acta materialia.* **79**, 84–92 (2014).
25. G. H. Haertling, and W. J. Zimmer, Analysis of hot-pressing parameters for lead zirconate-lead titanate ceramics containing two atom percent bismuth. *Am. Ceram. Soc. Bull.* **45**, 1084–1089 (1966).
26. D. Xu, W. L. Li, L. D. Wang, W. Wang, W. P. Cao, and W. D. Fei, Large piezoelectric properties induced by doping ionic pairs in $BaTiO_3$ ceramics. *Acta mater.* **79**, 84–92 (2014).
27. I. Fujit, K. Nakashima, N. Kumada and S. Wada, Structural, Dielectric and piezoelectric properties of $BaTiO_3$–$Bi(Ni_{1/2}Ti_{1/2})O_3$ ceramics. *J. Ceram Soc Jpn.* **120**, 30–34 (2012).

VITA

Name–Surname	Jitkasem Mayamae
Date of birth	6 June 1990
Province	Pattani
Education	**B.S.** (Industrial Chemistry – Analytical Instrumentation) King Mongkut's Institute of Technology Ladkrabang, Bangkok (2012)
	M.S. (Nanoscience and Nanotechnology) King Mongkut's Institute of Technology Ladkrabang, Bangkok (2013 - present)

Conferences

1. **Jitkasem Mayamae**, Usa Sukkha, Surasak Niemchareon, Rangson Muanghlua and Naratip Vittayakorn "Dielectric, ferroelectric and piezoelectric properties of the lead free $0.9BaTiO_3$-$(0.1-x)Bi_{0.5}Na_{0.5}TiO_3$-$xBi(Mg_{0.5}Ti_{0.5})O_3$ solid solution" The 9th Asian Meeting on Ferroelectrics and Asian Meeting on Electroceramics (AMF-AMEC-2014), Shanghai, China, October 26-30, 2014. (Poster Presentation)
2. **Jitkasem Mayamae**, Usa Sukkha, Surasak Niemchareon, Rangson Muanghlua and Naratip Vittayakorn "Dielectric, ferroelectric and piezoelectric properties of the lead free $0.9BaTiO_3$-$(0.1-x)Bi_{0.5}Na_{0.5}TiO_3$-$xBi(Mg_{0.5}Ti_{0.5})O_3$ ceramics system". The 40th Congress on Science and Technology of Thailand (STT 40), December 2-4, 2014 (Oral Presentation)
3. **Jitkasem Mayamae**, Wanwilai Vittayakorn, Surasak Niemchareon, Rangson Muanghlua, Soodkhet Pojprapai, Somsak Woramongkolchai and Naratip Vittayakorn "Effect of Sn^{4+} content on dielectric and piezoelectric properties for ternary systems of $(0.975-y)BaTiO_3$–$0.025SrTiO_3$–$yBaSnO_3$ ceramics" The 3rd International Congress on Advanced Materials (AM 2016) (Poster Presentation)

International publications

1) **Jitkasem Mayamae**, Usa Sukkha, Surasak Niemchareon, Rangson Muanghlua and Naratip Vittayakorn "Dielectric, ferroelectric and piezoelectric properties of the lead free $0.9BaTiO_3$-$(0.1-x)Bi_{0.5}Na_{0.5}TiO_3$-$xBi(Mg_{0.5}Ti_{0.5})O_3$ solid solution" *Ferroelectrics,* 490: 23-35 (2016).

2) **Jitkasem Mayamae**, Wanwilai Vittayakorn, Rangson Muanghlua, Somsak Woramongkolchai and Naratip Vittayakorn "Effect of Sn content on the dielectric and piezoelectric properties of the ternary system $(0.975-y)BaTiO_3$–$0.025SrTiO_3$–$yBaSnO_3$". *Journal of Materials science*, 52(12): 6928-6936 (2017).